Internal Loads of Semi-Submersibles at an Inconvenient Draft

An investigation into the non-linear response

R. Korte

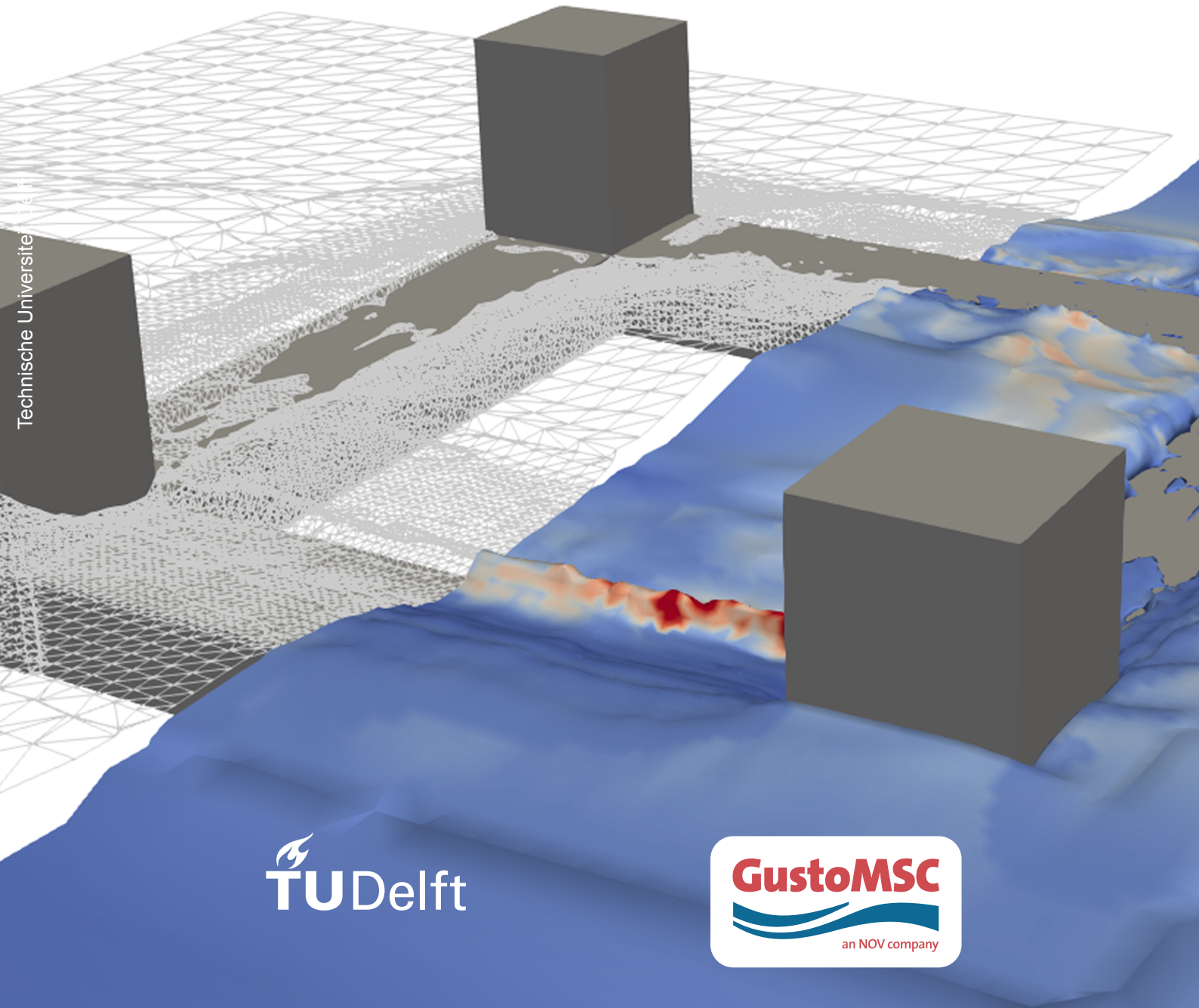

Technische Universiteit Delft

TU Delft

GustoMSC
an NOV company

Internal Loads of Semi-Submersibles at an Inconvenient Draft

An investigation into the non-linear response

by

R. Korte

to obtain the degree of Master of Science
at the Delft University of Technology,
to be defended publicly on June 26, 2019 at 14:40

Student number: 423274
Project duration: October 1, 2018 – June 26, 2019
Thesis committee:

Dr. ir. P. R. Wellens,	Delft University of Technology, *Chairman & Supervisor*
Dr. ir. G. H. Keetels	Delft University of Technology
Dipl. -Ing G. Jacobi	Delft University of Technology
Ir. E. J. Vlasveld,	GustoMSC

TU Delft

GustoMSC
an NOV company

Abstract

Once a semi-submersible is operating at an inconvenient draft (A shallow draft with limited water column above the pontoons), the passing waves over the pontoons can not keep their linear motion and energy will be transferred to higher harmonic wave frequencies. This means the hydrodynamic response will also contain energy at these higher frequencies. Conventional linear diffraction solvers are not able to solve the combined response of the wave frequency and its higher harmonics, which then result in a non-physical solution for the wave loads, motions and internal loads. This research aims to obtain a better insight into the hydrodynamic response at the inconvenient draft and ultimately on the internal loads of the semi-submersible.

In the first part of this research, model test solutions, linear potential solutions obtained with WAMIT and CFD solutions obtained with ComFLOW are compared. the comparison shows that ComFLOW is able to provide more accurate wave loads compared to the linear potential solver. The higher harmonics observed in the measured wave loads during model tests are correctly predicted by ComFLOW, although maximum deviations of 30% are still observed between measured and predicted wave-load amplitudes.

However, ComFLOW is not able to solve the motions of a free-floating semi-submersible correctly. Due to pressure peaks in the wave-exciting forces, solving the equation of motion results in an incorrect motion response and ultimately results in incorrect internal loads. Although a significant effort was made - in close collaboration with the ComFLOW developer - to improve this functionality, the results remained unsatisfactory.

Even so, in order to obtain an insight into the higher harmonic response contributions to the internal loads, a parameter study has been conducted, using tests in which the semi-submersible was held captive. This parameter study was conducted by systematically varying wave amplitudes and draft, and resulted in situational limits at which the higher harmonic response contribution becomes significant and the linear relation between the incoming wave and the hydrodynamic response is lost. This limit is shown to be dependent on the Ursell number. Furthermore, it is demonstrated that the significance of the higher harmonic response contribution increases from 10% to 40% throughout the inconvenient draft, while the most severe situations resulted in a higher harmonic response contribution of 50% of the total response amplitude.

In the final part of this study, an attempt is made to couple the wave loads from ComFLOW to internal loads. A quantitative analysis is made on the effect of the higher harmonic responses of the wave loads on the internal loads. The time domain simulator aNySim is used combined with the wave-exciting forces on a captive semi-submersible calculated with ComFLOW. A multi-body analysis is used to obtain the internal loads on the aft and front part of the semi-submersible. This did not provide the correct answers because the stiffness of the spring damping between the two sections affects the higher harmonic response contribution. This method overestimated the higher harmonic response contribution. A better understanding of the joint and the joint stiffness/damping of a dual-body simulation may solve the encountered problems.

Preface

This report is the final product of my MSc thesis project and is the final stage in obtaining the MSc degree Marine Technology at the Delft University of Technology. With my background in ship hydromechanics this thesis was a great opportunity to expand my knowledge on Computational Fluid Dynamics. Not only on the users side, but I also learned a lot on CFD development and challenges it brings.

I want to thank everyone at GustoMSC, for providing me the opportunity to use their knowledge and facilities. Fons, Rogier, Zana, Henry and Vincent thank you for your answers, feedback and input. A special thanks to my daily supervisor at GustoMSC Ebert Vlasveld, who has guided me throughout the project and provided me with the well-appreciated feedback. I want to express my gratitude to my supervisor and chairman of the graduation committee Peter Wellens, for his supervision during the complete project. I want to thank the graduation committee for taking the time to read my thesis and grade the graduation project. Thanks, Peter van der Plas and Joop Helder for the support with ComFLOW and the efforts providing the newest versions of ComFLOW.

Last but not least, I would like to sincerely thank my friends and family for their support during this project. In particular, I want to thank my girlfriend, who always supported me, even in the toughest times.

R. Korte
Delft, June 2019

Contents

List of Symbols

Symbol	Unit	Description
a	$[kg]$	Added Mass
A_{wl}	$[m^2]$	Water Piercing Area
c_c	$[Ns/m]$	Critical Damping
g	$[m/s^2]$	Gravitational acceleration
h	$[m]$	Wave Height
H	$[m]$	Water Depth of propagating wave
$H_{pontoon}$	$[m]$	Height of the pontoon
k	$[N/m]$	Spring Stiffness
$\kappa_{..}$	$[m]$	Radii of Gyration around specified axis
L_{gap}	$[m]$	Distance between Pontoons
λ	$[m]$	Wave Length
ω	$[rad/s]$	Radial Frequency
ω_{hh}	$[rad/s]$	Radial Frequency of hh'th harmonic frequency
ω_n	$[rad/s]$	Natural Radial Frequency
ω_{st}	$[rad/s]$	Radial Frequency of standing wave
ϕ	$[\circ]$	Rotation around Longitudinal Axis
ψ	$[\circ]$	Rotation around Vertical Axis
rho	$[kg/m^3]$	Fluid Density
T	$[m]$	Draft
T_p	$[s]$	Wave Period
θ	$[\circ]$	Rotation around Transverse Axis
u	$[m/s]$	Velocity in x direction
v	$[m/s]$	Velocity in y direction
w	$[m/s]$	Velocity in z direction
x	$[m]$	Longitudinal direction
y	$[m]$	Transverse direction
z	$[m]$	Vertical direction
ζ	$[m]$	Free surface elevation
ζ_a	$[m]$	Wave amplitude

List of Abbreviations

CFD	Computational Fluid Dynamics
CFL	Courant-Friedrichs-Lewy condition
EOM	Equation of Motion
FFT	Fast Fourier Transform
GABC	Generating Absorbing Boundary Conditions
iVoF	improved Volume of Fluid
MARIN	Maritime Research Institute Netherlands
RAO	Response Amplitude Operator

1 Introduction

1.1. Motivation

GustoMSC is a design and engineering company in the field of mobile offshore units and equipment. One segment of the mobile offshore units is the semi-submersible platform. These platforms are designed for offshore drilling, well-intervention, heavy lifting, crew accommodation and more. GustoMSC is currently working on a relative small semi-submersible called the OCEAN180. As this is a relative small semi-submersible, the air gap (the clearance between the free surface and the deck-box), is a limiting factor in the design. After an accident involving a deck-box impact on a semi-submersible in 2015, resulting in one casualty, DNV-GL tightened its rules and regulations with regard to air-gap requirements in storm conditions. For the OCEAN180 these air-gap requirements can only be met if the semi-submersible is at an inconvenient draft during a storm.

This inconvenient draft is not a set draft but rather a range of drafts combined with wave height and wave period. An indication of the inconvenient draft of a semi-submersible is shown in figure 1.1. At this inconvenient draft, the linear relation between the incoming waves and the hydrodynamic responses is reduced. This means that the hydrodynamic response consists not only of the wave frequency but also of higher harmonic frequencies. The conventional methods, use linearised potential flow and assumptions to linearise the problem; for example, no changes of water-line area are permitted. This linear relation is not present at this inconvenient draft, as rapid changes in water-plane area occur. This means that the solution provided by the conventional methods (motions and wave loads) may be too inaccurate.

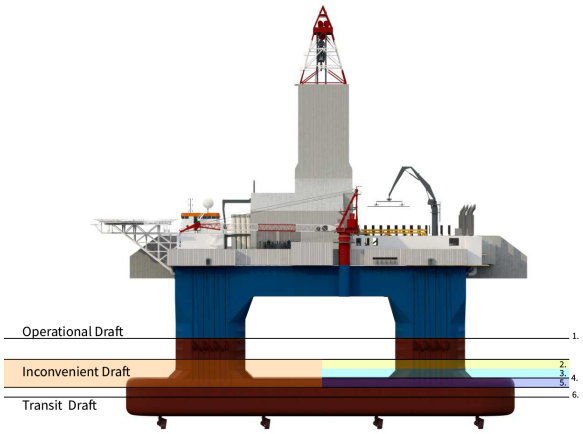

Figure 1.1: An indication of the range of inconvenient drafts for a semi-submersible.

As the internal loads (i.e. splitting loads) depend on both the wave loads and the motions, the internal loads calculated with the conventional methods may also yield an inaccurate prediction. These internal loads are an important input parameter in the structural verification of the mobile offshore unit.

Currently, GustoMSC has insufficient insight in the level of inaccuracy introduced by using the conventional methods for these inconvenient drafts.

A previous study, also done at GustoMSC and conducted by R. de Bruijn et al. (2011) [5], showed for a captive semi-submersible at an inconvenient draft that compared to both model tests and a CFD (Computational Fluid Dynamics) solver, the wave loads were generally overpredicted by the linear diffraction solver. For a prescribed motion, the linear diffraction solver typically resulted in higher internal loads compared to the loads calculated with a CFD solver. In this research no free-floating tests have been conducted and it remained unclear whether these conclusions can also be drawn for free-floating semi-submersibles. This study also showed that wave loads at the inconvenient draft consist of multiple harmonic frequencies; however, it is still not clear what the effect is of these higher harmonic wave loads on the internal loads, and whether the effect is significant with respect to the total internal loads. The other papers used as theoretical foundation of this research are shown in appendix A.

The academic value of this study is twofold:

1. From an economical point of view it means that the semi-submersible will not be over-dimensioned, potentially resulting in a more cost-effective structure.

2. From a safety point of view it means that the semi-submersible will not be under-dimensioned, potentially resulting in failure in more extreme events/sea states. If the wave loads, motions and internal loads can be predicted with more accuracy at these inconvenient drafts, currently operating semi-submersibles could be intentionally de-ballasted to an inconvenient draft to increase the air gap in storms, and so ensure the safety of the semi-submersible and the people on board.

1.2. Objective

The main problem that initiated this research is the lack of an engineering method to calculate the internal loads at an inconvenient draft. To arrive at such a method, it is essential to understand the physics of the problem, which makes the first objective of this study increasing the physical understanding of the higher harmonic response at the inconvenient draft. This means: looking into the conventional linear diffraction solvers, investigating the limitations, and researching the solutions of these methods at the inconvenient draft. Based upon this physical base, research can be directed at obtaining insight into the parameters that cause and influence the higher harmonic responses at the inconvenient draft. Limits should be set where the linear relation is no longer valid and conventional methods will no longer provide the correct solutions. Within these limits the internal loads should preferably be calculated with a different approach. This different approach is the final objective: to set up a method based on the correct physical foundation in order to estimate the internal loads at the inconvenient draft in a more accurate way. This should be an engineering approach and should be directed at solving the internal loads for all different geometrical and environmental situations, within an acceptable time span. These targets are all combined in one objective:

Determine the effect of non-linear wave loads on the internal loads of a semi-submersible at an inconvenient draft and develop a method which is able to approximate these internal loads.

1.2.1. Research Question

To structure the route to achieve the objectives, three main research questions have been set up. For each of these main research questions multiple sub-questions are defined. The research questions are as follows:

1. How do model-tests, linear potential solvers and CFD solvers compare?
   (a) What is the magnitude of the deviations between the different calculation methods and are there significant differences?
   (b) What is the physical explanation of the deviations?
   (c) Can ComFLOW be used to better approximate reality?
2. How does the higher harmonic response behave within the inconvenient draft?

(a) How do pontoon submergence and wave height impact the occurrence of higher harmonics in the wave-load response and can a clear relation be distinguished?

(b) What is the magnitude of the higher harmonic response on the internal loads, and does the influence reach a significant level?

(c) When do the (combined) pontoon submergence and wave height start to introduce significant non-linearities in the wave-induced internal load response

3. Can the calculations be simplified in such a way that the computational time is reduced without considerably affecting the accuracy?

(a) Why is an engineering method needed and what are the requirements?

(b) Is the engineering method capable of delivering the desired results?

1.3. Methodology

The methodology of this research are elaborated in twofold. First, the composition of the internal loads are discussed. As this is the common thread throughout this research. The next part of the methodology is the plan of approach.

1.3.1. Internal Load Components

The internal loads of a free-floating structure can be split into multiple load components. An overview of the load components is given in figure 1.2.

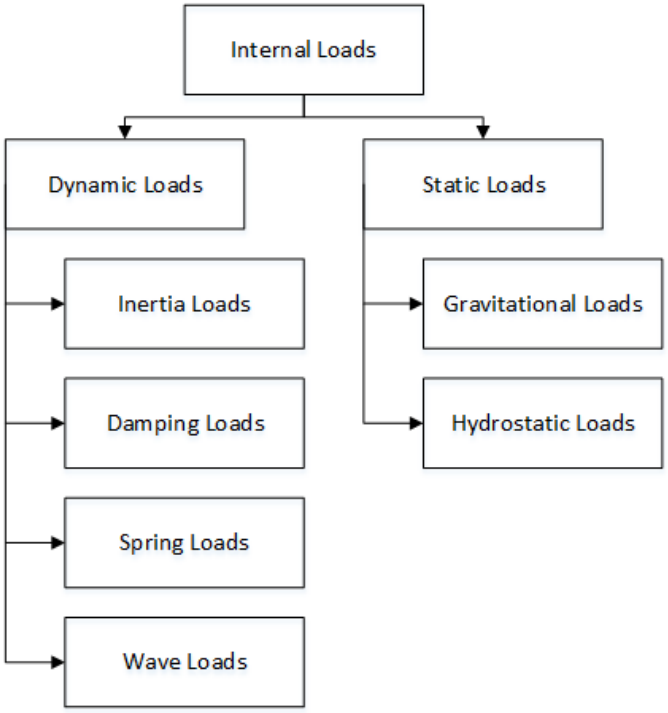

Figure 1.2: Internal Load Composition

- Static Loads
  - Gravitational Loads: The gravitational loads are the loads on the structure due to the mass of the structure itself. The gravitational loads depends on the pitch and roll rotation of a floating structure. The horizontal internal load is calculated with: $F_x = M \cdot g \cdot sin\phi$. The vertical force will generally be linearised so $F_z = M \cdot g$.
  - Hydrostatic Loads: Loads due to the still water buoyancy force.

- Dynamic Loads: To obtain the dynamic load component, the equation of motion(EOM) is solved. This consists of the following parts:
  - Inertia Loads: The inertia loads are the loads that result due to the accelerations of structure in combination with the mass distribution of the floating structure.
  - Damping loads: The damping loads correlates to the velocity of the semi-submersible, e.g. potential damping and viscous effects.
  - Spring loads: The hydrostatic loads represent the hydrostatic spring stiffness of the heave, roll and pitching motion. The water piercing area will determine the spring stiffness. In case of an inconvenient draft, the water piercing area can change rapidly, resulting in non-linear spring stiffness.
  - Wave Loads: The wave loads are the loads on the floating structure due to the wave passing. In case of an inconvenient draft, these wave loads consist of multiple harmonic frequencies.

The total of these components are summed for a part of the semi-submersible to obtain the internal loads. The difference of the internal loads of two sections provides the splitting loads. A schematic representation of a semi-submersible is given in figure 1.3b. If the internal loads on the forward section of the semi-submersible are desired, all components shown above are summed for the forward section. This will result in the internal loads as shown in figure 1.3a.

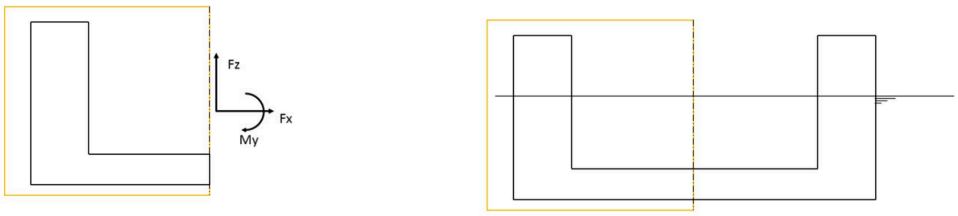

(a) Internal loads on schematic representation of Forward section of the Semi-Submersible

(b) Schematic representation of Semi-Submersible

Figure 1.3: Schematic Representation of Semi-Submersible and the Internal Load Definition

1.3.2. Plan of Approach

In this paragraph the approach to answer the three research questions mentioned in section 1.2.1 is further elaborated.

- The first step is to reproduce the semi-submersible at the inconvenient draft and corresponding results obtained by R. de Bruijn et al. (2011) [5]. Both in the linear/first-order diffraction solver WAMIT and in the CFD solver ComFLOW. The calculations with a fixed semi-submersible are made to analyse the model and to compare the calculations from the linear diffraction and CFD solver with existing model tests. This is done for both the 'linear' operational draft and the 'non-linear' inconvenient draft. Special attention is given to comparing ComFLOW with the model test, in order to check whether ComFLOW correctly calculates the forces acting on the semi-submersible.
- The second step involves solving the equation of motion at each time step within ComFLOW, a feature not available at the time of R. de Bruijn his research. This effectively provides ComFLOW with the ability to simulate free-floating wave tests, hopefully providing more insight into the physics involved.
- The third step is to perform a parameter study for both the draft and wave height, for a free floating semi-submersible. Multiple simulations are be performed in both the linear solver and the non-linear CFD solver, each time varying one parameter while the other parameters are fixed. In this way the different parameters can be isolated and their influence on the internal loads can be assessed. For the draft/submergence of the pontoon, six different draft zones are analysed,

of which two are expected to show a linear behaviour. These are the operational draft and an exaggerated transit draft. The other four zones are within the range of the inconvenient draft. These regions are stated in table 1.1 and are illustrated with the corresponding numbers in figure 1.1. The wave amplitudes are varied from small wave amplitudes to large wave amplitudes, associated with storm conditions. For GustoMSC it is important to know at which conditions the current diffraction method is no longer reliable and when they have to switch to a different method. This parameter study will present the limits at which non-linear effects start to occur and when the non-linear effects become significant enough to influence the accuracy of the hydrodynamic response.

- The fourth and final step is to develop an engineering method which is able to approximate the internal loads at the inconvenient draft to an acceptable degree of accuracy. The implementation of this method is highly dependent on the outcome of the previous steps of this research.

Draft		Specification
Operational Draft	1.	Linear behaviour of wave forces
Inconvenient Draft	2.	Small water column on top of the pontoon, without surface piercing motions
	3.	Small water column on top of the pontoon, with surface piercing motions
	4.	Draft at exactly pontoon height
	5.	Draft at pontoon width with waves overtopping pontoon
Transit Draft	6.	Linear behaviour of wave forces

Table 1.1: Overview of Drafts

1.3.3. Validation and Verification

To derive any conclusions or remarks from the result in this study, the calculations should be validated. There are model tests available of a semi-submersible at an inconvenient draft. These model tests consist of two parts, the wave loads on a captive model and the motions of a free-floating model. The tests are done on both an operational and an inconvenient draft. This means no internal loads are measured and the results of the internal loads at inconvenient draft cannot be validated directly. Instead, the answers the following validation and verification precautions will be made.

Grid Refinement Study
With regard to the CFD calculations, a different grid refinement can give different results. This means the grid on which the simulations are ran should be verified. To justify the selected grid size, it should be shown tat results are sufficiently converged. This is done by systematically adjusting the grid size and assessing the impact on the results.

Validate the wave loads and motions from ComFLOW with Model test
The wave loads and motions outputted by ComFLOW will be validated against a model test of a semi-submersible at an inconvenient draft. This validation will be done on both the wave-induced loads and the wave-induced motions.

Verify Engineering approach with results from ComFLOW
If the solution that ComFLOW provides is validated, the newly set up engineering method can be compared with ComFLOW. It will become possible to check whether the engineering method is producing acceptably accurate results within a shorter time span.

1.4. Outline

Chapter 2 gives the setup of the model test, linear diffraction solver WAMIT and the CFD solver ComFLOW.
Chapter 3 shows the steps that are taken to verify the CFD solutions. A grid study shown and the numerical parameters are selected.
Chapter 4 gives an overview of the simulations ran in model tests, the linear diffraction solver WAMIT and the CFD solver ComFLOW. The main objective of this chapter is to see the differences in outcome and to explain these differences.
Chapter 5 describes the parameter study. First the set up of the parameter study, which parameters are chosen to vary within which ranges. Next the results of this parameter study are discussed and conclusions are drawn. The main objective is to examine the transient behaviour from a linear behaviour to a non-linear behaviour and see at what limits the higher harmonics in the wave loads become significant.
Chapter 6 will discuss the engineering method used to compute the internal loads at an inconvenient draft. First the guidelines of this method are explained. Next, the set up of the method itself are elaborated. And finally, the results and initial findings are explained.

2

Model Description

This chapter gives the setup for each of the methods used to determine the hydrodynamic response of the semi-submersible. The model tests setup is shown in section 2.1, it shows which model is used, which conditions are tested and which responses are measured. In section 2.2 the setup of the linear diffraction solver is shown. Finally, in section 2.3 the setup of the CFD simulations is elaborated.

2.1. Model Test

Model tests are often assumed to be correct; however, they are prone to errors. In order to use and compare the model test results, the data should be analysed first. The main target of this section is to obtain trustworthy model test data that can be used in comparison with the solutions of the first-order diffraction solver and CFD solver.

In 2004, a model test study was conducted to obtain further knowledge on the hydrodynamic loads and motions of a semi-submersible at an inconvenient draft. The tests were conducted in the towing tank at Delft University of Technology and are documented in the report of J. de Weerd (2004) [6]. In these tests a ring semi-submersible was used, with a scaling factor of 1:100. The dimensions of the ring semi-submersible used in these model tests are shown in table 2.1. The drawings of the semi-submersible and the tank setup is shown in Appendix B, figure B.1. In total four different drafts were tested, $T = 25\ m$, $T = 17.5\ m$, $T = 14.5\ m$ and $T = 11.5\ m$. These drafts are within the range of the inconvenient draft from a particular wave amplitude. The tests are split into two parts: captive tests and free-floating tests.

Table 2.1: Full scale dimensions of the semi-submersible

Dimensions	Deep Draft	Inconvenient Draft
Draft	$25\ m$	$11.5\ m$
Length Floater	$59.5\ m$	$59,5\ m$
Width Floater	$13.5\ m$	$13.5\ m$
Height Floater	$7.5\ m$	$7.5\ m$
Length Columns	$14.0\ m$	$14.0\ m$
Width Columns	$14.0\ m$	$14.0\ m$
Height Columns	$39.5\ m$	$39.5\ m$
Pontoon Spacing	$73.5\ m$	$73.5\ m$

Table 2.2: Full scale mass properties of the semi-submersible

Dimensions	Deep Draft	Inconvenient Draft
Draft	$25\ m$	$11.5\ m$
Mass	$43670\ ton$	$32982\ ton$
KG	$26.15\ m$	$23.48\ m$
k_{xx}	$41.22\ m$	$42.00\ m$
k_{yy}	$41.22\ m$	$42.00\ m$
k_{zz}	$54.29\ m$	$54.57\ m$

For the captive tests the semi-submersible is retained at a fixed draft, even keel. In these tests the wave forces acting on the semi-submersible are measured in longitudinal (x) direction and vertical (z) direction. In these model tests only head waves are tested. This means the forces and motions in the surge, heave and pitch degree of freedom are obtained. The sway, roll and yaw are not measured. As a result only the surge, heave and pitch forces and motions are analysed throughout this research. The sway roll and yaw are left out of consideration.

Also, two wave probes are present, one in front of the model and one next to the model. From its time trace the wave amplitude and wave period can be determined. The setup of the captive test including the location of the wave probe is shown in Appendix B, figure B.3.

The free-floating tests are conducted to obtain the motions of the semi-submersible. In these tests the semi-submersible is softly moored with four springs that attached to the model, approximately at the height of the centre of gravity, each with a spring constant of 130 N/m. The spring constants of the mooring lines are selected such that its natural period is outside the wave-frequency range. For each draft, four regular wave frequencies are tested and one Neumann Spectrum with a peak period of 20s. This setup is visualized in Appendix B, figure B.4.

A complete overview form all the model tests used in this research is shown in table 2.3.

Table 2.3: Model test matrix

Draft	Inconvenient draft $T = 11.5\ m$				Deep Draft $T = 25\ m$			
	Desired		Obtained		Desired		Obtained	
	ω [rad/s]	ζ [m]	ω[rad/s]	ζ [m]	ω[rad/s]	ζ [m]	ω[rad/s]	ζ [m]
Captive Simulations	0.30	3.00	0.297	2.750	0.40	1.00	0.398	0.971
	0.40	1.00	0.398	0.980	0.40	2.00	0.390	1.941
	0.40	2.00	0.398	1.930				
	0.40	3.00	0.398	2.830				
	0.60	2.00	0.594	2.112				
	Desired		Obtained		Desired		Obtained	
	ω [rad/s]	ζ [m]	ω [rad/s]	ζ [m]	ω [rad/s]	ζ [m]	ω [rad/s]	ζ [m]
Free Floating simulations	0.26	2.00	0.251	2.159	0.26	2.00	0.257	1.439
	0.28	2.00	0.274	1.895	0.30	2.00	0.293	1.871
	0.40	2.00	0.390	1.902	0.40	2.00	0.391	1.933
	0.24	2.00	0.233	1.881	0.25	2.00	0.241	1.737

2.1.1. Wave-input analysis

In order to use the data obtained in the model tests and to compare them with the diffraction and CFD results, the model test data are analysed. First, the desired wave height and period is compared with the obtained wave height and period measured in the basin. Since the basin in which these tests are conducted is prone to a low frequency wave if the water level is at the correct height, the wave input on the semi-submersible needs to be checked for this low frequency wave. This low frequency wave can influence the response of the semi-submersible.

One major disadvantage of this data set is the lack of a calibration run. Normally, a calibration test is conducted for each wave frequency without the model in the basin,in which the water free surface elevation is measured at the anticipated location of the model. This provides the time trace of the wave which the model will experience during the model tests. As this is unknown, the exact wave the

model experienced is not known. During the tests with the model, the wave probe measures the wave amplitude in front of and next to the model. The wave amplitude obtained with these wave probes will consist of multiple wave patterns; incoming waves and the diffracted /reflected waves. The model reflects the waves in all directions, the time traces of both wave probes will thus consist of the initial wave generated by the wavemaker and the waves reflecting and diffracting from the model.

Low-frequency wave
As previously said, the basin in which the model tests are conducted is prone to having a low-frequency wave if the water level of the basin is filled to the correct mean free surface depth. At this point the wave-damping beach will reflect a low-frequency wave back into the basin. To check if this low frequency wave is present during these model tests, a Fast Fourier Transformation (FFT) has been applied to obtain the frequency spectrum of the waves in de basin. An example of a wave height time trace of a captive semi-submersible in regular waves is given in figure 2.1. In this figure both the time trace of the wave in front of the model and the FFT of this time trace is shown. In the FFT spectrum a clear peak can be distinguished around $\omega = 0.4\ rad/s$. This is as expected as this time trace is from one of the regular wave tests with a radial wave frequency of $\omega = 0.4\ rad/s$. Another small but important peak arises at $\omega = 0.03\ rad/s$. (period of around 200 seconds) This would mean one oscillation in the entire time trace. To better visualize this low frequency oscillation a FFT band-pass filter is used. A lower limit of $\omega = 0\ rad/s$ and an upper limit of $\omega = 0.05\ rad/s$ are used. In figure 2.2 this low-frequency oscillation is shown. It is visible that the amplitude of this oscillation is $0.09\ m$. This is equal to 5% of the total amplitude.

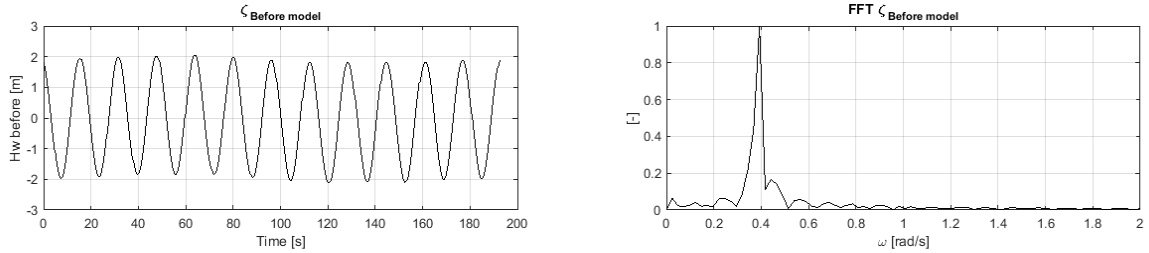

Figure 2.1: Wave amplitude and FFT of wave amplitude - Captive - $\zeta_a = 2m$ - $\omega = 0.4$

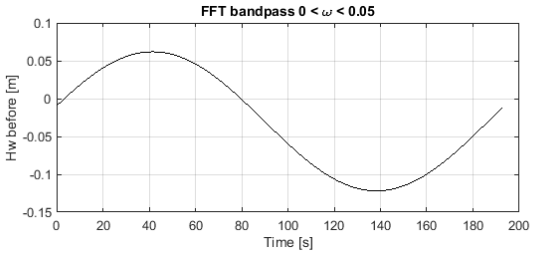

Figure 2.2: FFT bandpass filter $0 < \omega < 0.05$

For a free-floating test the same analysis is made. The time trace and frequency spectrum is shown in figure 2.3. In the frequency domain a peak is visible at $\omega = 0.4\ rad/s$ and a small peak is visible between $0 < \omega < 0.1\ rad/s$. This is also visible after the FFT band-pass filter with the same limiting frequencies as before. In figure 2.4 the low-frequency wave is shown, it also has a period around 200 second and an amplitude of $0.12\ m$, which is 6% of the total amplitude.

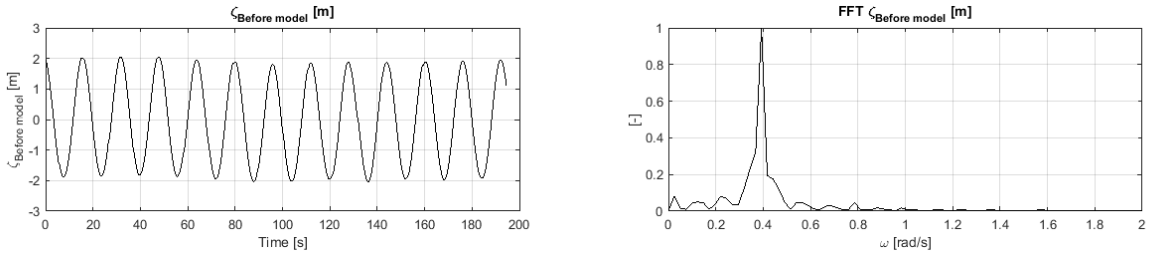

Figure 2.3: Wave amplitude and FFT of wave amplitude - Free Floating - $\zeta_a = 2m$ - $\omega = 0.4$

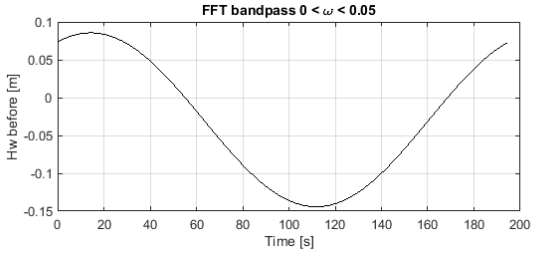

Figure 2.4: FFT bandpass filter $0 < \omega < 0.05$

As these tests are all performed with the model in the basin, the waves that diffract, reflect and radiate (free-floating only) from the semi-submersible are also captured in the wave amplitude time traces. However, in the case of wave diffraction and reflection, the low-frequency waves are less diffracted/reflected when compared to the high-frequency waves. In case of a free-floating semi-submersible, radiation of waves also occurs. The waves radiating from the semi-submersible will always have a frequency that is close to the frequency of the oscillations from the semi-submersible and in the case of regular waves, the frequency of the incoming waves. The low-frequency waves are thus caused by the basin and not by the model.

The low-frequency waves can be eliminated from the data with the same FFT band-pass filter, but with different limits. The lower limit is set at $\omega = 0.1\ rad/s$ and the upper limit at $\omega = 2\ rad/s$. Responses with frequencies above $\omega = 2\ rad/s$ are neglected, since these are typically not relevant for the response of the semi-submersible. This FFT filtering is also used for the response data of the captive tests. This will yield a better comparison with the linear diffraction solver and the CFD solver. In both methods only the regular input wave is simulated. In case of the free-floating semi-submersible, extra precautions should be taken. The waves that excite the semi-submersible are not perfectly regular, in which case the frequency spectrum would show a perfect peak around the wave frequency. As multiple waves with different wave frequencies travel trough the basin, higher order wave-drift forces should be taken into account. One of the consequences of having multiple wave frequencies is a low frequency surge force. This low-frequency response should be taken into account and should not be filtered out. This means that the lower boundary should always be checked for this low frequency response. As for all of the regular wave tests, there is not a wave frequency component within 0.1 rad/s of the applied regular wave frequency, this means the low-frequency response will not occur between 0 and 0.1 rad/s. The response obtained in the free-floating test can also be cleared of these frequencies.

2.2. First order diffraction

This section describes the hydrodynamic loads and responses obtained with linear tools, based on potential theory. For the calculation of the first-order hydrodynamic response WAMIT version 7.0 is used. WAMIT is able to solve the first-order diffraction and radiation problem. It uses a panel method to solve the velocity potential and the pressures acting on the floating object. Using Bernoulli's formula, the pressure field is calculated and from this pressure field the added mass, damping and wave forces are calculated. Finally, the motion and force RAOs can be calculated. A more elaborate explanation is given in the WAMIT user manual (2019) [12].

As the experimental data shown in section 4.1 only consist of one direction, the computations with

WAMIT will also be run for one direction. The hydrodynamic response are calculated on a hundred wave frequencies in total, ranging for 0.02 rad/s to 2.0 rad/s with increments of 0.02 rad/s.

The panel model of the semi-submersible at a draft of $T = 25\ m$ is shown in figure 2.5. The models for the three different drafts are the same, only the columns are cut at a lower level.

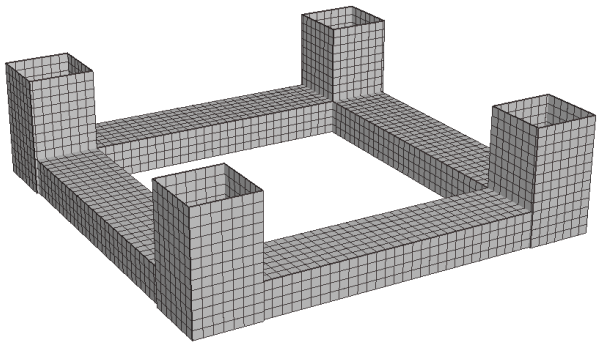

Figure 2.5: Panel Model at T=25m

WAMIT calculates the hydrodynamic data, and these are used to calculate the RAOs for motions and wave loads acting on the semi-submersible. Morison tubes are used to represent viscous damping. This quadratic damping is linearised using stochastic linearisation. As the free-floating tests are all at $\zeta_a = 2\ m$ and the captive test at $\zeta_a = 1,\ 2,\ 3\ m$ a wave amplitude of $\zeta_a = 2\ m$ is used to linearise the viscous damping.

2.3. Computational Fluid Dynamics

In this section the setup of the Computational Fluid Dynamics method are assessed. The solver used is ComFLOW4.1.1. Initially ComFLOW was developed to simulate the free-surface in a micro-gravity environment. This has been expanded to the hydrodynamic loading of marine structures. It solves the Navier-Stokes equation and uses an improved Volume Of Fluid (iVOF) to accurately capture the free-surface. An elaborate explanation of the theory behind ComFLOW is given by P. van der Plas(2017)[18].

This chapter consists of two parts, the initial setting are shown in section 2.3.1. The numerical parameters and solvers that are used in the CFD simulations are shown in section 2.3.2.

It should be noted that during this research several problems with ComFLOW have been encountered. This resulted in a close collaboration with the developers at MARIN[1]. This resulted in a new Alpha versions of ComFLOW in which attempts were made to solve the problem. As a result, multiple versions of ComFLOW are used in this research. In total three different ComFLOW versions have been used. These versions have been named A until C, as shown in table 2.4. This table gives the version names used in this research, ComFLOW build date and for which simulations this version is used. In Appendix E a complete description of this version is provided.

Table 2.4: ComFLOW Versions

Version	Build data	Usage
A	2018-02-05	Grid Study
B	2019-02-15	Captive Simulations
C	2019-04-11	Free-Floating Simulations

2.3.1. Initial Settings

Physical Parameters

ComFLOW is able to model both the liquid phase and the gas phase. The gas phase can be of importance in case of air entrapment; for example, impacts of breaking waves. This is not expected to

[1]Maritime Research Institute Netherlands

be of importance in the present simulations and thus a 1-phase model is used, which decreases the computational time, as the cells above the waterline are assumed to be void and the Navier-Stokes equation will not be solved in these cells. Still, an atmospheric pressure should be applied on the free surface. The atmospheric pressure, water density together with the other physical parameters are shown in table 2.5.

Table 2.5: Physical Parameters

Parameter	*Value*	*Unit*
Atmospheric Pressure	100 000	Pa
Density	1 000	kg/m^3
Viscosity	10^{-3}	Ns/m^2
Gravity	9.81	m/s^2

Domain

The semi-submersible is modelled in full scale. This means that the model basin should be scaled up to full scale. In this case the computational domain of the CFD simulations would be 11,000 x 276 x 120 meters. Such a large domain results in an impractical computational time. Common practice in CFD is to couple the length of the domain to the wavelength; this to reduce the influence of the reflected waves on the boundaries of the domain. However, as ComFLOW uses absorbing boundary conditions on the outflow boundaries this relation is not needed. Based on the recommendation from the ComFLOW development team, the domain length is reduced to 200 meters to minimize the computational time.

The full scale depth of the towing tank is 120 meters. This will also be the modelled depth in the CFD simulations.

For the width of the simulations the width of the full-scale basin is used, to allow the reflections that occurred in the model tests, to also occur in the CFD computations.

As the waves tested in the model tests are uni-directional, symmetry can be used to reduce half the cells and thus the computational time is reduced. If symmetry is used, the velocity normal to the symmetry plane is zero and no motions normal to the symmetry plane can be used. This means no sway, roll and yaw will occur in the simulations. One problem arises with the use of a symmetry plane in these simulations. The model of the semi-submersible is not centred in the model basin. This means that both sides of the tank are at a different distance from the model, which can influences the reflection of waves. To make sure that the symmetry plane is not subjected to large deviations, a symmetry check was conducted. A simulation with the symmetry plane is compared to a simulation with the full width and the non-centred location of the semi-submersible. In figure 2.6 both simulations are shown. No significant differences were found in the results for the resulting wave amplitude and the forces in the three degrees of freedom used.

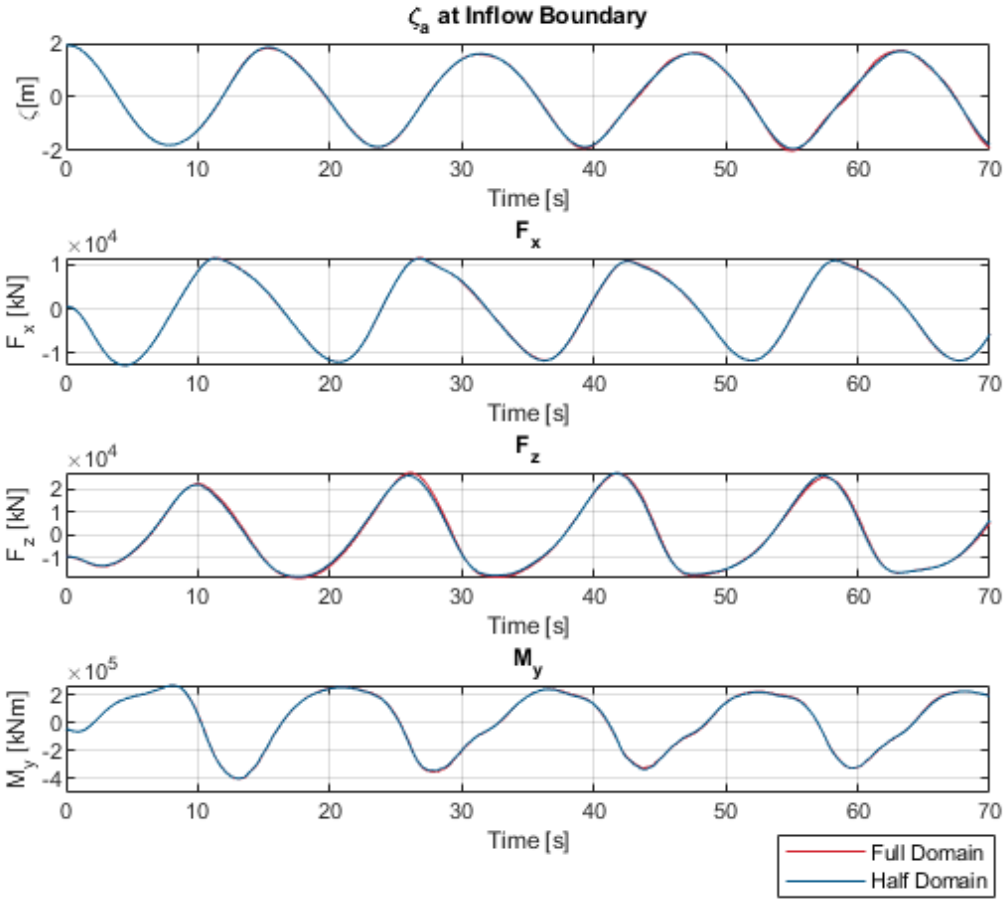

Figure 2.6: Wave load response on the full domain and on the halve of the domain cut at the symmetry plane.

Boundary Conditions

To make a wave propagate through the domain, inflow and outflow boundary conditions have to be defined. For these simulations, a simple form of the Generating Absorbing Boundary Condition (GABC) is used, a recommended in the ComFLOW manual (2015) [10]. An elaborate explanation of GABC is given in the paper of Xing Chang, Ido Akkerman, Rene H.M. Huijsmans and Arthur E.P. Veldman (2016) [4]. A GABC uses the orbital velocities and pressure field at the boundaries to determine the wave height and wave velocities at the boundary condition. As only regular waves are simulated in this research a simplified form of the GABC is used. Wave height and orbital velocities of the waves are determined based on the input parameters, such as wave period and wave number, which are subsequently prescribed on the inflow and outflow boundaries. This is also known as a Sommerfeld boundary condition.

An extra boundary condition is applied at the axis of symmetry. All flow variables are mirrored over the axis of symmetry and all normal velocities on the symmetry plane are equal to zero.

Waves

For the simulation of incoming waves, 5th order Stokes waves are used, as this yields the closest representation of the waves used in the model tests. A fully developed wave field is used in the initiation of the simulations without any ramping function to slowly initiate the waves. This means that the first 10 to 20 seconds of the simulation cannot be used because all reflecting/diffracting waves have not settled yet. No current is used in these simulations, since no current is present in the model tests.

2.3.2. Numerical Parameters and Solvers

In this section the selection of numerical parameters, the selection of the numerical solver for the momentum equations, and the time integration is discussed.

Time Integration

ComFLOW uses a numerical scheme to solve the time integration. This numerical scheme can be modified by changing different parameters. The general function of the numerical scheme is shown in equation 2.1. By changing the parameters, the numerical desired numerical scheme can be set up. Common numerical schemes such as a Forward Euler or an Adams-Bashforth can be used by selecting the correct parameters. The parameters for these two-time integration schemes are shown in table 2.6.

$$@ddtd\ u^{n+1} = @ddta\ u^{n} + @ddtb\ u^{n-1} + f(@feab1\ u^{n} + @feab2\ u^{n-1}) + ... \tag{2.1}$$

Both the Forward Euler and the Adams–Bashforth time integrator are simulated to analyse which numerical scheme has the optimal performance. Since the Forward Euler method resulted in unstable simulations and the Adams-Bashforth method with higher order solver proven to be stable, the latter method was selected as time integrator.

Table 2.6: Time Integration parameters

Name	Order	*ddtd*	*ddta*	*ddtb*	*feab1*	*feab2*
Forward Euler	1	1.0	1.0	0.0	1.0	0.0
Adams-Bashforth	2	1.0	1.0	0.0	1.5	-1.5

When the simulation is started not all diffracted and reflected waves are fully developed. This will take approximately two oscillations. This means the first few seconds of the simulation should not be used to compare the simulations. The duration of the simulations is therefore set to at least five wave periods of which the first two can be discarded as initiation oscillations.

The time step is adjusted and limited by two parameters. The maximum time step and the CFL limits.

- The first parameter is the maximum time step. To simulate a propagating wave correctly at least 250 time steps are needed per oscillation, as is advices in the ComFLOW manual [10].
- The second parameter is the Courant-Friedrichs-Lewy (CFL) condition. The formulation of the CFL condition is give in equation 2.2. It states that the velocity at the inflow of the cell x the time step cannot be greater than the width of the cell. Two separate CFL limits can be set, one for the flow and one for the waves. In both cases the CFL is set to $0.5 \leq CFL \leq 0.9$, this is based on advice given by the ComFLOW developers. If the CFL passes the upper limit, the time step is reduced by a factor of 2. If the CFL is lower than the lower limit for 10 consecutive time steps, the time step is increased by a factor of 2.

$$CFL = \frac{\Delta t|u|}{\Delta x} \leq 1 \tag{2.2}$$

Convection Scheme

For the discretization of the momentum equation and specifically for the convection, two main discretization schemes can be selected. A first-order upwind/second-order central scheme (b2) or a second-order upwind scheme (b3). These schemes are represented by equation 2.3 and equation 2.4 respectively. While using the first-order upwind scheme, artificial diffusion can be added to stabilize the discretization. The artificial diffusion can be set by a coefficient or as a changing parameter with a limiter. The different combinations and thus different convective schemes are shown in table 2.7.

$$u_x^+ = \frac{u_{i+1}^n - u_i^n}{\Delta x} \tag{2.3}$$

$$u_x^+ = \frac{-u_{i+2}^n + 4u_{i+1}^n + 3u_i^n}{2\Delta x} \tag{2.4}$$

Table 2.7: Convection Schemes

Scheme	Order of accuracy	Stability	Scheme	Artificial Diffusion	Limiter
1-st order upwind	1	++	b2	1.0	false
2nd-order upwind	2	+	b3	between 0.0 and 1.0	false
2nd-order central	2	+/-	b2	0.0	false
limited central	between 1 and 2	+	b2	0.0	true
partially upwind	1	+/-	b2	between 0.0 and 1.0	true

In figure C.5 all the different convective schemes are shown for one simulation. A first-order upwind discretization yields the most stable solution. This is the main reason why the first-order upwind is used as the discretization scheme for the convective terms. This scheme has a large artificial diffusion to keep the simulation stable. This can be a problem as too much energy is lost in the domain. If the time trace is analysed, it can be concluded that this loss of energy is not significant for this simulation. The wave amplitude does not change significant when the waves are propagating trough the domain.

Diffusion
Two discretization schemes for diffusion can be applied in ComFLOW, the manuals advices to use the LS-STAG scheme. This will yield a more accurate approximation of viscous stresses in cells at the edge of the floating geometry.

Turbulence Model
As this research is focused on large-scale phenomena such as wave loads and internal loads, turbulence will not have a significant influence on the hydrodynamic response, so that no turbulence model is used in the simulations.

3

CFD Verification

This chapter shows the precautions taken to obtain a sufficiently converged grid, the balance between the computational time and convergence of the solutions are optimized. The chapter is split into two parts; the different parts of the grid study is shown in section 3.1, after which the final grid is elaborated in section 3.2.

3.1. Grid Study

While using a CFD solver, a correct grid needs to be selected. When more grid cells are used, the simulation will represent reality more closely, at the expense of a longer calculation time. To obtain a balance between 'correct' solution and practical calculation time, the user should know which parameters/phenomena he is after. In this study the main targets are the wave loads, motions and internal loads on a semi-submersible. These are large-scale phenomena, so a coarse grid might be able to predict the outcome correctly. To test whether the grid results in sufficiently converged results, a number of tests are conducted. First, the waves that ComFLOW generates are analysed on different grid sizes and compared with the desired wave period and wave height. Next, two tests are conducted to check whether ComFLOW is able to simulate the hydrostatic forces. This is done for both heave and pitch. Finally, the complete grid is analysed, with a fixed and a free-floating semi-submersible.

3.1.1. Cells per Wave

For the simulation of the wave three different tests are conducted.

1. Amount of cells in x-direction per wave length
2. Amount of cells in z-direction per wave height
3. Amount of cells in combined x-z direction with fixed aspect ratio

The first part of the grid study is conducted on the propagation of waves. An incorrect grid size can cause dissipation of energy, which will mean a wave height that will degrade while propagating through the computational domain. To reduce the computational time, these simulations are conducted in 2D. First, the number of cells per wave length is analysed, engineering guidelines generally recommend 60 cells per wave length. This grid together with one coarser grid and two finer grids are analysed. In figure 3.1 a time trace is plotted from the two wave probes measuring the wave height. The first one shows the wave amplitude at the inflow boundary of the domain. The second one gives the wave amplitude at the centre of the domain. In table C.1 and 3.1 shows the absolute and relative differences between the specified input values and the simulated values as seen in the ComFLOW simulation.

For each of the different grids the waves at the inflow boundary show show the correct result. Only the coarsest grid with 30 cells in each wave length shows a step-like behaviour. The period of the waves is correctly simulated at each grid size and the wave amplitude at each grid is approximately 6% to high with respect to the specified wave amplitude input.

If the wave is analysed in the middle of the domain, it can be clearly seen that the coarse grid in particular has a large loss of amplitude and a decrease in wave period. For the other three grids, it can

be concluded that a decreasing cell size will cause a decrease in dissipation. The change of period is hardly influenced and changes are within 0.3%. The wave amplitude in the middle of the domain is in good agreement for the tree finer grids and the specified wave amplitude. Only the most coarse grid has a large deviation of almost -50% Only the Finally, it can be concluded that the minimum amount of cells in each wave length should indeed be 60.

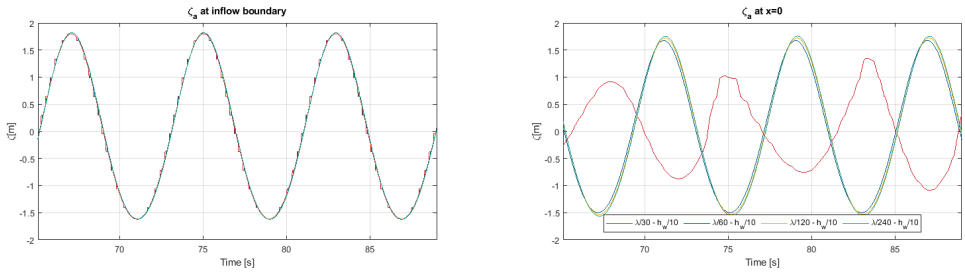

Figure 3.1: Grid study: Varying number of cells in each wavelength

Table 3.1: Relative Differences for different number of cells per wavelength

	Input vs. BC		Input vs Mid		Dissipation BC vs Mid	
	$Period[\%]$	$\zeta_a[\%]$	$Period[\%]$	$\zeta_a[\%]$	$Period[\%]$	$\zeta_a[\%]$
$\lambda/30\ h_w/10$	-0.01	+5.07	-4.16	-48.51	-1.24	-53.11
$\lambda/60\ h_w/10$	0.00	+6.22	-0.23	-0.64	-0.29	-7.33
$\lambda/120\ h_w/10$	0.00	+6.27	-0.13	+1.45	-0.16	-5.19
$\lambda/240\ h_w/10$	0.00	+6.21	-0.11	+3.09	-0.13	-3.36

In the second part, the number of cells per wave height is analysed. A typical engineering guideline is to use at least 10 cells. Four grids are analysed from 4 to 16 cells per wave height. In figure 3.2 the time traces of the above-mentioned wave probes are shown and in tables C.2 and 3.2 the absolute and relative differences, respectively, are shown. When a more detailed analysis is made, it appears that the inflow period is exactly as required The wave amplitude at the inflow boundary is just as in the previous section approx. 6% too high. For all grids the dissipation of wave height until the middle of the domain is approximately 5%. It appears that the increase in cells per wave height has a limited influence on the outcome and thus it suffices to use a coarse grid. Therefore a number of 8 cells is preferred and in some cases 4 cells may be enough.

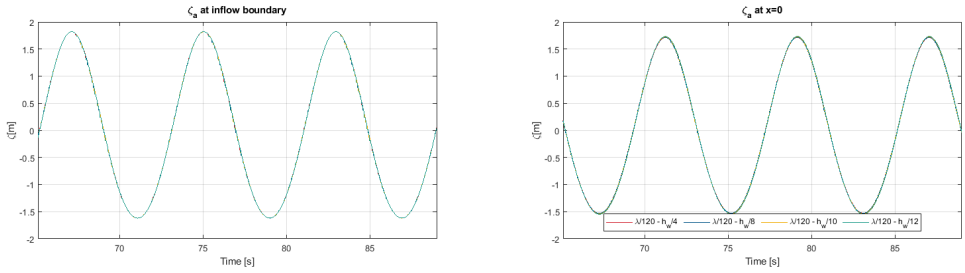

Figure 3.2: Grid study: Varying number of cells in each wave height

Table 3.2: Relative Differences for different number of cells per wave height

	Input vs. BC		Input vs Mid		Dissipation BC vs Mid	
	$Period[\%]$	$\zeta_a[\%]$	$Period[\%]$	$\zeta_a[\%]$	$Period[\%]$	$\zeta_a[\%]$
$\lambda/120\ h_w/4$	0.00	+6.27	-0.12	+1.10	-0.15	-5.58
$\lambda/120\ h_w/8$	0.00	+6.26	-0.13	+1.20	-0.16	-5.46
$\lambda/120\ h_w/12$	0.00	+6.27	-0.12	+1.70	-0.15	-4.91
$\lambda/120\ h_w/16$	0.00	+6.28	-0.11	+2.09	-0.14	-4.48

In the third and last step to determine which grid size is best suited to simulate the incoming waves correctly, different cell sizes with a fixed aspect ratio are analysed. In figure 3.3 the time traces of the above-mentioned wave probes are shown and in table C.3 and 3.3 the absolute and relative differences are shown. The input waves for all grids are again around 6% to high w.r.t. the specified wave amplitude and a decrease in cell size gives a decrease in dissipation. All grids results in the correct solution with no large deviation. The only thing that should be mentioned is a dissipation of 10% when the coarsest grid is used.

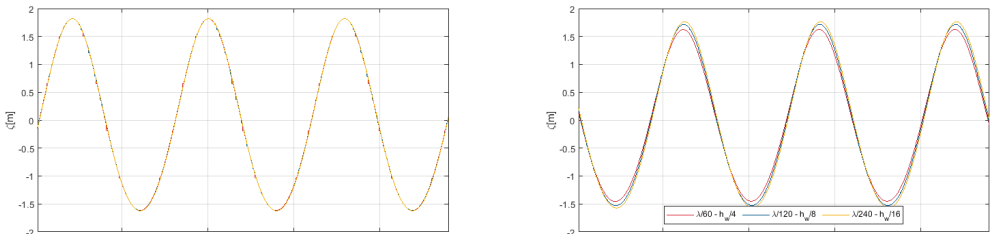

Figure 3.3: Grid study: Varying number of cells with fixed aspect ratio

Table 3.3: Relative Differences for different number of cells with a fixed aspect ratio

	Input vs. BC		Input vs Mid		Dissipation BC vs Mid	
	$Period[\%]$	$\zeta_a[\%]$	$Period[\%]$	$\zeta_a[\%]$	$Period[\%]$	$\zeta_a[\%]$
$\lambda/60\ h_w/4$	+0.01	+6.21	-0.18	-3.10	-0.15	-10.09
$\lambda/120\ h_w/8$	0.00	+6.26	-0.13	+1.20	-0.16	-5.49
$\lambda/240\ h_w/16$	0.00	+6.23	-0.08	+3.49	-0.14	-2.93

3.1.2. Hydrostatics - Heave

To analyse for which grid size the hydrostatic solution converged to an acceptable level. The submergence check is conducted to see whether the solutions of ComFLOW matches the analytic solution. Five different grids are analysed, the cell size varies between $2\ m - 1\ m - 0.5\ m - 0.33\ m - 0.25\ m$, each with an aspect ratio of 1. To solve the hydrostatics at multiple drafts numerous simulations need to be ran. To quickly check the hydrostatic response at different draft the semi-submersible is submerged with a low constant velocity. A constant velocity of $w = -0.1\ m/s$. This velocity is so low that the hydrodynamic solution is insignificant w.r.t. hydrostatic solution.

As the waterline of the semi-submersible does not change after a draft of $T = 7.5\ m$, the relation between draft and buoyancy force should be linear. In figure 3.4a the buoyancy force is shown for a draft of $T = 11\ m$ to $T = 15.5\ m$. Although the data for all grids shows a close correlation with the analytic solution, a repetitive pattern can be recognized. This pattern is caused by the labelling of the cells in ComFLOW. As the draft of the semi-submersible increases, the semi will 'jump' from cell to cell; and a pressure peak is caused. A finer grid will have more of these peaks but will have less amplitude. Next to these peaks a small osculation can be recognized in the data of the different grids. This is caused by waves that are radiated from the structure. As the semi-submersible has a constant velocity some waves are radiated. If this velocity is decreased the wave-like pattern would decrease; however, this will cause an increase in computational time.

Comparing the responses obtained with the different grids to the analytic solution, it is observed all grids have a slightly higher buoyancy force. This can be declared by the hydrodynamic force due to the

constant downward velocity of the semi-submersible. All grids are within a 1% error margin, only the peaks show larger differences which can increase to 10% for the 2m cells but quickly reduce to less than 3% for the 1m cell. For the other three grids this difference is just below 2%. This indicates that the cell size should be at least 1 meter to obtain a solution without pressure peaks that are too high.

3.1.3. Hydrostatics - Pitch

An inclination test of the semi-submersible is performed to check which grid size is needed to obtain the restorative moment. These tests have been conducted on three different grids; the cell size varied between $2\ m\ -\ 1\ m\ -\ 0.5\ m$ also with a fixed aspect ratio of 1. The resulted are to the hydrostatic restoring moment with $GM = 6.04\ m$, as results form the mass properties in table 2.2.

Both the ComFLOW solutions and the analytic solution for the restoring moment are shown in figure 3.4b. The agreement between the analytical solution and response from ComFLOW is acceptable expected for the coarsest grid; however, all of them have a slightly lower gradient. The coarsest grid shows an oscillation around the analytic solution. These oscillations are smaller for the grid with 1m cells and even smaller for the finest grid. The optimal grid to use is the grid with cells of 1m in all directions, since this grid has limited oscillations around the analytic solution and the computational time is shorter compared to the finest grid. The results are deemed sufficiently converged at this grid size.

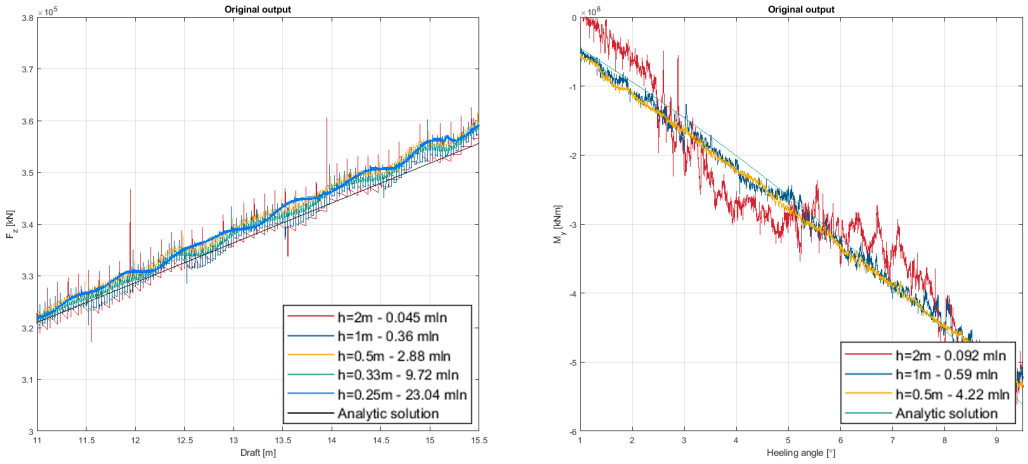

(a) Buoyancy test (b) Inclination test

Figure 3.4: Grid Study on calculation of hydrostatic forces in still water.

3.1.4. Full Domain

The next and final step in the grid study is to analyse the behaviour of the complete simulation on different grid sizes. The three different grids that are compared are shown in table 3.4, including the cell size at its finest level and the total number of cells in the domain. In figure 3.5 the wave loads on the captive semi-submersible are shown. Grid 2 is not able to simulate the waves correctly; this can be seen on the wave probe before the model. The mean water level in the domain rises, which also causes the heave force to have an increasing mean. No large deviations are visible between the responses and wave shape obtained for grid 1 and grid 05. This means grid 1 is the most optimal with respect to accuracy and computational time, grid 05 would have a slightly higher accuracy but the computational time would increase by a factor 8.

Table 3.4: Number of cells for different grid refinements

Grid	Δ [m]	N cells
Grid 2	2.0	303 840
Grid 1	1.0	1 582 866
Grid 05	0.5	10 183 056

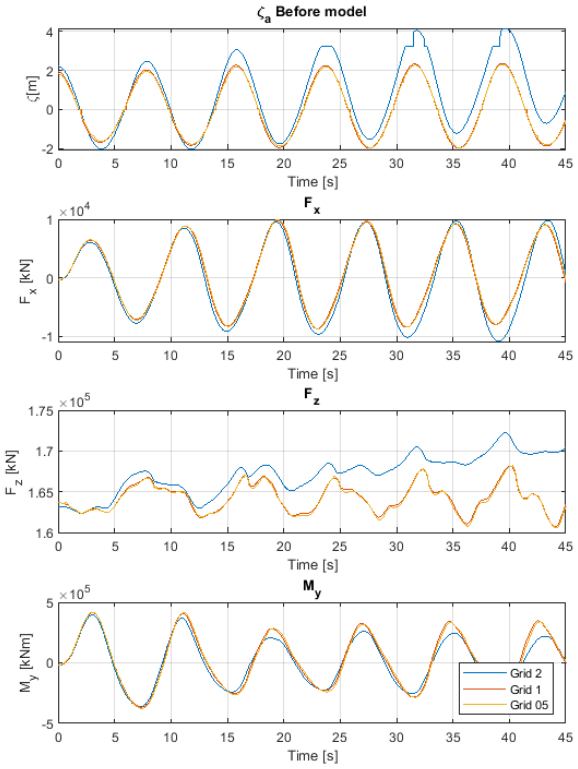

Figure 3.5: Grid Study on full domain. Wave amplitude, surge force, heave force and pitching moment are shown for multiple grid sizes.

3.2. Final Grid

To conclude the grid study and this chapter on the verification of the CFD solver, the findings of the gird study are shown and the final grid, that is used in the further parts of this research, is presented.

To conclude the grid study the following 3 rules should be obeyed:

- 60 cells in longitudinal x direction per wavelength
- 8 cells in vertical z direction per wave height
- Minimal cell size of $\Delta = 1\ m$

One major remark can be made on the conclusions with respect to the number of cells per wave height and per wavelength. At the time of the grid study, it was unknown that the number of integration point per cell has a large influence on the propagation of the waves. As more integration point per cell is defined, the water free-surface can be better represented and reconstructed more accurately. This means the number of cells in a vertical direction can be drastically reduced if the number of integration points is increased. This is preferred as it reduces the computational time. The number of integration points is increased with a factor of 4, meaning ComFLOW is able to simulate the waves with only two cells per wave height.

The main points of interest are the free-surface, the flow above the pontoons and the fluid-structure interface. These are at the highest refinement layer. Also in the case of free-floating simulations. The finest cells in the domain have a size of $0.78\ m$ in each direction and thus an aspect ratio of 1. To optimize the computational time, 4 refinements layers have been applied. Each with a refinement factor of 2. A cut-out is made in between the pontoon of the semi-submersible to further decrease the number of cells and reduce the computational time.

An example of the grid used in further simulations is shown in figure 3.6. This is a grid for the simulation with the semi-submersible at a draft of $T = 25\ m$. Combining the symmetry plane, refinement layers and refinement layer cut out, the number of cells is reduced to approximately 300 000 cells.

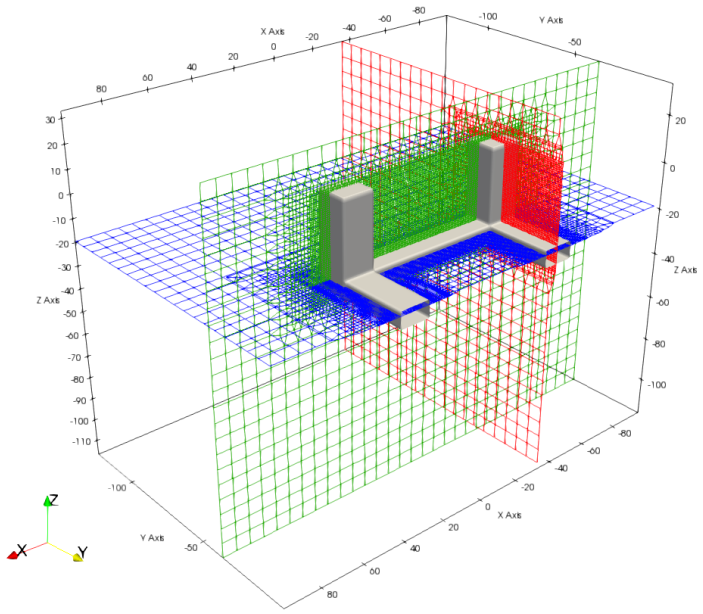

Figure 3.6: Final grid for a draft of $T = 25\ m$

4

Comparison

In this chapter the results of the three different methods to determine the wave loads, motions and internal loads of a semi-submersible are discussed. The model tests are used as a basis and are compared against results from conventional tools(based on linear theory) and results from CFD calculations, which should capture the non-linear effects. This chapter answers the first research question:

How do model-tests, linear diffraction and CFD solvers compare?.

In section 4.1 the initial finding from the model test data are discussed. In section 4.2 the wave loads, motions and internal loads obtained with the linear diffraction solver WAMIT are discussed and compared to the model test results. The core of this chapter in section 4.3, in which the three different methods are compared and analysed. Limitations of different methods are assessed and the differences are discussed. In section 4.4 the effects that cause the non-linear response are assessed. Based upon these sections, conclusions are provided in section 4.5.

4.1. Model tests

After the low frequency waves are removed, the model test data can be analysed. The wave loads obtained with the captive tests are first analysed and the effects of a reducing draft and the effects of a changing wave amplitude are assessed; both for a 'linear' deep draft at $T = 25\ m$ and the shallowest draft of $T = 11.5\ m$. This shallow draft is chosen as it is expected to show the highest significance of the higher harmonic response. For the free-floating model tests the motions are analysed for a change in draft. For each of the time traces visible in this section, a FFT spectrum has been made. In this section the frequency spectra are normalized. Instead of looking at the total energy present at a frequency range, the contribution in the total response of the different higher harmonic frequencies is analysed. This procedure shows the differences in distribution of energy more clearly.

4.1.1. Wave Loads

Change of Draft

The change in response that occurs due to a change in draft is analysed at a wave frequency of $\omega = 0.2\ rad/s$. The draft is changed from the deepest draft at $T = 25\ m$ to the shallowest draft of $T = 11.5\ m$. In figure 4.1 the incoming wave, horizontal force, vertical force and pitching moment are shown. The input waves have the same amplitude of $\zeta_a = 2\ m$ and in general no large deviations are visible for the incoming wave. The largest draft gives the largest surge force, but reducing de draft will not give a reduction of surge force for each step, as the surge force increases from $T = 17.5\ m$ to $T = 14.5\ m$. A change in draft will also cause a change in natural periods; these shift towards the wave frequency and the response amplitude increases accordingly.

In case of the three deepest drafts, almost no differences are present in the heaving force. Only for the most shallow draft some change is visible when the heave force is at its minimum. At this point a wave trough is passing the semi-submersible. At this point there is just 1.5m water above the pontoons, the water above the pontoon gets isolated from the rest of the wave and a small phase shift occurs.

If the free surface rises again, the flow of water above the pontoon is caught back into the flow of the wave and the force will merge with the heave force of the other drafts.

The pitching moment shows two distinctive groups. The two deepest drafts show the same response with almost the same amplitude. The response of the smaller drafts has a lower amplitude and more frequency components. This can also be seen in the response spectrum. The frequency spectrum of the smaller two drafts shows multiple peaks with higher frequencies. This means that the response of the wave loads is non-linear with respect to the incoming wave. For this semi-submersible, in waves with a frequency of $\omega = 0.2\ rad/s$ and a wave amplitude of $\zeta_a = 2\ m$ that draft is below $T = 17.5\ m$.

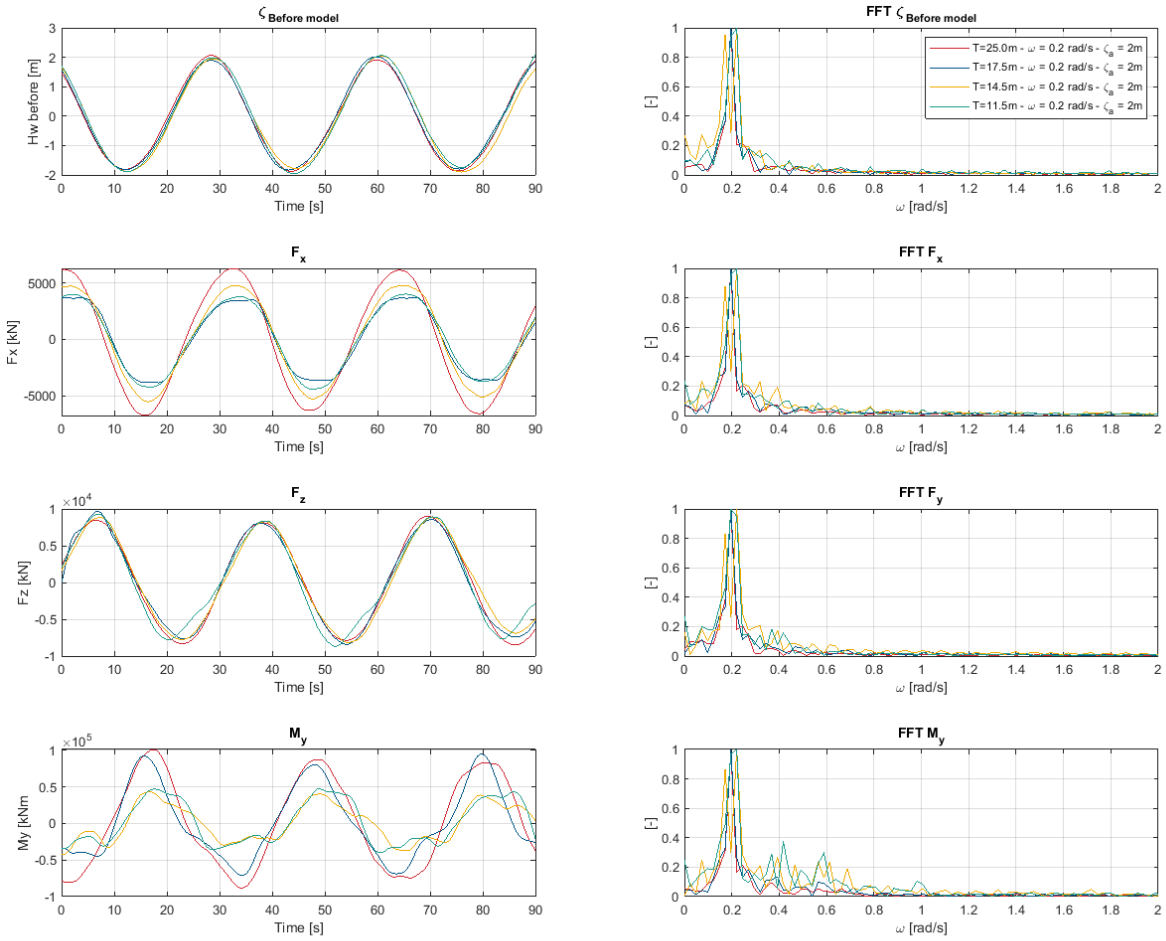

Figure 4.1: Model test data at $T = 25,\ 17.5,\ 14.5,\ 11.5\ m$ with $\omega = 0.2\ rad/s$, $\zeta_a = 2\ m$

Change of Wave Height

If the wave amplitude is increased, the clearance between the free surface and the top of the pontoon will decrease. In figure C.2 three runs are shown, each at a draft of $T = 25\ m$ with a wave frequency of $\omega = 0.4\ rad/s$. The wave amplitudes shown are $\zeta_a = 1,\ 2,\ 3\ m$. At this deep draft the response is linear with respect to the incoming wave. Only the heave force can be checked as the horizontal surge force is not correctly registered for a majority of the runs at $T = 25\ m$.

In case of the shallowest draft, $T = 11.5\ m$, linear scaling with the wave height is no longer valid, as can be seen in figure C.3. With a shallow draft the pontoons will get closer to the free surface, locally resulting in shallow water behaviour of waves. This means the linear relation is lost at a lower wave amplitude compared to a deep draft. A wave amplitude of $\zeta_a = 1\ m$ still shows this linear relation, but an increase to $\zeta_a = 2\ m$ already shows some non-linear response. This can clearly be seen by the pitching moment. In the time trace an increase in wave amplitude means the response does not show a linear relation. When the frequency spectra is analysed, the higher harmonic response frequencies

have increase in significance.

For a fully linear response with regard to the wave height, the normalized frequency spectra would show a single peak at the wave frequency. An increase in wave amplitude would not cause any change in the normalized frequency spectra. For this shallow draft the response at the higher harmonic frequencies of $\omega_2 = 0.8\ rad/s$ and $\omega_3 = 1.2\ rad/s$ is more significant at a larger wave height.

4.1.2. Motions

All free-floating tests were done at one wave amplitude of $\zeta_a = 2\ m$. This means only one frequency can be analysed for two different drafts and no variation in wave height can be analysed. The time traces of both wave probes and the hydrodynamic responses are shown in figure C.4. The response shows a linear relation with respect to the incoming wave. In case of the shallow draft, the amplitude of the motions is increased for all three motions because the wave frequency lies closer to the natural frequencies. The normalized frequency spectra for both drafts show almost the same behaviour,without the higher harmonic frequencies. This indicates a less significant contribution to the higher harmonic frequencies, as seen for the wave loads.

4.2. First order Potential Theory

The solution obtained with the linear diffraction solver WAMIT is compared with the model test data in this section. It will show the limitations and deviations of the hydrodynamic response calculated with a conventional method at an inconvenient draft.

4.2.1. Wave Loads

The wave load RAOs and corresponding phase differences are shown in figure 4.2, together with the force measurements in the model tests. For a draft of $T = 25\ m$ the surge force is not measured. This means the surge force can not be compared. The pitching moment is calculated based on the observed surge and heave force. The surge force is missing, meaning the pitch moment can not be calculated. This means for the captive wave load simulations at a draft of $T = 25\ m$ only the heave forces can be compared. This is not the case of the other 3 drafts and the three degrees of freedom can be compared.

The surge force at the lower frequencies ($\omega \leq 0.5\ rad/s$) shows in each model test situation a lower force compared to the surge force obtained by WAMIT. At frequencies $\omega > 0.6\ rad/s$, the differences become more profound.

For the heave response at $T = 11.5\ m$, the model tests with a different wave amplitude show a different amplitude (force divided by the corresponding wave amplitude). This means the amplitude of the response does not scale linear with the wave amplitude. At the deep draft of $T = 25\ m$, the response of the model test at different wave amplitudes results in the same RAO value, which means that in this situation the responses are linear, as expected. This linear situation is also in good correlation with the values obtained with the linear diffraction solver WAMIT.

The pitch moment response is correctly captured by the linear theory for $\omega < 0.4\ rad/s$. For $0.4 < \omega < 0.8\ rad/s$, the measured response deviates from the linear response, especially for the shallower drafts.

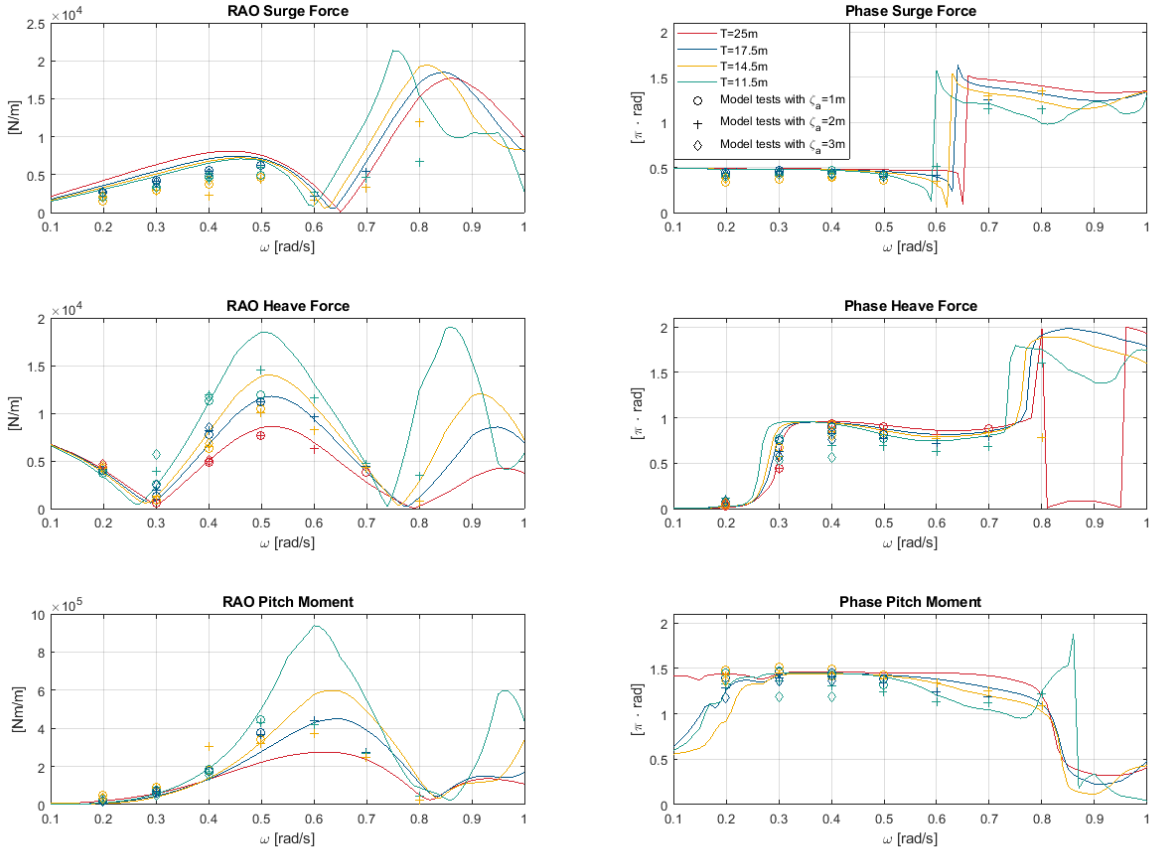

Figure 4.2: Wave Force RAOs and corresponding phase. The continues line represent the solution obtained by WAMIT, the symbols represent the model tests results at different wave amplitudes.

4.2.2. Motions

In figure 4.3 the motion RAOs and corresponding phases are plotted for the four separate drafts. The model test data are added, for the tested frequencies.

The motion response obtained by model tests and linear calculations are in good agreement. For heave and pitch, the model test points coincide with the linear calculation for both the amplitude, as well as the phase shift. A slight discrepancy is observed for the low-frequency surge response, which is attributed to the soft mooring present in the model tests (resulting in a higher response near the natural frequency of this mooring), but which was not included in the calculations.

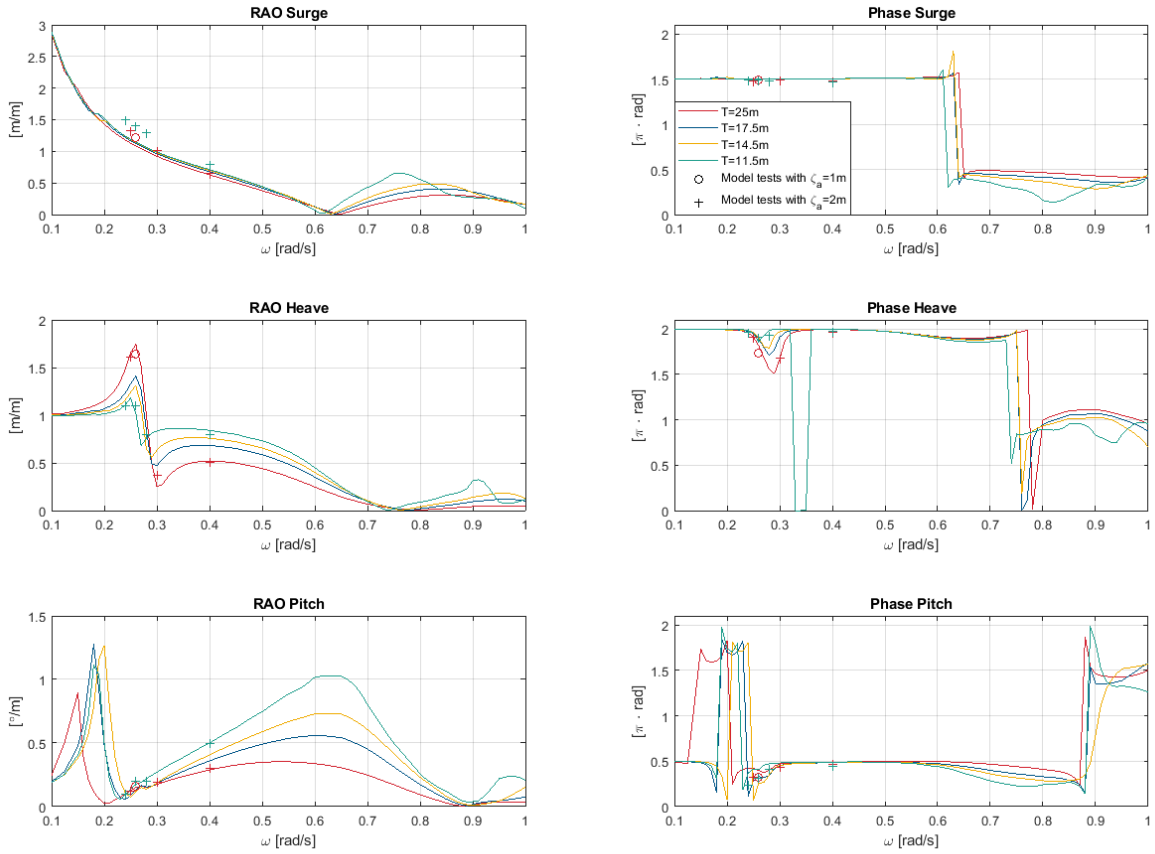

Figure 4.3: Motion RAOs and corresponding phase. The continues line represent the solution obtained by WAMIT, the markers represent the model tests results at different wave amplitudes.

4.2.3. Internal Loads

In Dynload, integration boxes can be specified to obtain internal loads acting on a specific part of the structure. For this research an integration box has been defined around the forward and aft part of the semi-submersible, splitting the semi-submersible in two halves.

In figure 4.4 the internal loads on the aft part of the semi-submersible are shown. Unfortunately, no model test data are available on the internal loads and thus a comparison between model tests and the linear solution is not available. In the final part of this chapter 4.3 these internal loads are compared and analysed with the internal loads obtained with the CFD solver ComFLOW.

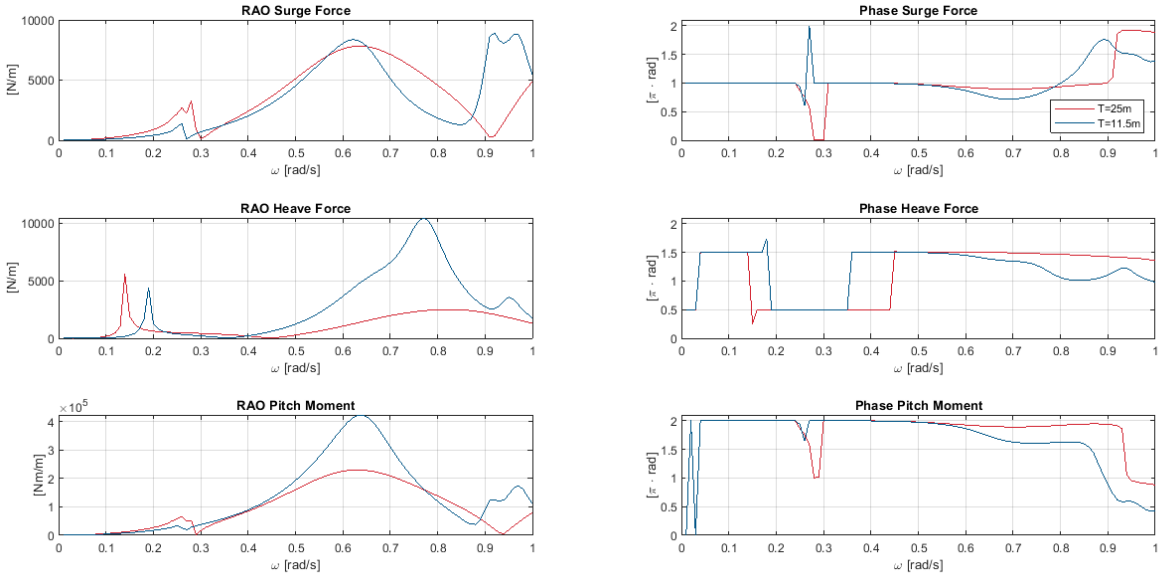

Figure 4.4: Internal Load RAOs and corresponding phase on Aft part of Semi-Submersible for two drafts, obtained by Dynload

4.3. Computational Fluid Dynamics

In this section the results from the model tests, the linear potential solver and the CFD solver are compared. This comparison is made for the wave loads, motions and internal loads. The main objective of this section is to analyses the differences between the three methods. At the same time it is checked whether ComFLOW is better able to solve these responses compared to the results from the linear potential solver. This is not always the case, as is shown in the following paragraphs. For each of the following paragraphs the conditions that cause a linear response are compared first; after which the conditions that show a non-linear response are compared and analysed.

4.3.1. Waveloads

First, the wave loads acting on a captive semi-submersible are analysed. In paragraph 4.1, the analysis of the model tests, it is shown that a deep draft gives a linear wave-load response with regard to the incoming wave. It is expected that both the linear potential solver and the CFD solver ComFLOW are able to solve the correct wave loads for this deep draft. Figure 4.5 shows a comparison between the three methods used to solve the wave forces and moments at the deep draft. At this draft the response of all methods shows a first-order response and no responses of a higher harmonic frequency are present in the solution. This can also be seen in all of the frequency spectra of the responses. Only a distinctive peak is present at the wave frequency. The surge force amplitude in case of the model tests is slightly higher compared to the other two, no phase shift exists. The heave force shows good agreement for all three methods. In the case of the pitching moment, the model tests has the largest response amplitude. The linear calculations and CFD results show a similar, but slightly lower, response amplitude. No large deviations are visible in these comparisons. Both the linear potential solver and the fully non-linear CFD solver are able to solve the wave-load response for the deep draft.

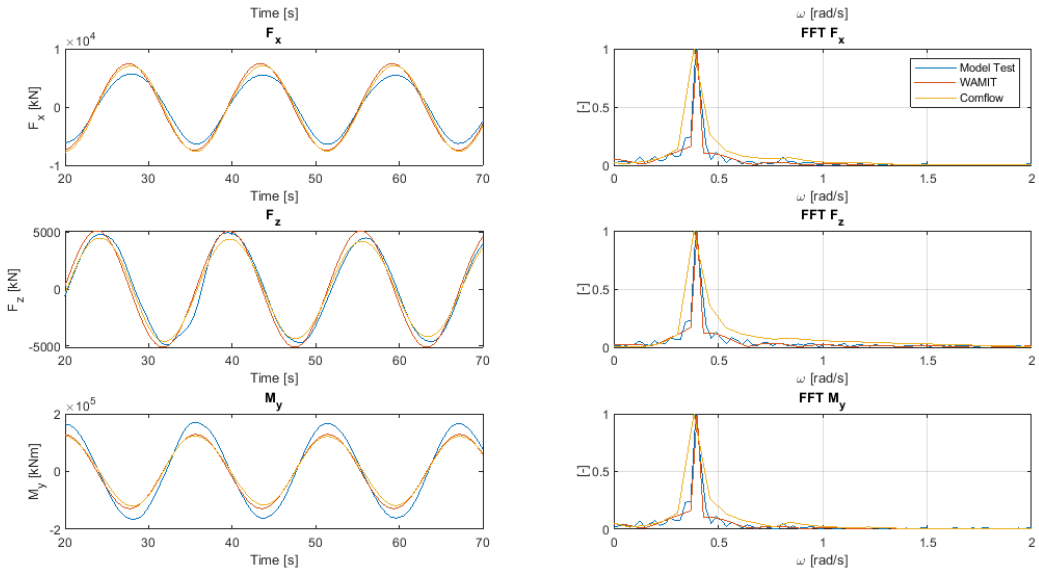

Figure 4.5: Wave loads at $T = 25\ m$, $\omega = 0.4\ rad/s$ and $\zeta_a = 0.9\ m$

When the same wave condition is compared at a draft of $T = 11.5\ m$, discrepancies show up. The linear relation between wave height and response at $\omega = 0.4\ rad/s$ is no longer valid from $\zeta_a = 2.9\ m$. The responses of the three methods are shown in figure 4.6. While the waves travelling alongside the model are almost the same, the amplitude of the surge force differs. The model tests show the lowest response, the linear method the highest response and the CFD response is in between. Also, a the time traces show a tilting behaviour in the model test and CFD data. This means the peak of the response will shift forwards within its oscillation. As this is a higher order phenomenon, it is not seen in the linear solution but is also present in the frequency spectrum of the surge response. At the second harmonic of the wave frequency a peak is visible. This tilting of the time trace is also visible for the heave force. The amplitude of the heave force is still in good agreement. In case of the pitching

moment, the response shows a non-linear response for the model test data and CFD data. This is substantiated when the response is compared in the frequency domain. Three peaks are visible in the response of the model test and ComFLOW. These peaks coincide with the second and third harmonic wave frequency. When the wave height is decreased to $\zeta_a = 0.9\ m$ and $\zeta_a = 1.9\ m$, the conclusions on the surge and heave response are confirmed but less obvious. This is shown in figures C.7 and C.8. Both figures show almost the same second and third harmonic response. If the wave height is increased, an increasing phase shift occurs for the surge and heave force. The linear potential solver will keep showing a linear/first-order response.

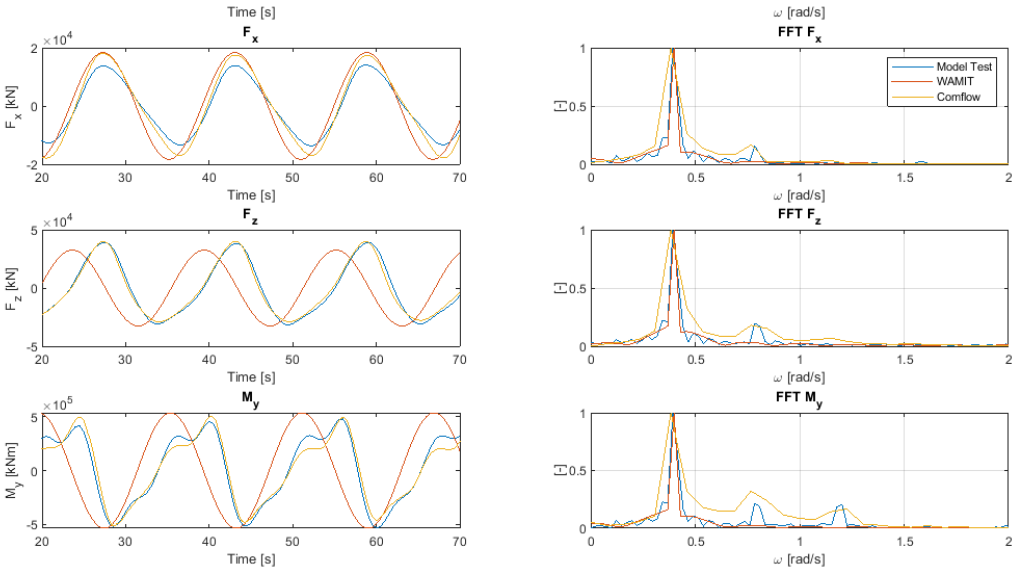

Figure 4.6: Wave loads at $T = 11.5\ m$, $\omega = 0.4\ rad/s$ and $\zeta_a = 2.9\ m$

Figure C.10 shows the comparison at a lower wave frequency of $\omega = 0.3\ rad/s$. The surge force shows a similar tilted time trace. The peaks of the surge force of the model test seem to be capped from a certain force. The amplitude of all three methods remains in the same order. When the heave force is analysed, immediately stands out that the model tests and CFD response give a force amplitude that is twice2 as high compared to the linear method. The response at the higher order frequencies is captured by CFD in a correct way. The same thing happens with the pitching moment, the amplitude is underestimated by the linear calculation, and again CFD shows a good correlation with the model test data.

At a higher frequency $\omega = 0.6\ rad/s$, the heave force shows a more linear response while the surge force will show a response with a higher harmonic frequency; see figure C.11. The surge force is under-predicted by the linear calculation. The CFD solver shows a close fit with the model tests. Only the peak values are slightly lower in case of the CFD solver. This might be caused by the refraction of wave present in the model basin, which is identically simulated in the CFD solver. This can be seen in the wave height in the first plot. The pitching moments of the CFD and model tests are again in good agreement. This time the linear calculations give a large over-prediction of forces.

For all cases the surge force calculated with ComFLOW differed between +16.7% and +2.53% in model tests. The linear potential theory shows a large difference compared to model tests, -74.1% to +56.5%. The heave force calculated with ComFLOW had a difference between -14.6% and +11.9%, and the linear potential a difference between -71.3% and +33.2%. The largest difference of amplitude occurred at the pitching moment. ComFLOW had a difference between -30.2% and +27.3%, while linear potential had a difference between -50.8% and +114.3% with regard to the model tests. For each run the relative difference between the model test and ComFLOW is shown in table 4.1. The relative difference between model tests and linear potential solver is shown in table 4.2.

On the comparison of the wave load several remarks can be made. The CFD solver ComFLOW is able to capture the wave frequent response and also the higher harmonic responses. In all cases where the response consisted of the wave frequency and higher harmonics of the wave frequency, ComFlOW

shows the correct frequencies with an energy level close to the model tests. Especially in cases where the response consisted of higher harmonic frequencies, the response calculated with ComFLOW had a much better approximation compared to the linear potential solver. It also shows ComFLOW still has a maximum deviation of $\pm 27\%$ with model tests. The average deviation for the wave loads on a captive semi-submersible obtained with ComFLOW is $\pm 15.4\%$ larger than the model test solutions.

Table 4.1: Wave Load comparison differences in response amplitude: Model test and ComFLOW

Draft [m]	25	11.5				
ω[rad/s]	0.398	0.398	0.398	0.398	0.594	0.297
wave height [m]	1.93	1.85	3.77	5.76	4.50	5.42
Surge Force difference [%]	24	17	25	15	20	21
Heave Force difference [%]	3	-8	3	1	12	-15
Pitch Moment difference [%]	30	-23	-20	6	27	7

Table 4.2: Wave Load comparison differences in response amplitude: Modeltest and WAMIT

Draft [m]	25	11.5				
ω[rad/s]	0.398	0.398	0.398	0.398	0.594	0.297
wave height [m]	1.93	1.85	3.77	5.76	4.50	5.42
Surge Force difference [%]	36	28	40	32	-74	57
Heave Force difference [%]	3	-18	-18	-18	33	-71
Pitch Moment difference [%]	-23	-5	17	18	114	-51

4.3.2. Motions

The next step is to compare the motions of the semi-submersible. The CFD simulations are conducted with ComFLOW version C, the full version information is shown in Appendix E.3. For a deep draft the motions are shown in figure 4.7. The motion response should be linear with respect to the incoming wave at this deep draft, as concluded in the analysis of the model tests. This is also seen in the surge motion response calculated with ComFLOW. The amplitude of the surge response is in good agreement with the surge response as seen in model tests and in linear potential theory. When analysing the heave response of the semi-submersible a large difference can be observed. Besides the large difference in amplitude, multiple peaks are bserved in the heave response spectrum of the CFD simulation at harmonic frequencies. This should not occur in this linear case,only a peak at the wave frequency is expected.The pitch response also deviates from the expected response. The semi-submersible oscillates around a mean pitch angle of 0.5° and has a sharp non-physical change of direction around a pitching angle of 0.0°. This indicates ComFLOW is not able to solve the motions of the semi-submersible in a correct way.

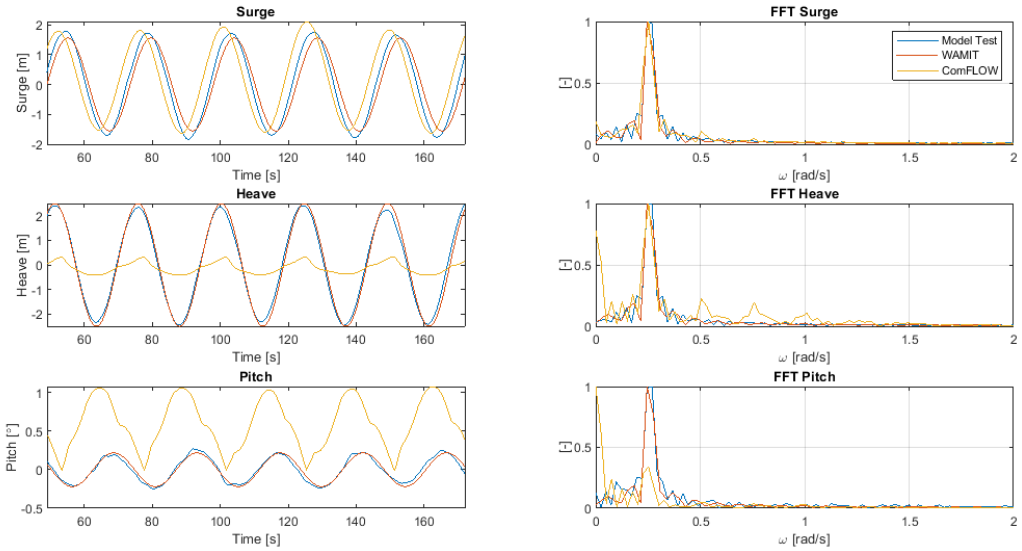

Figure 4.7: Motions at $T = 25\ m$, $\omega = 0.26\ rad/s$ and $\zeta_a = 1.4\ m$

When the motions of the semi-submersible at a shallow draft of $T = 11.5\ m$ are analysed, large differences become visible. The motion responses are expected to be rather linear, as explained in section 4.1.2. Only in case of a wave frequency near the natural frequency of the heaving motion does the pitch response show a higher harmonic response at twice the wave frequency. This can be seen in both figure C.13 and C.14. At this natural frequency more deviations of the ComFLOW solution are visible, while model tests and first-order potential theory show a good comparison. For the surge response there is a slight phase shift and an overestimation of the amplitude around 21%, for pitch the rotation is overestimated with almost 50%. The heaving amplitude is underestimated with 63%. When a different case is analysed at a wave frequency further away from the natural frequency of the heaving motion, the three methods of solving show slightly better agreement. This is shown in figure C.16. The differences in amplitude are still significant, as can be seen in table 4.3.

Table 4.3: Modeltest and ComFLOW

Draft [m]	25	11.5			
$\omega\ [rad/s]$	0.26	0.23	0.25	0.27	0.39
Surge difference [%]	7.31	33	24	32	46
Heave difference [%]	-86	-55	-64	-61	-20
Pitch difference [%]	302	554	67	38	-42

ComFLOW integrates the pressures along the hull to obtain the total forces and moments. These are used in solving the equation of motion (EoM). The fluid forces that are used in the EoM show a highly ragged response. This can be seen in figures C.17 to C.21. As the semi-submersible travels through the grid, each time the semi-submersible jumps to the next integration point, a force peak is generated. During the captive tests the semi-submersible does not move and these force peaks are therefore not present in the solution. The force peaks are so significant that they influence the motions of the semi-submersible. Due to the continuous motion of the semi, a large number of these pressure peaks are generated. It also means the peaks of multiple time steps can merge together and add up to a duration of more than a second. The sum total of all these peaks will become significant and will influence the motions of the semi-submersible. Due to this behaviour, it can be concluded that ComFLOW is not able to solve the motions of a semi-submersible in waves.

Due to these incorrect motions, a close collaboration with the developers of ComFLOW was achieved. Multiple attempts to improve the motion solution where made, with multiple versions of ComFLOW. Despite the effort motion solution which could be used in the further parts of this research were not achieved.

4.3.3. Internal Loads

In the previous paragraph it is shown that ComFLOW is not able to solve the motions of the semi-submersible. This has a consequence for the calculations of the internal loads. The internal loads are the sum of the wave loads, gravitational loads and inertia loads. Since the gravitational and inertia loads are caused by the motions and accelerations of the semi-submersible, these cannot be correctly predicted. The wave-load part of the internal loads is the pressure integration over a specific part of the semi-submersible. The pressures integrated in the free-floating simulations show a highly ragged response. This is used in the calculation of the internal loads and will lead to a highly ragged internal load response and to some extend the wave loads are also influenced by the incorrect motions of the floater. This means that the internal loads cannot be solved for the free-floating semi-submersible while using the free-floating simulations in ComFLOW.

To see whether it is still possible to obtain insight into the higher harmonic response of the internal loads, simulations on a captive semi-submersible are ran. These simulations are compared to the solution from the linear diffraction solver WAMIT, which means that only the wave-load parts of the internal loads are compared. The gravitational and inertia loads are left out of the consideration.

No model test data are available for the internal loads and direct comparison is not possible. However, the sum of the wave-load part of the forward and aft section is equal to the total wave loads. This can be compared with model tests to validate the obtained internal loads with ComFLOW. A second check can be made to compare the results of a 'linear' situation, as the use of Dynload.

The results of the first check are shown in figure 4.8 which shows the wave loads on a captive semi-submersible. This show a precise correlation, only for the pitching moment a small discrepancy is visible.

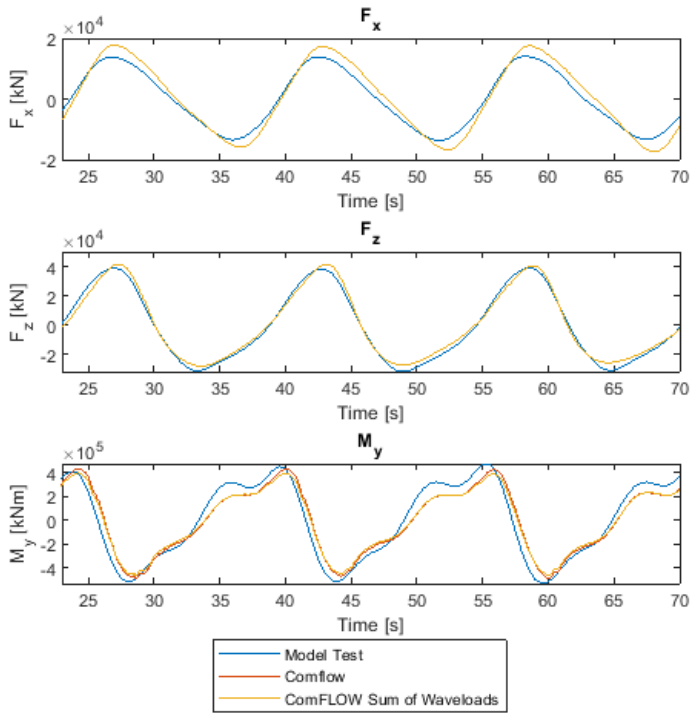

Figure 4.8: Comparison of Total Wave loads on Semi-Submersible, including the sum of the Wave load components of the Internal load calculations

Figure 4.9 shows the comparison between the internal loads on the aft section. The solutions obtained with Dynload and ComFLOW are both plotted. The situation simulated is at a deep draft of $T = 25\ m$ with a wave amplitude of $\zeta_a = 0.92\ m$. ComFLOW is able to solve the internal loads in good agreement with the linear Dynload solution. The surge force is off by -5%, the heave force difference is slightly higher at -14%, the pitching moment has a difference of -9%. These differences are in the same order of magnitude for the wave loads shown in figure 4.3.1. These two test show that the captive simulations conducted with ComFLOW to obtain an insight into the wave-load part of the internal loads

can be used. The relative differences with respect to the model tests are of the same magnitude of the total.

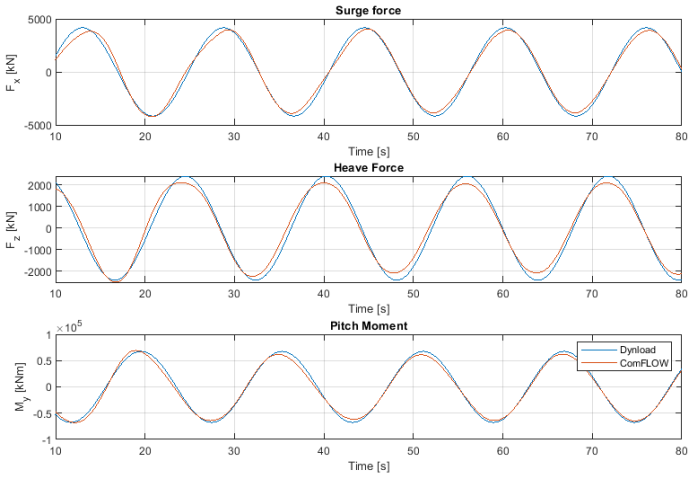

Figure 4.9: Internal loads of the aft section of the semi-submersible at $T = 11.5\ m$, $\omega = 0.39\ rad/s$ and $\zeta_a = 0.92\ m$

Finally, a comparison is made at an inconvenient draft. A draft of $T = 11.5\ m$ and a wave amplitude of $\zeta_a = 2.88m$ is selected, as it is the most shallow draft with the highest wave amplitude of the model tests. Figure 4.10 shows the internal load in this situation. There are large differences between the responses obtained with Dynload and ComFLOW. ComFLOW shows a response consisting of multiple higher harmonics. Dynload is not able to solve the response on these higher harmonic frequencies. This causes the time traces to show a different shape and large deviations in amplitude.

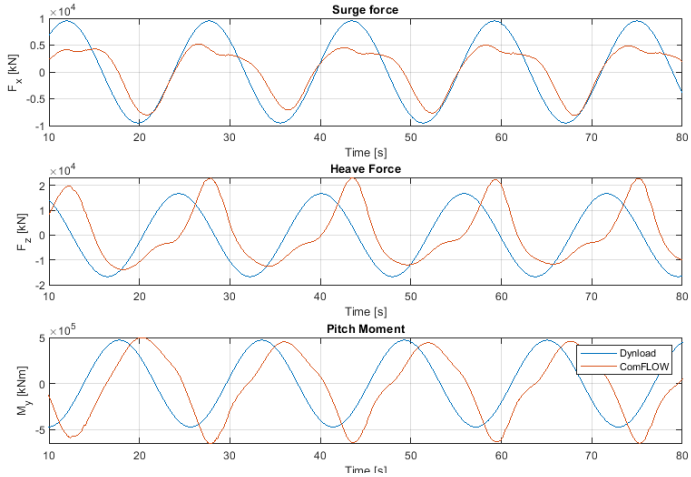

Figure 4.10: Internal loads of the aft section of the semi-submersible at $T = 11.5\ m$, $\omega = 0.39\ rad/s$ and $\zeta_a 2.88 =\ m$

4.4. Physical Cause

The sudden decrease in water depth above the pontoons of the semi-submersible will cause wave shoaling and at a certain height the waves will break. In the paper written by K. Iwata, K. Kawasaki and D. Kim (1996) [9], they investigate this wave deformation and breaking due to a submerged structure. They state that the harmonic wave frequencies start to gain energy above the submerged structure. This is caused by the transfer of energy from the fundamental wave frequency to the second and higher harmonic components. The transfer of energy is caused by the non-linear interaction between the wave and the structure. Since now higher harmonic waves are generated above the pontoon, the wave loads on the semi-submersible will also consist of these higher harmonic frequencies. As stated in the paper, most energy is transferred to the second harmonic wave frequency. This can be seen in the figure but also in most of the model tests, where a response occurred at the second harmonic wave frequency.

This is also confirmed by a test conducted at Delft University of Technology by J.A. Battjes and S. Beij (1991) [2]. The test analysed the spectral evolution of waves over a shoal, and an increase in wave non-linearity was seen when the waves travelled over the shoal.

A test has been conducted to see if these higher harmonic waves are present in the simulations in ComFLOW. For this small test the simulation with $\omega = 0.4\ rad/s$ and $\zeta_a = 2.9\ m$ is used. At three different locations the wave amplitude is measured: before the model, above the forward pontoon of the semi-submersible and above the aft pontoon of the semi-submersible. Figure 4.11 shows the time trace of these tests. Also, the frequency spectrum is calculated to see which frequencies are present in the solution. It becomes clear that in front of the model the wave only consist of wave frequent oscillations. Above the forward pontoon, the significance of the second harmonic wave frequency has increased. For the wave amplitude above the aft pontoon the third harmonic component increases. This indicates that the same physical phenomenon is occurring above the pontoons of the semi-submersible. If the same test is done at a deep draft, only waves at the wave frequency will occur and no waves at a higher harmonic are present. This also explains the linear response in these cases. The wave amplitude of the spectrum can be seen in figure C.23.

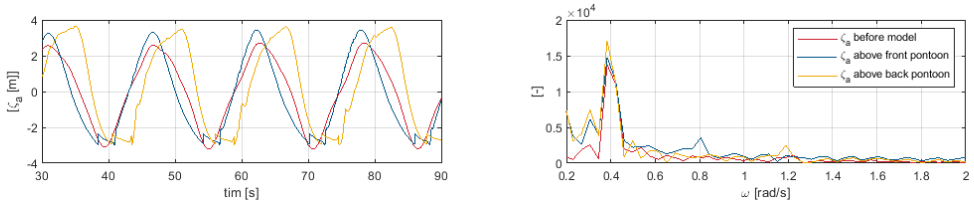

Figure 4.11: Wave amplitude on three locations

4.5. Conclusion

At the start of this chapter the question was asked:

"*How do model tests, linear diffraction and CFD solvers compare?*"

The answer will first be given in three separate parts which come together at the end of this section in one conclusion.

What is the magnitude of the deviations between the different calculation methods and are there significant differences?
In the 'linear' cases the potential solver and the CFD solver show good comparison with the model test for the captive wave loads. Cases which are in the inconvenient draft show higher harmonic wave frequencies, resulting in discrepancies between the responses. The linear potential solver is not able to capture the response at these frequencies. The response amplitude can be over-predicted and under-predicted by the linear potential solver, depending on the phase shift between the harmonic frequencies. This phase shift between the harmonic frequencies depends again on the initial wave frequency. ComFLOW is able to solve the wave-load response at the higher harmonics of the wave frequencies, resulting in a better approximation of the response amplitude. Still the deviations of response amplitude are $\pm 30\%$ with regard to. the model test, which is better compared to the $\pm 50\%$ deviation of the linear potential solver.

The motions of the free-floating semi-submersibles tell a different story, as no higher harmonics are observed in the motion response measured during the model tests; however, these motions are predicted to an acceptable level of accuracy by the potential solver. This is visible in all the test cases, also at the inconvenient draft. The responses ComFLOW calculates do not coincide with the model tests. Large deviations occur not only in response amplitudes but also in the frequency spectra, and are the result of incorrectly calculated wave loads by ComFLOW when simulating a free-floating body. These calculated wave loads are influenced by a large number of non-physical pressure peaks. As the wave loads are not correct, the resulting motions will not be correct either.

The incorrect motions and wave loads in case of a free-floating semi-submersible also cause an incorrect internal load solution. Yet, to obtain an insight into the higher harmonic behaviour of the internal loads at the inconvenient draft, simulations are ran to analyses ComFLOW's solution at the captive

tests. This means that only the wave-load parts of the complete internal loads are calculated. For the deep linear case, the internal load response shows good comparison with the solution based on the linear potential theory. At the inconvenient draft large differences between the response obtained with Dynload and ComFLOW are seen. ComFLOW shows a response consisting of multiple higher harmonics. Dynload is not able to solve the response on these higher harmonic frequencies.

What is the physical explanation of these differences?
There is one main physical explanation of these differences; the occurrence of higher harmonic wave frequencies above the pontoons. Due to a rapid change in water depth, energy from the wave frequency is transferred to the higher harmonic wave frequencies. This will cause waves on a higher harmonic wave frequency on top of the pontoons. The force response on the semi-submersible will thus consist of the wave frequency and the higher harmonic wave frequencies. It depends on the phase shift between the wave frequency and the higher harmonic frequencies whether the forces on the structure are increased or decreased with regard to the linear solution.

Can ComFLOW be used to represent reality with high enough accuracy?
The answer to this question depends what is investigated. In case of wave loads on a captive semi-submersible, ComFLOW is able to simulate the surge response with a difference around $+20\%$ with regard to model tests. The heave force is more accurate with a difference of around $+10\%$. The pitching moment is least accurate with a difference of $\pm 30\%$. Although these differences are not negligible, the physics of the problem (i.e., the wave energy being transferred to higher harmonic frequencies) are well captured; this results in ComFLOW being significant more accurate than linear diffraction methods. ComFLOW is not able to simulate the motions of a free-floating semi-submersible correctly. There are many non-physical pressure peaks in the wave-load solution for a free-floating semi-submersible, so that the subsequent solving of the equation of motion yields incorrect results. This also means the internal loads of a free-floating semi-submersible cannot be calculated with ComFLOW, since they depend on both the wave loads and the motions. The internal loads for a captive semi-submersible can be calculated with reasonable accuracy, which is in the same order as the wave loads on a captive semi-submersible.

How do model-tests, linear diffraction and CFD solvers compare?
As there are higher harmonic wave frequencies present above the pontoon at the inconvenient draft, the wave forces on the semi-submersible cannot be scaled linear with regard to wave height. This means linear potential theory calculates an unphysical response with large deviations regarding the model tests response. The CFD solver ComFLOW is able to capture these responses over both the wave frequency range and higher harmonic frequencies. This means the solution of wave forces is in good agreement with model test. During free-floating tests in ComFLOW, the wave loads are dominated by non-physical pressure peaks. As the wave loads are incorrect, the motions also deviate strongly with the motions obtained in model tests, which therefore results in an incorrect solution of the internal loads.

5

Parameter Study

To obtain a better insight into the transient behaviour of the linear to fully non-linear response, a parameter study has been conducted for the internal loads of a semi-submersible at an inconvenient draft. This chapter elaborates on the parameter study that is conducted to check the effect of changes in wave amplitude and draft. Previous research only investigated the top zone of the inconvenient draft, as shown in table 1.1 and figure 1.1. This parameter study will broaden its limits and will investigate the other zones within the inconvenient draft. The main research question that is answered in this chapter is:

How does the higher harmonic response behave within the inconvenient draft?

Detailed attention is given to the effect on the higher harmonic response contribution by a change in wave amplitude and draft throughout the inconvenient draft; the magnitude of the response on the higher harmonic frequencies and the limits at which the response on these higher harmonic frequencies becomes significant and will change the outcome. All are linked to the influence on the internal loads.

As ComFLOW is not able to solve the motions of the semi-submersible, the parameter study is conducted on a captive model. This has multiple consequences. The diffraction problem is exaggerated, since the relative velocity between the water particles and the semi-submersible is of greater magnitude.

The radiation problem is not solved because there are no motions of the semi-submersible. The internal loads consist of the gravitational loads, inertia loads and wave loads. The gravitational and inertia loads both depend on the motions of the semi-submersible. The motions will not be solved, and thus only the wave-load part of the internal loads can be solved. This is the part where the higher harmonic contribution of the response is most significant.

During the captive parameter study, the close collaboration with the developers of ComFLOW was still ongoing. The intention with this captive parameter study was to combine it later with free-floating simulations. The result from the captive simulations could be linked to the results of the free-floating simulations. Unfortunately, the free-floating simulations within ComFLOW did not provided the desired results at the end of this study and only the captive simulations could be conducted and analysed.

In the first section, the methodology of the parameter study is explained. It is clarified which situations are simulated and why these situations are selected. In the second section, the results of the parameter study are discussed. In the final section, conclusions are drawn and the research questions are answered.

5.1. Methodology

In this section the selection of conditions is explained. Time wise, it is not feasible to simulate all possible situations. Certain ranges need to be set up and boundaries should be set to obtain a good understanding within an acceptable time span. The methodology is split up into two parts: first, the range at which the draft is tested is discussed, followed by the selection of the range of simulated wave amplitudes. No change in wave period is assessed, since this would significantly increase the number of runs and the required computational time.

5.1.1. Draft

The draft of the semi-submersible is varied from a deep draft of 25 meter to a exaggerated transit draft of 5.5 meters. In this way all the zones of the inconvenient draft are tested. The step size at which the draft is changed is not uniform. The 'linear'deep drafts are of less interest compared to the different zones in the inconvenient draft. This means the step size is larger at the deeper drafts and smaller at the shallow inconvenient drafts. For the transition zone around the top of the pontoon at $T = 7.5\ m$, a step size of $\Delta T = 1\ m$ is used, while for the deeper drafts a step size of $\Delta T = 3\ m$ up to $\Delta T = 4.5\ m$ is used. All drafts tested are shown in table 5.1.

5.1.2. Wave Amplitude

The range at which the wave amplitude can be varied is limited by two physical boundaries. The maximum wave amplitude is limited by the draft of the semi-submersible. As the semi-submersible is held captive in the waves, wave amplitudes larger than the draft of the semi-submersible will cause the bottom to fall dry. This will cause all kinds of different phenomena, such as slamming. For the simulations at a deeper draft, small wave amplitudes are not of interest since all the responses are linear. To minimize the number of 'linear' runs, the waves are simulated from $\zeta_a = 2m$ up to $\zeta_a = 10\ m$ at the deeper drafts. With the exception of $T = 25\ m$, as multiple linear simulations are needed to obtain a clear picture of the limits of the inconvenient draft. At the inconvenient draft the step size is reduced to $\Delta\zeta_a = 1\ m$. Waves from $\zeta_a = 1\ m$ up to $\zeta_a = 8\ m$ are tested. The wave frequency will not be changed as the effects of a change in wave frequency can be predicted beforehand. The wave frequency used in this parameter study is fixed to $\omega = 0.4\ rad/s$.

Draft [m]	ζ_a [m]
25.0	0.5-1-1.5-2-4-6-8-10
21.5	2-4-6-8-10
17.5	2-4-6-8-10
14.5	2-4-6-8-10
11.5	2-4-6-8-10
9.5	1-2-3-4-5-6-8
8.5	1-2-3-4-5-6
7.5	1-2-3-4-5-6
6.5	1-2-3-4-5
5.5	1-2-3-4-5

Table 5.1: Simulation Matrix, all simulations are a wave frequency of $\omega = 0.4\ rad/s$

The Ursell number can be calculated for the water column above the pontoon to check which kind of waves are present. This will give a limit at which the wave above the pontoon can not be linear any more and energy is transferred to waves at a higher harmonic frequency. An increase in wave frequency will yield a shorter wave. This will mean a lower Ursell number. As a consequence the waves can obtain higher wave amplitudes or shallower drafts before the linear relation is lost. This also means waves with a low frequency are influenced by the higher harmonic frequencies, even for small wave amplitudes or deep drafts.

5.2. Results

The results of the parameter study are analysed in two ways. First, the time traces and frequency spectra are analysed. This is shown in the first section. Next, a general remark is made on the presence of standing waves and how these standing waves will influence the outcome. The main part of this section concerns the analyses of the contribution of the first four harmonic frequencies. For each of the 5 zones within the inconvenient draft the contribution of the higher harmonics is analysed. At each situation the total wave-load response is discussed, as well as the wave loads on the forward and aft of the semi-submersible. This gives an indication which sections experience a higher harmonic loading and if the significance of the higher harmonics is also visible in the wave-loads part of the internal loads.

5.2.1. Time Traces

The time traces of the forces and the moment give a good indication of the physical phenomena that cause the higher harmonic responses, since it becomes clear in which part of the wave oscillation the changes occur regarding the linear response. At the deep draft with small wave amplitudes the responses show a linear response. Increasing the wave amplitude will lead to a tilting in the time traces of the surge and heave force. This tilting means the time trace of the force will show a different gradient at an increase in force versus the decrease in force. In general the surge force will have a negative tilt, which means that the increase in force has a higher gradient compared to the decrease in force. However, the heave force shows a positive tilt, which means that the decrease in force has a larger gradient compared to the increase in force. This tilting is the first indication that the linear correlation between the incoming wave and the response is broken, and something that is also seen in the model tests in section 4.1.

When the wave amplitude is increased or the draft is decreased, the higher harmonic components become more and more significant; until the waves start to break over the pontoons and the pontoons start to penetrate the free surface. For example, in the situation of a draft of $T = 9.5\ m$ and a wave amplitude of $\zeta_a = 3\ m$. In figure 5.1 the positive surge force shows the same response as a linear response, whereas the negative surge forces are capped; this is caused by the breaking of waves. As the orbital motion of the water particles is lost, the minimum surge force is less than the maximum surge force. This can also be deduced from the heaving force time trace; however, only with a large maximum force compared to the minimum force. As the crest is at the semi-submersible, the heave force is at its maximum. At this point the particle velocity of the water above the pontoon is at its highest, causing breaking waves and loss of energy. This means that the maximum heave force is lower than the heave force obtained with the linear solution, which can be seen in the lower part of figure 5.1.

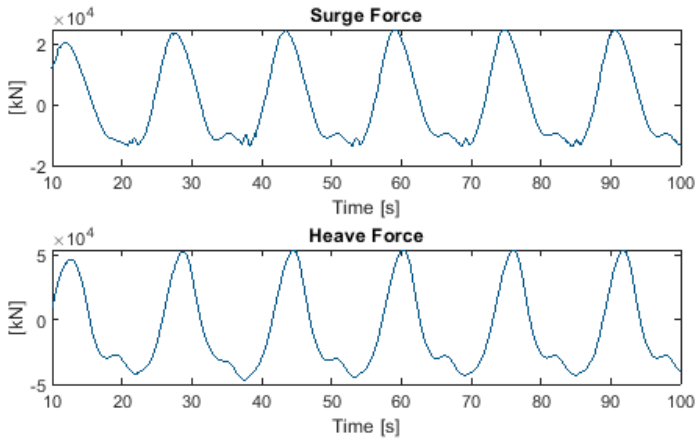

Figure 5.1: Surge and Heave Time Trace at $T = 9.5\ m$, $\zeta_a = 3\ m$ and $\omega = 0.4\ rad/s$

This behaviour is also seen at the lowest zone of the inconvenient draft; a transit draft where the waves topple over the pontoon top. The time traces for this situation are shown in figure 5.2. In this figure the situation at a draft of $T = 6.5\ m$ and wave amplitude of $\zeta_a = 4\ m$ is shown. It shows a large minimum compared to the maximum heave force. An increase in wave amplitude will increase the mass located above the pontoons and as a consequence the breaking of waves will cause the orbital path to be lost. At the wave troughs, no water is present above the pontoons, but the waves are still able to obtain their orbital movement.

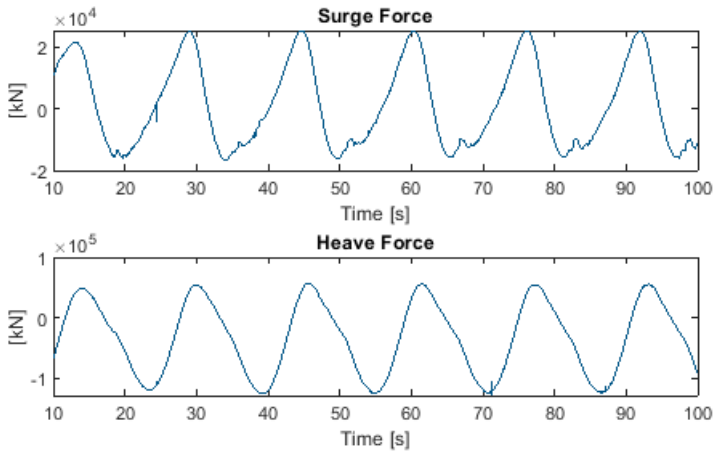

Figure 5.2: Surge and Heave Time Trace at $T = 6.5\ m$, $\zeta_a = 4\ m$ and $\omega = 0.4\ rad/s$

These two variations are visible in all the responses of the parameter study. For each draft and wave amplitude combination the response will show these phenomena. The severity of these phenomena will depend on the contribution of the response at the higher harmonic frequencies.

5.2.2. Standing Waves

There is one important remark that should be made before analysing the results of the parameter study, and that is the presence of standing waves between the pontoons of the semi-submersible, which cause resonating waves at certain frequencies and also a response at these frequencies. The linear diffraction solvers are able to solve these standing waves, because they can be predicted with linear potential theory. This is a different phenomenon that has a limited connection with the higher harmonic response at the inconvenient draft. However, a problem arises when the frequencies of these standing waves are close to the higher harmonic wave frequencies above the pontoons; for example, at an exaggerated transit draft, a draft of $T = 5.5\ m$. With the wave amplitude smaller than the clearance between the mean water line and the pontoon top ($\zeta_a \leq 2\ m$), the response is expected to be linear, as the water-piercing area does not change and no water is present on top of the pontoons.

The contribution of each of the higher harmonic frequencies to the total response is shown in figure 5.3. This figure shows the contribution of the first four harmonic frequencies for wave amplitude, surge force, heave force and pitching moment. To calculate the contribution at each harmonic frequency, the contribution at the desired frequencies is divided by the total contribution of the first four harmonic frequencies. This means the sum of contribution will always be 1, and a contribution of 1 for the first harmonic frequency indicates a linear response.

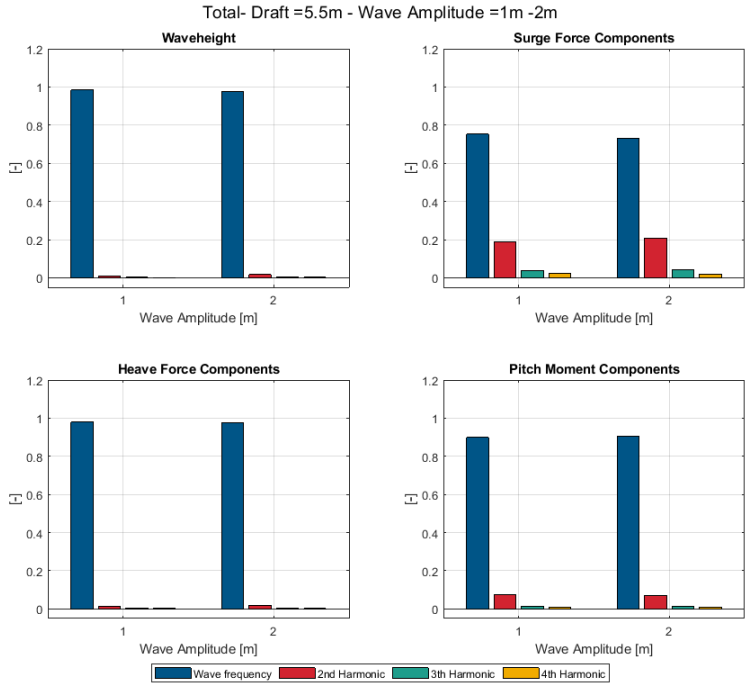

Figure 5.3: Higher harmonic components of the total wave loads at $T = 5.5\ m$

At these linear cases at $T = 5.5\ m$ the surge force shows a higher harmonic contribution of 25% and 27%, indicating a non-linear response. However, this is not caused by the shallow water effect and the phenomena investigated by this research, but is caused by standing waves between the pontoons of the semi-submersible. This is also proven by analysing the wave amplitude time traces, one in front of the semi-submersible and one between the pontoons of the semi-submersible. The time trace and frequency spectra are shown in figure 5.4. It shows an uniform input wave at a frequency of $\omega_1 = 0.4\ rad/s$. The time trace of the wave between the two pontoons shows a different story. A large number of wave frequencies is present between the pontoons, of which some will coincide with the higher harmonic wave frequencies at $\omega_2 = 0.8\ rad/s$ and $\omega_3 = 1.2\ rad/s$. These frequencies can be linked to the natural frequencies of the standing waves.

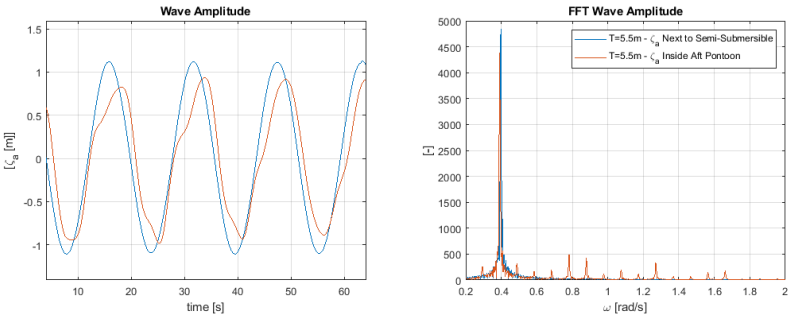

Figure 5.4: Time trace and FFT of Wave Amplitude before and within the semi-submersible at $T = 5.5\ m$ and $\zeta_a = 1\ m$

At the deep operational draft with small wave amplitudes this standing wave has much less influence. This can be seen in figure D.10. The contribution of the higher harmonics is lower compared to the exaggerated transit draft. The standing waves will only be present between the two columns, and have less area for the pressures to act on and thus less influence on the standing waves within the total response. Another influencing factor is the entrapment of the waves. At a deep operational draft, the diffracted waves can propagate outwards; whereas at transit draft the waves are trapped within the

gap of the semi-submersible. This will also cause more wave frequencies to resonate within the gap of the semi-submersible at $T = 5.5\ m$. The time trace and frequency spectra of the wave front and within the semi-submersible for a draft of $T = 25\ m$ are shown in figure 5.5.

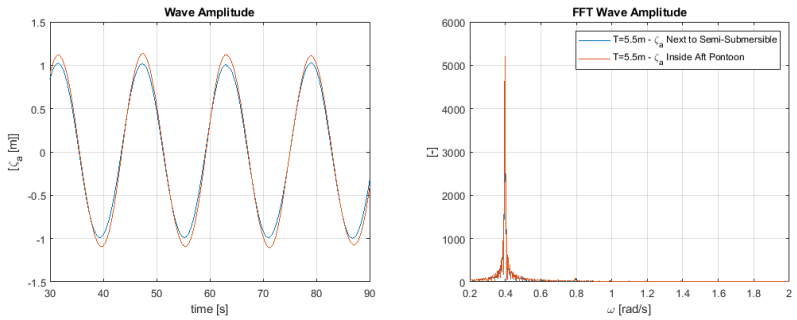

Figure 5.5: Time trace and FFT of Wave Amplitude before and within the semi-submersible at $T = 25\ m$ and $\zeta_a = 1\ m$

To calculate the natural frequency at which the standing waves will resonate equation 5.1 is used, with $\Delta X = \frac{L_{gap}}{0.5,1,1.5,\ldots}$. With $L_{gap} = 59.5m$. The frequency peaks seen in figure 5.4 can each be linked to one of the natural frequencies calculated analytically. The frequency peaks calculated with the response from ComFLOW are shown in table 5.2. Here these frequency peaks are linked to the different eigenmodes of the standing waves.

$$\omega_{st} = \sqrt{\frac{2\pi g}{\Delta X}} \tag{5.1}$$

Eigenmode	Analytic Frequency [rad/s]	ComFLOW peaks [rad/s]
0.5	0.72	0.80
1	1.02	1.00
1.5	1.25	1.20
2	1.44	1.40

Table 5.2: Frequency of standing waves linked to peaks in wave spectra calculated with ComFLOW

The final check is made to ascertain that this response is caused by the standing waves. A simulation is run with a different regular wave frequency of $\omega = 0.5\ rad/s$. The wave amplitude and the corresponding FFT are shown in figure 5.6. This also shows a peak around $\omega = 0.8\ rad/s$, but is much less significant compared to the same peak with the incoming wave frequency of $\omega = 0.4\ rad/s$.

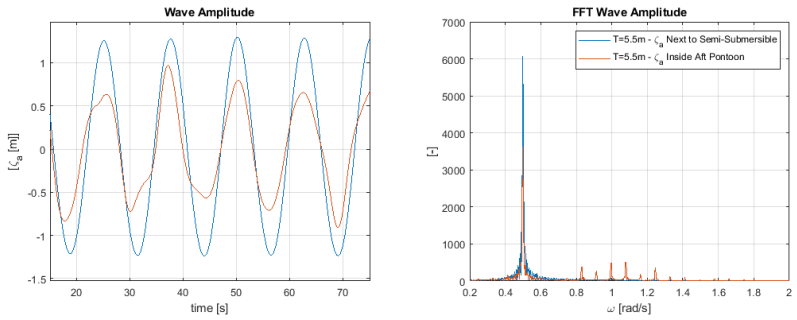

Figure 5.6: Time trace and FFT of Wave Amplitude before and within the semi-submersible at $T = 5.5\ m$, $\zeta_a = 1\ m$ and $\omega = 0.5\ rad/s$

This means that at shallow drafts the influence of these standing waves will influence the outcome of the parameter study. This should be taken into account when analysing the data.

5.2.3. Higher Harmonic Contribution

Zone 1 - Deep draft with a wave amplitude smaller than the clearance between the free surface and the pontoon top

In this zone the waterline is above the pontoon and the wave amplitude is smaller than the water depth above the pontoon. This means the pontoon top is submerged throughout the complete wave cycle. In this zone the transition from linear response to the non-linear response occurs as the higher harmonic responses come into play. In table 5.3 all the simulations in this zone are stated.

Draft [m]	ζ_a [m]
25.0	0.5-1-1.5-2-4-6-8-10
21.5	2-4-6-8-10
17.5	2-4-6-8
14.5	2-4-6
11.5	2

Table 5.3: Situations in zone 1

The top limit of the inconvenient draft is at an operational draft. If the draft is decreased or the wave amplitude is increased, at some point the free surface waves are changed is such way that the linear relation between the hydrodynamic responses and the incoming wave is no longer valid. In this zone the point at which the linear relation will not be valid is sought and a connection is made with the Ursell number.

The Ursell number is given in equation 5.2. The Ursell number gives the degree of non-linearity of waves, based on wave steepness and relative wave depth. In this formula λ is the wave length, H is the wave height and h is the water depth. A more elaborate explanation of the Ursell number is given in the book *Waves in Oceanic and Coastal Waters* by Leo H. Holthuijsen [8]. An Ursell number under $U_r \leq \frac{32\pi^2}{3} \approx 105.28$ will give a linear wave, whilst a Ursell number higher will give a wave with non-linear components.

$$U_r = \frac{H\lambda^2}{h^3} \tag{5.2}$$

The composition of the harmonic frequencies present in the response are shown in figures D.6 to D.10. These figures show the different harmonic contribution for a fixed draft with increasing wave amplitude. Figures D.31 to D.35 show the harmonic contribution for a fixed wave amplitude with a varying draft. With the deeper drafts and smaller wave amplitudes it is expected that the response has a linear relation w.r.t. the incoming waves.

The first thing that immediately stands out is the constant 20% to 30% contribution of the second harmonic surge force. This can be linked to the standing waves explained in section 5.2.2

In case of the heaving force in this zone it can be seen that for small wave amplitudes the response is still linear. However, when the wave becomes larger the higher harmonic components increases to a significant contribution. When using the Ursell number of $U_r = \frac{32\pi^2}{3} \approx .105,28$, the cases that will give a linear response can be determined beforehand. The cases that should be linear according to this theory are at a draft of $T = 25\ m$ to a maximum wave amplitude of $\zeta_a = 2\ m$and at a draft of $T = 21.5\ m$ to a maximum wave amplitude of $\zeta_a = 1\ m$. When looking at the higher harmonic contribution, it becomes clear that some cases with a higher Ursell number also cause a linear response with respect to the incoming wave. Even up to an Ursell number of $U_r = 1600$ ($T = 14.5\ m$ - $\zeta_a = 2\ m$).

The Ursell number can be used as a limit, because all situations with a $U_r \leq\approx .105,28$ will yield a linear response that can be calculated correctly with the linear diffraction solver. A higher Ursell number is less decisive, as most of the situations tested with a higher Ursell number show a significant contribution of higher harmonic response, but not all of them.

This is also backed by the relative differences between the linear solution and the solution obtained by ComFLOW. For each case at a draft of $T = 25\ m$ the Ursell number, relative error between the two solutions and the contribution of the first harmonic are shown in table 5.4. For all the conditions with an Ursell number lower than $U_r \leq 105.28$, the first harmonic frequency (regular wave frequency) causes more than 93% of the total response for all three degrees of freedom. These cases also show small

differences between the solution obtained with the linear diffraction solver and with ComFLOW; to a maximum difference of 11.22% for the pitching moment. If the wave height increases further, the Ursell number will be larger than the set limit. From this point the first harmonic contribution starts to drop and the relative differences start to increase.

	Wave Amplitude [m]	0.5	1	1.5	2	4	6	8	10
	Draft [m]	25	25	25	25	25	25	25	25
	Ursell Number [-]	26.3	52.6	78.9	105.2	210.3	315.5	420.7	525.8
Surge	Error [%]	-2.86	-2.61	-2.55	-2.82	-3.92	-3.67	-3.49	-4.03
	Contribution First Harmonic [%]	96.90	94.18	94.16	94.89	91.82	88.85	88.28	87.37
Heave	Error [%]	-6.97	-7.06	-6.60	-5.66	-1.17	4.83	12.22	19.84
	Contribution First Harmonic [%]	98.10	95.95	95.66	95.48	93.26	91.29	89.04	87.21
Pitch	Error [%]	-9.47	-9.70	-10.17	-11.22	-20.31	-28.27	-31.76	-26.09
	Contribution First Harmonic [%]	97.86	94.25	93.52	93.52	86.33	79.12	74.02	69.92

Table 5.4: Relative error w.r.t. linear solution and contribution of first harmonic of the wave load response on the complete semi-submersible

The contribution of higher harmonics in the wave loads acting on the forward section of the semi-submersible are shown in figures D.16 to D.20 and in figures D.36 to D.40. The wave loads acting on only the forward section of the semi-submersible show the same behaviour as the total wave loads and will increase up to a higher harmonic contribution of 20%. When analysing the first harmonic contributions together with the relative differences, shown in table 5.5, it becomes clear that situations below the Ursell limit show a large first harmonic contribution and this is the case for all three degrees of freedom larger than 93%. The differences between the ComFLOW and the linear diffraction solver are also of small magnitude, except for the pitching moment when the relative difference at the lowest wave amplitude starts at 16.87%.

	Wave Amplitude [m]	0.5	1	1.5	2	4	6	8	10
	Draft [m]	25	25	25	25	25	25	25	25
	Ursell Number [-]	26.3	52.6	78.9	105.2	210.3	315.5	420.7	525.8
Surge	Error [%]	-1.32	-0.32	1.21	2.32	4.25	6.37	10.96	17.41
	Contribution First Harmonic [%]	97.19	96.67	95.46	95.12	92.30	90.11	85.57	82.42
Heave	Error [%]	-4.80	-2.86	-0.84	1.24	10.14	19.91	31.92	43.59
	Contribution First Harmonic [%]	98.27	96.64	95.26	94.77	91.14	88.62	82.84	79.16
Pitch	Error [%]	-16.87	-20.07	-23.04	-26.00	-41.68	-51.10	-50.13	-40.25
	Contribution First Harmonic [%]	97.10	96.04	94.13	93.26	86.75	79.42	69.41	62.80

Table 5.5: Relative error w.r.t. linear solution and contribution of first harmonic of the wave load response on the forward section

The contribution of higher harmonics of the wave loads acting on the aft section of the semi-submersible is shown in figures D.26 to D.30 and in figures D.41 to D.45. The heaving forces in this case show an almost constant second-order contribution of 10% for a draft of $\zeta_a = 1\ m$ up to 22% for a draft of $\zeta_a = 10\ m$.

When analysing the first harmonic contributions together with the relative differences, shown in table 5.6, it shows slightly lower first harmonic contributions compared to the forward section, up to a minimum of 88.38%. However, it shows the same behaviour as the Ursell limit, because the first-order contribution drops after the limit has been exceeded. The relative differences are smaller compared to the forward section where the maximum difference is 16.40% for the pitching moment.

With regard to the heave force, it it becomes clear that the higher harmonic in each zone of the inconvenient draft is larger for the aft section. The wave will travel over the forward pontoon, which will result in a transfer of wave energy to the higher harmonic wave frequencies and travel onwards to the aft section. When this wave group will pass over the aft pontoon, an increasing amount of the wave energy is transferred to the higher harmonic frequencies. This means that the higher harmonic contribution for heave is more significant on the aft section.

	Wave Amplitude [m]	0.5	1	1.5	2	4	6	8	10
	Draft [m]	25	25	25	25	25	25	25	25
	Ursell Number [-]	26.3	52.6	78.9	105.2	210.3	315.5	420.7	525.8
Surge	Error [%]	-2.64	-3.99	-5.01	-5.69	-9.09	-9.89	-10.16	-8.50
	Contribution First Harmonic [%]	94.74	90.54	90.64	88.34	76.05	69.30	66.78	66.63
Heave	Error [%]	-9.23	-11.26	-12.05	-11.99	-10.59	-6.05	-0.63	8.03
	Contribution First Harmonic [%]	97.30	94.73	92.79	90.64	81.16	75.26	72.79	74.24
Pitch	Error [%]	-6.26	-3.23	-0.78	0.90	1.37	1.67	7.45	16.40
	Contribution First Harmonic [%]	97.53	93.53	93.90	92.95	83.10	78.75	77.81	79.43

Table 5.6: Relative error w.r.t. linear solution and contribution of first harmonic of the wave load response on the aft section

Zone 2 - Deep draft with a wave amplitude larger than the clearance between the free surface and the pontoon top

The second zone that is analysed is a deep draft with a wave amplitude larger than the clearance between the free surface and the pontoon top. This means there is no water on parts of the pontoon top in some phases of the wave oscillation. It is expected that all situations in this zone will give a response with a significant contribution of higher harmonic frequencies. All the situations tested in this zone are shown in table 5.7.

Draft [m]	ζ_a [m]
17.5	10
14.5	8-10
11.5	4-6-8-10
9.5	2-3-4-5
8.5	1-2-3-4-5

Table 5.7: Situations in zone 2

The contribution on the total wave-load response in the higher harmonic frequencies in this zone are shown in figures D.4 to D.8. For the smaller draft of $T = 8.5\ m$ and $T = 9.5\ m$ it shows an increasing response contribution in case of the first harmonic component, meaning the response becomes more 'linear' when the wave amplitude is increased. This is contrary to expectations and can be explained that[zo correct? Check zin aub] the standing waves between the pontoons are better able to resonate for the smaller wave amplitudes, compared to the more violent flow at higher wave amplitudes. This is also backed by simulations at a larger draft, at $T = 11.5\ m$ and $T = 14.5\ m$. For these simulations the standing waves between the pontoons will become less significant. The response at the higher harmonics is dominated by the waves on top of the pontoons. This shows an increase in contribution of the higher harmonics for increasing wave amplitude, as was expected beforehand.

The contribution of the higher harmonics in the heave force can also be split into two different types of behaviour. The smaller drafts of $T = 8.5\ m$ and $T = 9.5\ m$ show a constant contribution to the higher harmonics, in total around 18% to 23%, whereas for the larger draft from $T = 11.5\ m$ the higher harmonic contribution increases to a maximum of almost 40%.

The contribution to the wave-load response on the forward section of the semi-submersible at different the harmonic frequencies in this zone is shown in figures D.14 to D.18. The same conclusions can be drawn in case of the surging force only on the forward section as well as at the total surging force. At lower draft the contribution of higher harmonic contributions decreases, whereas it increases for the deeper drafts to just above an 30%. The heaving force shows increasingly higher harmonics for an increasing wave amplitude to a maximum of around 25%.

The contribution on the wave-load response on the aft section of the semi-submersible on the different harmonic frequencies in this zone is shown in figures D.24 to D.28. Again, for both the surge and heave force the higher harmonic contributions show the same trends. However, in general the higher harmonic contribution is larger at the aft section and even has a maximum of 50% for the total contribution for both the higher harmonic surge and heave-force response.

Zone 3 - Draft is at pontoon top
The third zone in the inconvenient draft is when the draft is exactly at the height of the pontoon top. The top side of the wave will topple over the top of the pontoon while the lower half of the wave will hit the side of the semi-submersible. In table 5.8 all simulations in this zone are stated. As this zone is a one-set draft, a change in draft is impossible and only a draft of $T = 7.5\ m$ is used.

Draft [m]	ζ_a [m]
7.5	1-2-3-4-5

Table 5.8: Situations in zone 3

The contribution of higher harmonics in the total wave loads is shown in figure D.3. The composition of the surge forces first increases to 30% at a wave amplitude of 2 meter. If the wave amplitude is increased further, it will drop down to 20% at a wave amplitude of 5 meter. In case of the heaving force, it becomes clear that the higher harmonic contributions increase when the wave amplitude is increased; from 6% at a wave amplitude of 1 meter to 20% for a wave amplitude of 3 meter. For higher wave amplitudes the second harmonic does not increase to a higher contribution; the third and fourth harmonic keep on increasing.

The distribution of the harmonic contributions for the forces on the forward section of the semi-submersible are shown in figure D.13. This case shows an almost constant distribution of higher harmonic frequencies in case of the surge force. Only the smallest wave amplitude of 1 meter has a slightly lower second harmonic contribution of 21%. All cases at this draft with a higher wave amplitude show a second harmonic contribution of almost 30%. For the heaving force, total contribution of the higher harmonics slowly increases from 10% to 20%.

While looking at the aft section of the semi-submersible, different trends can be distinguished. The distribution of the harmonic contributions for this case are shown in figure D.23. With regard to the surge force, instead of an almost constant contribution to the higher harmonics, the second harmonic contribution will drop while the third and fourth harmonic contributions will increase. The total contribution of the higher harmonics will decrease slightly from 25% to 20%. At the largest wave amplitude of $\zeta_a = 5\ m$, the third harmonic contribution is higher than the second harmonic. In case of the heaving force, the second harmonic contribution increases to a wave amplitude of $\zeta_a = 6\ m$, a higher wave amplitude will give a same contribution from the second harmonic; just above 20%. This is also seen in the first harmonic contribution as it levels around 72%.

For the situation when the draft is exactly at the height of the pontoon top, two conclusions can be drawn. The first conclusion concerns the significance of the higher harmonic components in case of the surge force. For low wave amplitudes the higher harmonic contribution is at about the same level, whereas for an increasing wave amplitude the higher harmonic contribution will become more significant on the forward section. This is caused by the breaking of waves, since the larger waves will break over the forward pontoon. Energy is dissipated and less wave energy will reach the aft pontoon. The second conclusion concerns the heaving force at the aft section. The higher harmonic contributions are more significant compared to the forces on the forward section. This may be caused by the lower wave energy; at the forward pontoon the wave will break and a violent flow is present above the pontoon. As less wave energy is propagated to the aft section, the flow above the pontoon will become less violent and the higher harmonic waves will propagate over the pontoon top.

Zone 4 - Transit Draft, wave amplitude larger than freeboard
The fourth zone at which the captive wave loads on the semi-submersible are analysed is a transit draft with a wave amplitude larger than the clearance between the free-surface and the pontoon top. This means that part of the wave will topple over the pontoon top. These waves will always break as there is no water depth above the pontoon. Two drafts are tested in this zone with multiple wave amplitudes. The overview of all the situations tested is shown in table 5.9.

Draft [m]	ζ_a [m]
6.5	2-3-4-5
5.5	3-4-5

Table 5.9: Situations in zone 4

The contributions to the total wave load response in the different harmonic frequencies in this zone are shown in figure D.1 and D.2. In both drafts the surge force shows an almost constant significance of the second harmonic contribution, 25% for $T = 5.5\ m$ and 20% for $T = 6.5\ m$. This also indicates an increase in draft and leads to a reduction in higher harmonic contributions because there is less water above the pontoon tops. At large wave amplitude the decrease in contribution of the first harmonic is mainly caused by the third and fourth harmonic. In case of the heave response, the general trend shows an increasingly higher harmonic contribution for a higher wave amplitude. However, this increase in higher harmonic contribution only applies to waves with a wave amplitude that is more than 1 meter larger than the clearance between the free surface and the pontoon top. Waves with an amplitude that are more than 1 meter larger than the clearance still show a linear heave response. This can be seen in the case of $T = 5.5\ m$ with $\zeta_a = 3\ m$ and $T = 6.5\ m$ with $\zeta_a = 2\ m$. Both cases show a significant contribution of the response at the wave frequency, 97% of the total response.

The contribution of the wave loads integrated on the forward section are shown in figures D.11 and D.12. The same behaviour as on the total loads is observed on the forward section and shows a highly non-linear response as the first harmonic order contribution lies only on 60% for a draft of $T = 5.5\ m$ and 65% for a draft of $T = 6.5\ m$. For the heaving force on the forward section of the semi-submersible, an almost linear behaviour is observed for all wave amplitudes at a draft of $T = 5.5\ m$ since the first harmonic contribution will contribute to more than 90% of the total response. For a draft of $T = 6.5\ m$, the significance of the higher harmonics starts to increase for the larger wave amplitudes, up to $\zeta_a = 5\ m$. The significance at this largest wave amplitude is 10% for the second harmonic and 4% for the third harmonic; thus the heaving force on the forward pontoon in this zone can be calculated with linear diffraction solvers.

The contribution of the wave loads integrated on the aft section are shown in figure D.21 and D.22. Again the same behaviour as for the total and forward wave loads is observed, which is a constant second harmonic contribution and a gaining third harmonic contribution. The contribution of the first harmonic lies for the aft section around 70% for a draft of $T = 5.5\ m$ and 75% for a draft of $T = 6.5\ m$. The heave response on the aft section shows a large higher harmonic contribution compared to the forward section. Also, at a draft of $T = 5.5\ m$, an increasingly higher harmonic significance is seen, up to 40% of the total response for the largest wave amplitude.

Two conclusions can be drawn for this zone. First, if the free surface is closer to the pontoon top, the second harmonic contribution will drop for the surge force but increase for the heave force. In case of the surge it was noticed that the contributor of the second harmonic is a standing wave between the floaters; for larger waves this standing wave is less profound and thus the forces present in these higher harmonic frequencies are less significant.

The second conclusion is that the significance of the second harmonic contribution is for surge force larger on the forward section and for the heave force more profound on the aft section, whereas the third harmonic frequency reacts in the opposite way.

Zone 5 - Transit Draft, wave amplitude smaller than freeboard
The fifth zone that is analysed is also at the transit draft; however, in this case the waves are smaller than the clearance between the free-surface and the pontoon top. This means that there is no change in water plane area and that the steep walled assumption is valid again. The Ursell number in this situation is small, with $U_r \leq 1$. As there is no water on top of the pontoon, the depth that is used is the

total water depth. This is also tested for two drafts with multiple wave amplitudes. The overview of the situations tested is shown in table 5.10.

Draft [m]	ζ_a [m]
6.5	1
5.5	1-2

Table 5.10: Situations in zone 5

The distribution of the harmonic harmonic contributions for the total wave load is shown in figures D.1 and D.2. The wave loads on the forward section in figures D.11- D.12, and the contribution of the harmonic frequencies of the wave loads on the aft section of the semi-submersible is shown in figures D.21- D.22.

The surge forces show similar trends as for the linear cases in zone 1, and show a second harmonic contribution around 18% to 20% for all situations in this zone. When the forward and aft wave loads are compared, almost no differences are present; there is less than 4% difference between the contribution of the wave frequent response.

The heave forces for the total, forward and aft integration show an almost perfect linear response, as the total higher harmonic contributions for each of these situations are less than 4%.

This means the responses at this zone can be calculated correctly with the linear diffraction methods and shows the lower limit of the inconvenient draft. This can be defined as in equation 5.3

$$\frac{\zeta_a}{H_{pontoon} - T} \leq 1 \tag{5.3}$$

Change in Draft

The higher harmonic response contributions is elaborated for each of the separate zones in the inconvenient draft. However, a change of draft trough all the zones of the inconvenient draft should also be analysed. The wave amplitude and the wave period of the incoming wave does not change, this means the wave steepness does not change. Any change in the contribution of the responses at the higher harmonic frequencies can be assigned to the interaction between the semi-submersible and the waves. In figure 5.7 the higher harmonic response contributions for all drafts with a wave amplitude of $\zeta = 2\ m$ is shown.

The heave force response components show a linear relation at the deepest drafts. At a draft of $T = 14.5\ m$ the higher harmonic response contribution start to gain significance. The maximum higher harmonic response contribution for the heave force at this draft is seen at a draft of $T = 9.5\ m$. When all the wave amplitudes are combined it is seen that the maxima will always occur when the wave amplitude is 1 to 1.5 the clearance between the pontoon top and the free surface. This can be written as in formula 5.4. In which ζ_a the wave amplitude represents, T the draft and $H_{pontoon}$ the pontoon height.

$$1 \leq \frac{\zeta_a}{T - H_{pontoon}} \leq 1.5 \tag{5.4}$$

At even shallower drafts or higher wave amplitudes the higher harmonic response contribution is reduced further. This is caused by the loss of the orbital wave motion of the water particles. The wave can not retain their orbital motion in the limited water column present above the pontoons. Eventually the response will retain its linear relation with the incoming wave again at the transit draft and when the wave amplitude is smaller than the clearance between the free-surface and the pontoon top.

In case of the surge force both the effects of the standing wave at the exaggerated transit draft and the standing waves between the columns at deep draft can be seen. The second harmonic is dominant in case of the transit draft and for the deepest draft a small second harmonic wave frequency contribution is still present.

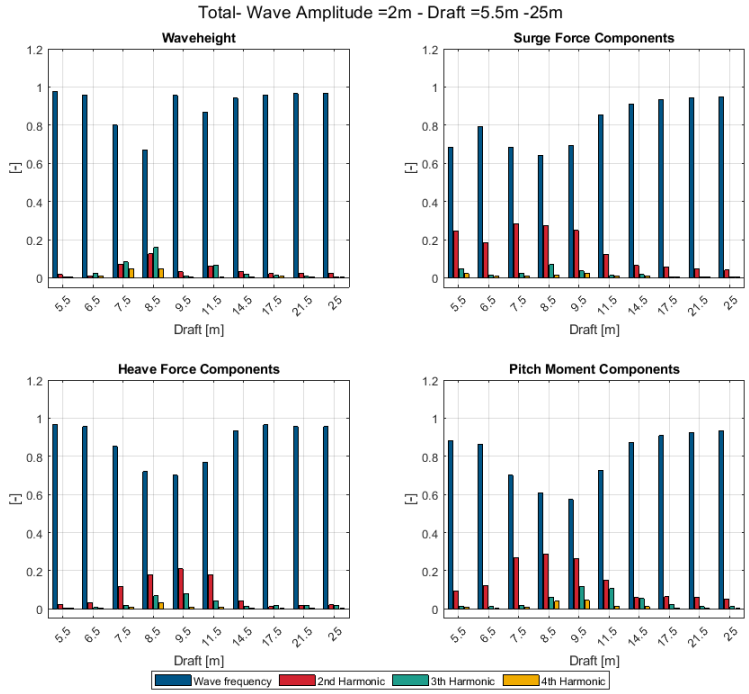

Figure 5.7: Higher harmonic components of the total wave loads response at a wave amplitude of $\zeta_a = 2\ m$

5.3. Conclusions

The research question asked at the start of this chapter was:

How does the higher harmonic response behave within the inconvenient draft?

This question are answered with the help of the three questions stated below.

How do pontoon submergence and wave height impact the occurrence of higher harmonics in the wave load response and can a clear relation be distinguished?
An increase in wave amplitude will cause an increase in the higher harmonic response contribution. This is valid for the total wave loads or for wave loads integrated over a particular section. For the surge force, the higher harmonic response contribution is found to be larger on the forward section in each of the zones of the inconvenient draft, which is due to the standing waves in between the pontoons and not the result of the change in wave pattern on top of the pontoons. This phenomenon is especially significant for the most shallow drafts. As the pontoons get closer to the free surface, or even penetrate the free surface, a large part of the wave energy is reflected and retained inside the pontoons. This causes a higher harmonic response contribution that can be as high as 50% of the total response.

For the heave force, a clear correlation between the higher harmonic response contribution and the wave amplitude can be distinguished, since below an Ursell limit of $U_r \leq \frac{32\pi^2}{3}$ the heave response shows a linear relation with the incoming wave. Furthermore, situations with a higher Ursell number have an increasing higher harmonic contribution of at least 10%.

The pitching moment is a consequence of the surge and heaving force. This means that there is always a slight constant higher harmonic contribution due to the surging force, and an increasingly higher harmonic contribution due to the heaving force. It can be concluded that an increase in wave amplitude will lead to a more dominant contribution to the response at a higher harmonic frequency.

A changing draft has a dominant effect on the generation of higher harmonics. This effect will largely depend on the zone of the inconvenient draft that the semi-submersible is situated in. In the deep 'operational' draft the higher harmonic contribution will quickly increase and reach a maximum when $1 \leq \frac{\zeta_a}{T - H_{pontoon}} \leq 1.5$. After this stage the flow becomes too violent, waves start to break and the

wave energy is dissipated. The higher harmonic contribution will reduce further when the draft is reduced towards the transit draft, and eventually, the linear relation is restored when the wave amplitude is smaller than the clearance between the free surface and the pontoon top.

What is the magnitude of the higher harmonic responses on the internal loads and is the influence at a significant level?
It isimportant to realise that this only concerns the wave-load-induced part of the total internal load. In most cases the wave-load responses on the higher harmonic frequencies contribution vary between 10% to 40% of the total response at the inconvenient draft. In some severe cases it can increase to a maximum of 50%, which means that the first harmonic wave frequency only contributes to 50% of the total response amplitude. This large contribution of responses on higher harmonic frequencies also makes that the solutions greatly differ from the linear solutions;even up to an difference of 40% in response amplitude.

When do the (combined) pontoon submergence and wave height start to introduce significant non-linearities in the wave-induced internal load response?
One of the most important aspects of calculating the internal loads is to know at which limits the linear diffraction solver will provide a solution that is considered too inaccurate. From these limits onwards, another method should probably be used to calculate the internal loads. The limits determined in this research express the upper and lower boundaries of the inconvenient draft.

The upper limit of the inconvenient draft is found to be equal to the Ursell limit. If $U_r = \frac{H\lambda^2}{h^3} \leq \frac{32\pi^2}{3}$, the response may be assumed to be linear and correct calculations can be made with the linear diffraction solver. For situations with a higher Ursell number, the higher harmonic contribution will increase and consequently the difference in response amplitudes will also increase. This Ursell limit is a conservative limit, as some situations will still be linear even at higher Ursell numbers.

The lower limit of the inconvenient draft is at a transit draft when the wave amplitude is smaller the the clearance between the free-surface and the pontoon top. This limit can be given by the formula: $\frac{\zeta_a}{H_{pontoon}-T} \leq 1$.

How do the higher harmonic responses behave within the inconvenient draft?
The behaviour of the higher harmonics in the response depends on the combination of the clearance between the pontoon top and the free surface, the wave amplitude and wave length. When the Ursell number of the waves above the pontoon top exceeds $U_r = \frac{H\lambda^2}{h^3} \leq \frac{32\pi^2}{3}$, part of the wave energy is transferred to higher harmonic frequencies. An increase in wave amplitude will yield an increase in higher harmonic response contribution, up to a maximum of 50%f of the total response. Decreasing the water column above the pontoon and increasing the wavelength will also increase the higher harmonic response contribution. The higher harmonic response contribution is at its maximum when the free surface is 2 or 3 meters above the pontoon with the largest waves. A deeper draft will cause the higher harmonic contribution to decrease. At a transit draft with a wave 1 meter larger than the freeboard, the response is again linear.

6

Quantification of the non-linear wave loads onto the total internal loads

Since the internal loads cannot be directly calculated using the available tools (as shown in section 4.3.3), an effort is made to at least assess the impact of non-linear wave load behaviour at an inconvenient draft onto the total internal loads.

The applied method combines the captive wave loads obtained in chapter 5 with the time domain simulator aNySim to calculate the total internal loads, including the inertia and gravitational loads. More information on aNySim are shown on the website of MARIN [11].

The first section will discuss the setup of this method, which input is used, and which assumptions are made. This is shown in section 6.1 Next, the method is validated and verified, using a comparison with model tests, seen in section 6.2. Finally, the results are shown and conclusions on this chapter is drawn. This is shown in respectively section 6.3 and section 6.4.

6.1. Methodology

In this section the setup of the quantitative analysis is explained. The underlying idea is to impose the captive wave loads from the CFD solver ComFLOW on the free-floating semi-submersible. The wave loads will set the semi-submersible in motion. The time domain simulator will solve the equation of motions, which will include all the terms of the internal loads. This means that the total internal loads can be calculated at the inconvenient draft. There is however one limiting factor, as a single body model the internal loads can not be calculated/outputted by aNySim. That is why a dual body model is needed.

The method will first be set up for a single-body semi-submersible and then for a dual body submersible; this is done for two separate drafts. One deep draft at $T = 25\ m$, which should show a linear response with regard to the incoming wave; as shown in section 4.1. And a draft of $T = 11.5\ m$ is selected because it should show a non-linear response. This brings the total number of models to four.

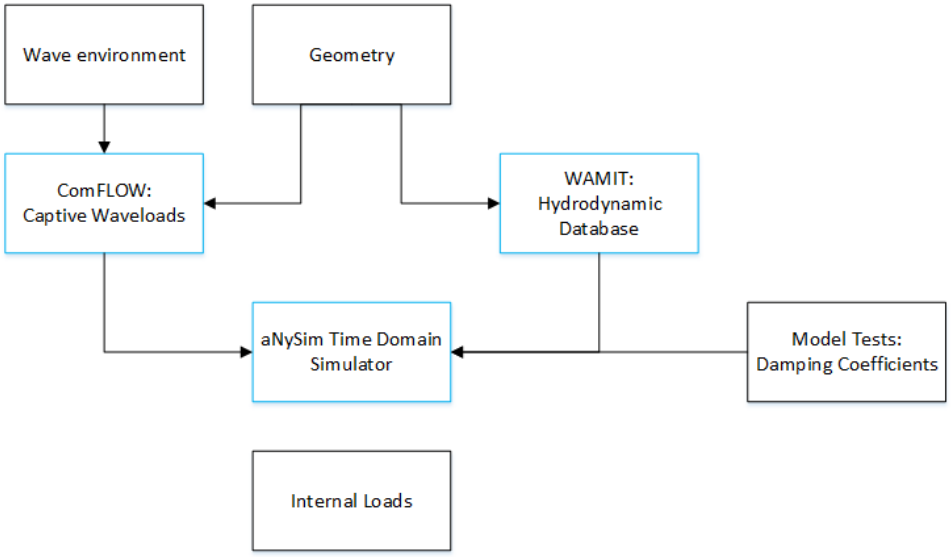

Figure 6.1: Overview of the quantitative analysis scheme Single Body

For the dual body model the semi-submersible is split up into two parts, the forward section and the aft section. These two sections are connected in the time domain simulator aNySim, using a *Joint*, the numerical equivalent of a 6-component frame. Separation of the model has some consequences for the setup for each of the used software packages. These effects and the way WAMIT, ComFLOW and aNySim are set up are discussed in the following paragraphs. The overview of the dual body models is given in figure 6.2.

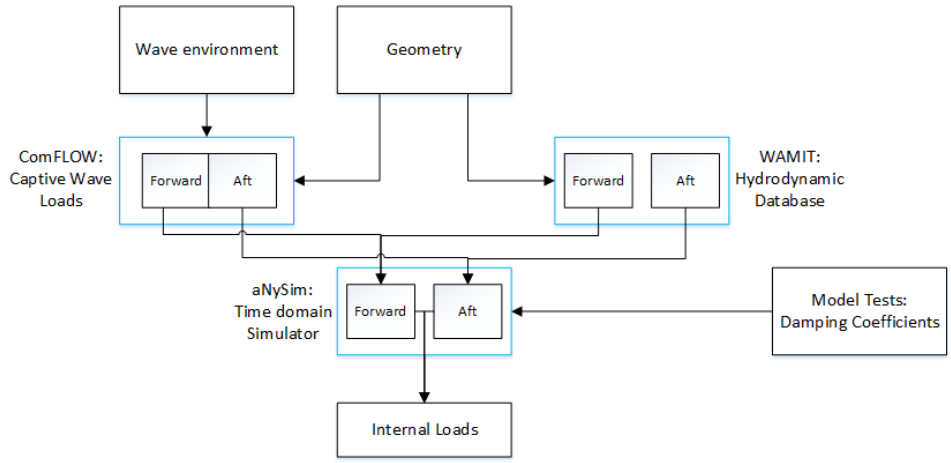

Figure 6.2: Overview of the quantitative analysis scheme Dual Body

For the present time-domain calculations, the following input is required to perform reasonable accurate calculations:

- Frequency dependent hydrodynamic added mass and potential damping. See section 6.1.1
- Hydrostatics and Mass properties (Mass, radii of gyration, COG position). See table 2.2
- Viscous damping. See section 6.1.2
- Applied Wave Loads. See section 6.1.3
- Joint stiffness. See section 6.1.4

6.1.1. Hydrodynamic Database

For the single body models, the WAMIT is set up in the same way as in section 4.2. For the dual body models, the setup of WAMIT is slightly different. The model is split up into two symmetrical parts. No panels are modelled at te symmetry plane. The forward section for the dual-body model is shown in figure 6.3.

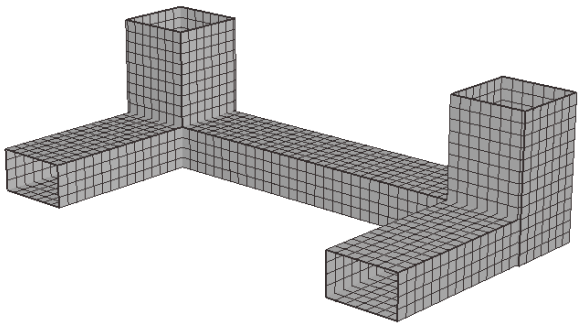

Figure 6.3: Model of the forward section of the semi-submersible

The results obtained with the multi-body calculation are the frequency dependent added mass and potential damping, in the form of 12x12 matrices. This includes the single-body effects(on each symmetrical body) as well as the coupling terms describing the hydrodynamic interaction between the two bodies.

6.1.2. Viscous Damping

The spring and damping coefficients are determined with a P-Q analysis, this is based on the method of J.J. van der Vegt(1984) [19], as shown in the paper of S. Burmester et al. [3].

The spring and damping coefficients of the dual body model are obtained with the single-body models. As the total damping is the same and both sections are symmetrical, the damping per section is 50% of the total damping. This holds for both the linear and the quadratic damping.

6.1.3. Applied Wave Loads

In ComFLOW it is not required to split the model into two sections, as the sectional wave loads are obtained with the method shown in section 2.3 and chapter 5.

With the single-body models, the total wave loads are applied at the COG of the semi-submersible. For the dual body simulation, the sectional wave loads obtained by ComFLOW are imposed separately onto the corresponding section. This will result into the motions of the semi-submersible and into the internal loads between the two sections.

6.1.4. Joint Stiffness

To connect the two halve of the dual body simulation, a joint is used and placed in the COG of the semi-submersible. This joint gives the direct output of the forces on the COG meaning the splitting loads. The two bodies should not be able to move separately from each other. To ensure that the relative velocity between the two sections will remain as low as possible, the joint is given high spring stiffness in all six degrees of freedom, in order to limit relative motions. For the initial simulations the maximal allowable relative motion of the two bodies is set to $\Delta x_{max} \leq 0.01\ m$, $\Delta z_{max} \leq 0.01\ m$ and $\Delta \phi_{max} \leq 0.01^{\circ}$. The damping of the joint is set on 70% of the critical damping.

6.2. Validation & Verification

To make sure the model provides the correct solution, multiple test have been conducted;

1. Excursion tests to calculate the hydrostatic response

2. Free decay tests to calculate the mass, inertia, stiffness and damping terms. The dual body models should behave exactly as the single body models for all tests.

A different draft means different wave loads from ComFLOW, a different hydrodynamic database from Wamit and different stiffness and damping setting in aNySim. This means the deep draft model and inconvenient draft model are be validated separately.

6.2.1. Excursion Check

Excursion tests are performed for heave and pitch. The first excursion test that was run is the heave test. A constant downwards force is applied onto the models. The force is increased linearly between $t = 0s$ and $t = 500s$, after which it is kept at a constant level. The analytical heave excursion is calculated in advance with equation 6.1; where z represents the vertical translation, F the applied force, A_{wl} the water-piercing area, ρ the density of the water and g the gravitational constant. The water-piercing area is equal in the inconvenient daft as well as the deep draft model. This means the excursion is at the same magnitude if the same force is applied. The force applied is $F = 7.691 \cdot 10^3\ kN$.

$$z = \frac{F}{A_{wl}\rho g} = \frac{7691 \cdot 10^3}{784 \cdot 1000 \cdot 9.81} = 1\ m \tag{6.1}$$

The excursion of the deep draft model is shown in figure 6.4. This figure shows for the both the single body and the dual-body model an increase in draft of $1\ m$ due to the applied force. This is in correlation with the analytically calculated magnitude.

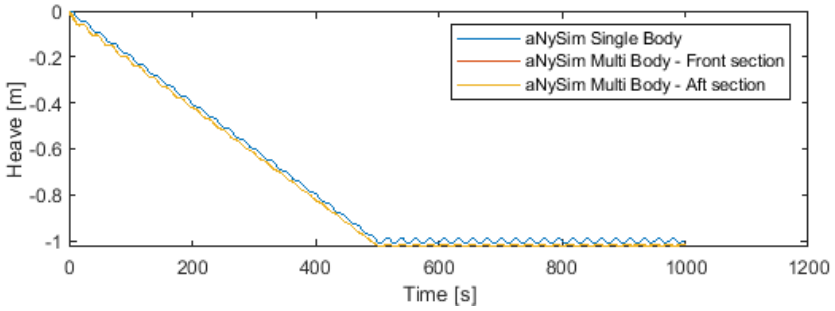

Figure 6.4: Heave Excursion Tests Deep Draft models

The excursion of the inconvenient-draft model is shown in figure 6.5. Again, both the single-body and the dual-body model show an increase in draft of $1\ m$ due to the applied force. This is equal to the analytic value.

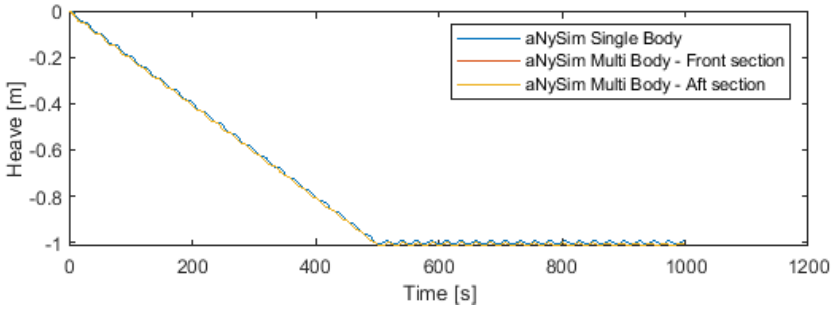

Figure 6.5: Heave Excursion Tests Inconvenient Draft models

The same models will also be tested with an inclination test. This time a linear increasing moment is applied on the models. Equation 6.2 gives the analytic solution of the pitch excursion due to the applied moment. In this equation ϕ is the resulting pitching angle, M is the applied moment, GM is

the metacentric height and ∇ the displacement. The analytically calculated pitching excursion for both deep model and inconvenient model is also shown in this equation. The moment applied is $M = 1.43 \cdot 10^5\ kNm$

$$\phi = sin^{-1}(\frac{M}{GM \cdot \rho g \nabla})$$

$$\phi_{deep} = sin^{-1}(\frac{1.43 \cdot 10^8}{6.04 \cdot 10^3 \cdot 9.81 \cdot 43697.5}) = 3.16° \tag{6.2}$$

$$\phi_{inconvenient} = sin^{-1}(\frac{1.43 \cdot 10^8}{13.17 \cdot 10^3 \cdot 9.81 \cdot 33113.5}) = 1.92°$$

In figure 6.6 the pitch excursion test of the deep-draft model is shown. In figure 6.7 the pitch excursion test of the inconvenient-draft model is shown. All four models show the correct inclination due to the applied moment, no deviations are visible between the single-body models and the dual-body models.

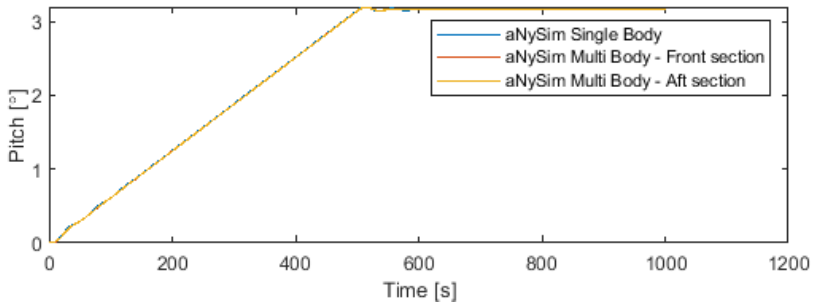

Figure 6.6: Pitch Excursion Tests Deep Draft model

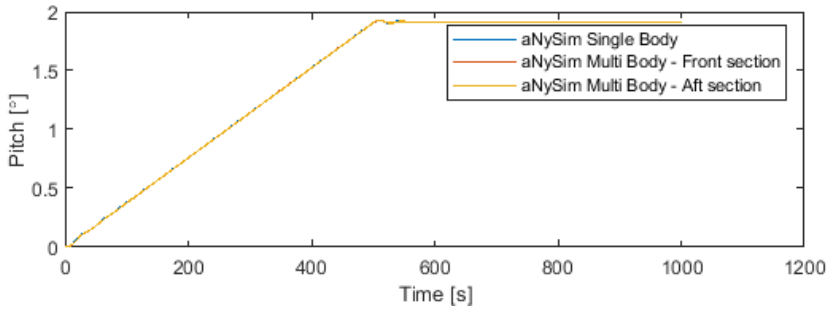

Figure 6.7: Pitch Excursion Tests Shallow Draft model

6.2.2. Free Decay tests

The next step in the validation and verification of the models is the free-decay tests. In this part the free-decay tests conducted with the four models are compared to the free-decay model tests. With the free-decay tests the damping properties of the models and the natural periods are validated. The free-decay tests conducted for the model tests are not all equally good, as some of the free decay model tests consist of high frequent response. The model test free decay tests for the pitching motion are only conducted once per draft and from this particular test only three useful oscillation are obtained. This means the damping needs to be tuned with respect to these three oscillations; in other words, this means a rough estimate of the added linear potential and quadratic damping.

First, the free-decay tests of the deep-draft model are analysed for both heave and pitching motion. Next, the free-decay tests for the inconvenient-draft model are analysed. In each case, the model test results are compared to both the single-body and dual-body models.

The free-decay for the heave motion of the deep-draft model is shown in figure 6.8a, and shows good comparison with the model test and the two aNySim models. This shows a good correlation between the model test and time domain simulated free decay test. The decay of the pitch amplitude is also in good agreement, as shown in figure 6.8b. No change in period between the single-body and the dual-body model is visible.

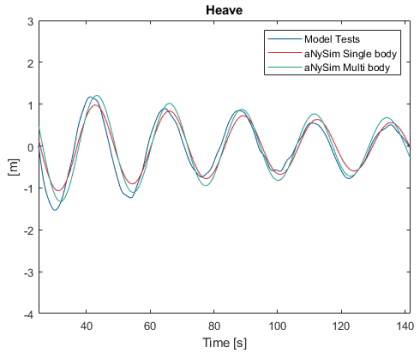

(a) Free Decay Tests Heave Deep Draft model

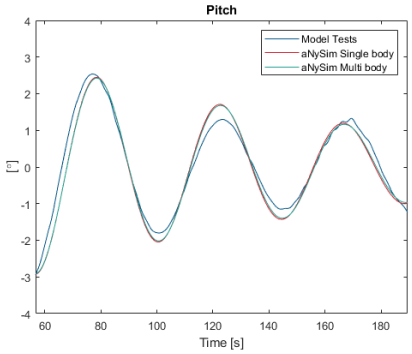

(b) Free Decay Tests Pitch Deep Draft model

The next step is to validate the models at the inconvenient draft. The free-decay for the heave motion of the inconvenient-draft model is shown in figure 6.9a. The decay of the heave amplitude is in good agreement with the model test result for both the single-body model and the dual-body model. The same is concluded for the pitching motion of the inconvenient-draft model, this is shown in figure 6.9b, and shows a good comparison between the free-decay tests of model tests and the models in aNySim.

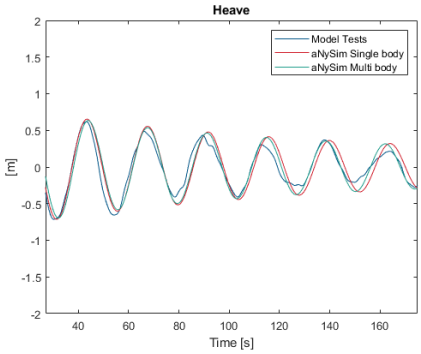

(a) Free Decay Tests Heave Shallow Draft model

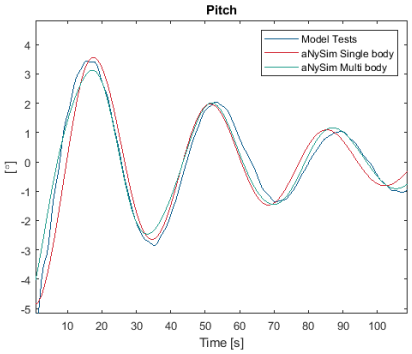

(b) Free Decay Tests Pitch Shallow Draft model

6.3. Results

The next step is to apply the forces obtained in the captive simulations in ComFLOW to the models in aNySim. The first step in this section is to analyse the initial results. The motions are analysed and the internal loads are compared to the linear solution. In the second step, extra attention is given to the joint stiffness, since it is shown that joint stiffness has an effect on the internal load response.

6.3.1. Initial Results

The first model that is analysed is the deep-draft model, and model tests have shown that the motion and wave-load response have a linear relation with respect to the incoming wave. This means that the internal loads are accurately approximated with the linear diffraction solver combined with a mass model. The motion solution of the semi-submersible at this deep draft is compared using the model tests, the linear solution based on RAOs, the aNySim single-body model and the aNySim dual-body model.

In figure 6.10 the motions of the semi-submersible are shown, as well as the corresponding frequency spectra. The time traces show the motion for a free floating semi-submersible in case of the

model tests and the Motion RAO response. The aNySim models both show the resulting motions due to the applied captive wave loads. It is concluded that the motions show a linear relation with respect to the regularly incoming waves. This is also substantiated by the motions response spectra. Both aNySim models show a good comparison with the motions obtained with the model tests and the linear diffraction solver.

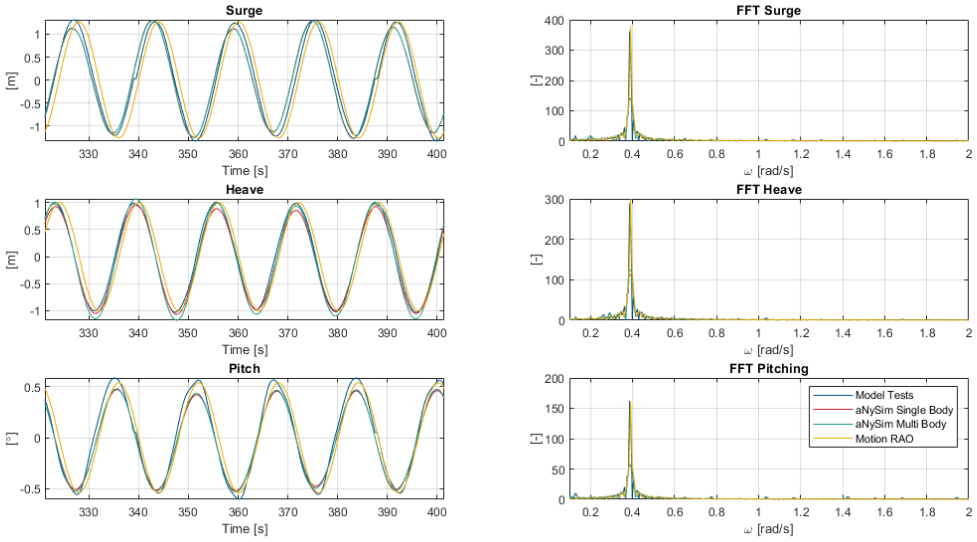

Figure 6.10: Motion response obtained with model tests, Dynload, aNySim single body model and aNySim Dual body model at $T = 25\ m$

The motions of the semi-submersible at the inconvenient draft is shown in figure 6.11. Again both the single-body and the dual-body aNySim model show good comparison with the motions obtained with model tests but also with the motions from the linear diffraction solver. The linear relation between the incoming waves and the motions of the semi-submersible is still valid.

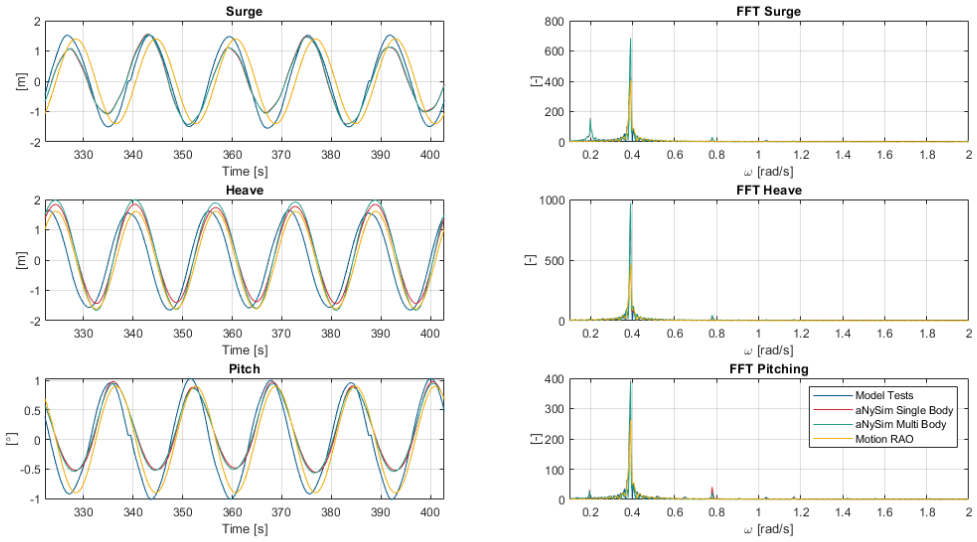

Figure 6.11: Motion response obtained with model tests, Dynload, aNySim single body model and aNySim Dual body model at $T = 11.5\ m$

The next step is to compare the internal loads. The output of Dynload shows the total internal loads

on a part of the section; for this research the forward and aft section. The aNySim joint (stiffener-damper) reports the forces and motions between the two sections. This means the response from Dynload on the forward section is deduced from the aft section to obtain the same internal load definition.

The left-hand side of figure 6.12 shows the applied forces on the deep-draft model, which are obtained with the captive ComFlow simulations. The forces on the aft section, forward section and total forces are shown separately in the first column. The second column shows the corresponding frequency spectra of these applied forces. The right side of this figure shows the resulting difference of internal loads between the forward and the aft section.

The motions of the semi-submersible have been shown to have a linear relation with the incoming wave; combined with the linear forces applied on the model, a linear relation between the incoming wave and the internal loads between the two sections is expected. This also means that the internal loads obtained with Dynload are expected to be a good approximation. The internal loads in horizontal direction shows an almost linear response, only a small peak is visible on the second harmonic wave frequency of $\omega = 0.8\ rad/s$. The amplitude of the force reported in aNySim is however a magnitude smaller compared with the output from Dynload. The vertical internal loads show a different result, the amplitude between Dynload and the dual-body model show good agreement. However, a higher frequency response are seen in the time traces, which is also supported if the frequency spectra are analysed. This shows a significant peak at $\omega = 0.8\ rad/s$ and a smaller peak at $\omega = 1.2\ rad/s$. The moment acting in the joint shows again a linear response, but the amplitude is only half the amplitude obtained with the Dynload. As Dynload is able to solve the internal loads with good accuracy in this 'linear' case, the solutions obtained with the dual-body simulations should be quite similar.

Although the verification of the methodology is not yet completed, the same procedure is also applied to the case with an inconvenient draft, see figure 6.13. The applied forces consist of multiple higher harmonic frequencies as is shown in chapter 5. It is expected that the harmonic response frequencies will propagate into the internal load; however, to which extend is not known. On the right side of this figure, the internal load difference between the forward and aft section of the semi-submersible is shown. The Dynload solution is shown next to the dual-body solution. In this case the Dynload solution might not give the correct answer, as it is not known whether the linear relation between the internal loads and the incoming wave is still valid. When analysing the internal load response obtained with the dual-body model, one comment is be made. A large part of the response is at a higher harmonic wave frequency. The total contribution is much larger than the higher harmonic response contribution in the applied forces. As the motions still show a linear relation, the higher harmonic contribution in the internal loads cannot be larger than the higher harmonic contribution in the applied wave loads. However, here this is the case, especially for the vertical force. The most dominant response contribution is at the second harmonic frequency, this is more dominant than the first harmonic wave frequency.

Both the deep-draft model and the inconvenient-draft model do not provide the correct answers and thus cannot be validated. This may be caused by the way the dual-body is constructed and the influence of the joint in the internal loads response.

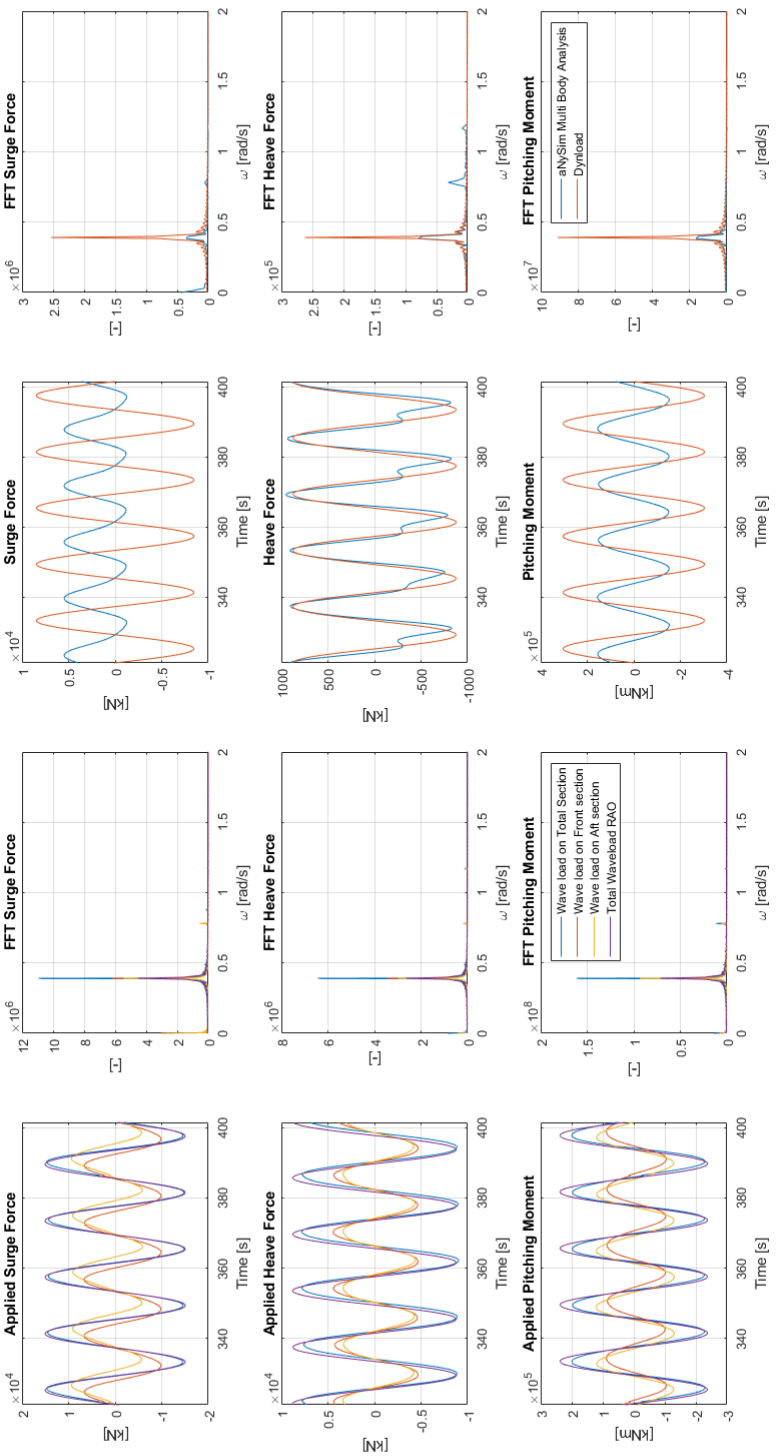

Figure 6.12: Applied wave loads obtained with captive ComIFLOW simulations (left) and Internal Load response response obtained with the aNySim Dual body model and Dynload at $T = 25\ m$(right)

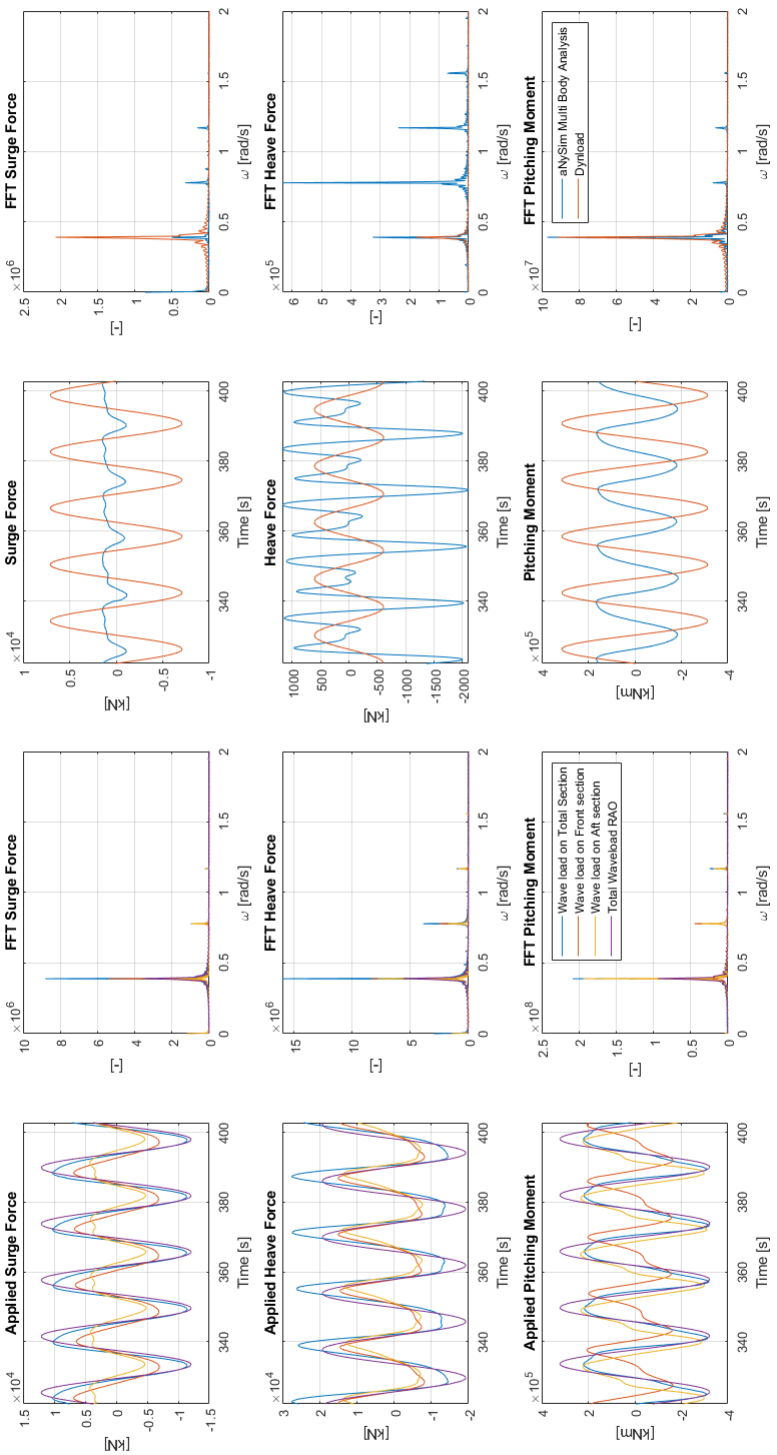

Figure 6.13: Applied wave loads obtained with captive ComlFLOW simulations (left) and Internal Load response response obtained with the aNySim Dual body model and Dynload at $T = 11,5\ m$(right)

6.3.2. Joint Stiffness

Based on the results described in section 6.2, dynamic excitation of the spring-damper system (i.e. the joint) seems to pollute the dynamic response. Therefore extra attention is given to the joint stiffness connecting the two bodies in the dual-body model. The stiffness and damping tested is derived from the internal loads and obtained with Dynload. Using the formula to compute the spring stiffness given in equation 6.3, the desired spring stiffness is calculated. In this formula k is the spring stiffness in $\frac{N}{m}$ or $\frac{Nm}{degree}$, F the force or moment amplitude and δ the maximal allowable displacement or rotation between the forward and aft section. In table 6.1, five different levels of string stiffness are presented. The corresponding natural frequencies of the joints are shown in table 6.2. It shows that the natural frequencies for the Weak and Medium joint are within the typical response frequency of the semi-submersible. For the stiff joint only the vertical natural frequency is within this range. The natural frequency of the two stiffest joint are out of the this range.

$$k = \frac{F}{\delta} \tag{6.3}$$

	δ			Corresponding spring stiffness		
	[Δx]	[Δz]	[$\Delta \phi$]	[N/m]	[N/m]	[Nm/degree]
Weak	1	1	1	$8.31 \cdot 10^{6}$	$8.61 \cdot 10^{5}$	$1.70 \cdot 10^{10}$
Medium	10^{-1}	10^{-1}	10^{-1}	$8.31 \cdot 10^{7}$	$8.61 \cdot 10^{6}$	$1.70 \cdot 10^{11}$
Stiff	10^{-2}	10^{-2}	10^{-2}	$8.31 \cdot 10^{8}$	$8.61 \cdot 10^{7}$	$1.70 \cdot 10^{12}$
Extra Stiff	10^{-3}	10^{-3}	10^{-3}	$8.31 \cdot 10^{9}$	$8.61 \cdot 10^{8}$	$1.70 \cdot 10^{13}$
Extra Stiff 2	10^{-4}	10^{-4}	10^{-4}	$8.31 \cdot 10^{10}$	$8.61 \cdot 10^{9}$	$1.70 \cdot 10^{14}$

Table 6.1: Joint stiffness of the 5 tested joints

	Natural Frequency		
	ω_x [rad/s]	ω_z [rad/s]	ω_{psi} [rad/s]
Weak	0.71	0.23	0.59
Medium	2.24	0.72	1.86
Stiff	7.10	2.28	5.88
Extra Stiff	22.45	7.23	18.61
Extra Stiff 2	70.99	22.85	58.84

Table 6.2: Natural Frequency of the 5 tested joints

The internal load response calculated with the different joint stiffness are shown in figure 6.14. The time traces including the response spectra are shown in figure F.1 up to and including figure F.4.

The surge force show a no large deviation in amplitude due the changing joint stiffness. Only the Weak joint shows a slightly deviating surge force response. The heave force is more influence by the joint stiffness. It is seen that an increase in joint stiffness causes an increase in higher harmonic response contribution. It also shows that the solutions are converging, as the increase for Stiff to Extra Stiff has hardly any influence. At the highest spring stiffness(not shown in this graph) the forces become ragged; due to the high spring stiffness peak forces start to occur in the internal load response, distorting the outcome. This is shown in figure F.4.

The pitching moment shows the same response for each of the different joints.

The internal load response is converging for an increase in spring stiffness, this means the pollution of the higher harmonic response components in the internal load can not be pinned on the setup of the joint stiffness. The higher harmonic response contributions will remain in the solution.

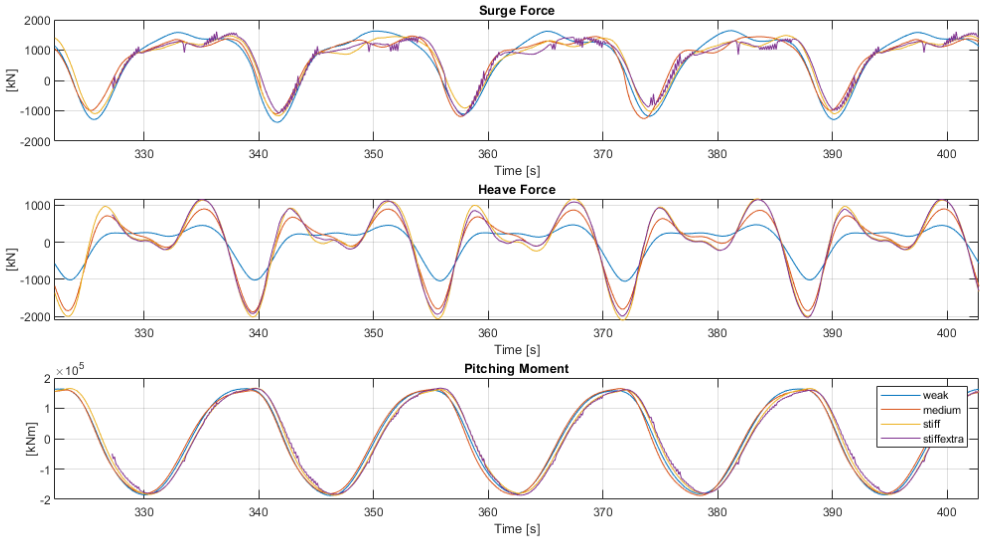

Figure 6.14: Internal load response with varying joint stiffness

All the tests mentioned above are conducted with a damping of 70% of the critical damping. Two tests have been conducted to analyse the effects of the damping. One test with a damping of 100% of the critical damping is conducted, and one test with a damping of 10% of the critical damping. The results of these two tests are shown in figure F.6 and figure F.7, respectively. Although the influence of a change in damping is limited, one thing is noticeable. The higher damping is reducing the response contribution at the higher harmonic frequencies. This is as expected, since higher frequencies yield higher relative velocities, these are damped more with higher damping ratios.

6.4. Conclusions

To perform a quantitative assessment of the impact of non-linear wave loading on the total internal load response, the time domain simulator aNySim is used in combination with wave loads obtained by captive CFD simulations in ComFLOW. It is shown that both the model at a deep draft and the model at an inconvenient draft are able to solve the motions of the semi-submersible in good agreement with the model tests and the linear diffraction solver. The internal loads obtained with this method still represent a challenge. In the deep 'linear' case the dual-body model provides a non-linear internal load response for the vertical load. This is even the case when the applied force and motions have a linear relation with the incoming wave, which means that there are higher harmonic response frequencies present where they should not be. This pollution of the response signal is also seen for the model at an inconvenient draft. The response at higher frequencies is much more dominant compared to the applied wave forces, and combined with the linear motions this cannot be correct. The higher harmonic wave frequencies in the internal loads should be less than in the applied wave loads, because the resulting motions are linear.

The dual-body model uses a joint (spring damper) to connect the two sections of the semi-submersible. The stiffness of this joint influences the higher harmonic response contribution. It was noticed that a weak joint will yield a linear response in case of the deep-draft model; however, this would mean that the relative motion of the two sections will become too large and would be in the order of meters. The solutions for simulations with increasing joint stiffness converge to a solution with a polluted higher harmonic response contribution. The damping of the joint has limited effects on the internal load solution. The amplitude of the response does hardly change and only the higher harmonic wave frequencies are damped slightly more when a high damping is used. A more elaborate study is needed to see whether the joint stiffness-damping can be set in such a way that the internal load can be calculated correctly. Or if the current method to extract the internal loads from the time domain simulator is the correct one.

7

Conclusion & Recommendations

The main problem that initiated this research is the lack of a method to calculate the internal loads at an inconvenient draft. The first objective was to obtain an insight into the effects of the non-linear wave loads on the internal loads of a semi-submersible at an inconvenient draft. The second objective was to set up a method which is able to approximate these non-linear internal loads. This chapter gives the conclusions and recommendations on both objectives. In the first section the conclusions are given and to finalize this thesis recommendations are given in the last section.

7.1. Conclusion

Due to a rapid change in water depth above the pontoons of the semi-submersible, energy from the wave frequency is transferred to the higher harmonic wave frequencies. This will result in waves on a higher harmonic wave frequency on top of the pontoons. The force response on the semi-submersible will thus consist of the wave frequency and the higher harmonic wave frequencies.

As there are waves at higher harmonic wave frequencies present above the pontoon at the inconvenient draft, the wave forces on the semi-submersible cannot be scaled linear with regard to wave height. This means linear potential theory calculates a non-physical response with large deviations from the responses found in the model tests. The CFD solver ComFLOW is able to simulate all the wave frequencies, including the higher harmonic components. This means that the solution of wave forces is in good agreement with model tests. The motions computed with the current version of ComFLOW are incorrect. During free-floating tests in ComFLOW, the wave loads are dominated by pressure peaks. This is used to solve the motion of the semi-submersible. As the wave loads are incorrect, the motions also deviate strongly from the motions obtained in model tests, which then results in an incorrect solution of the internal loads.

After extensive collaboration with the developers of ComFLOW the motions of the semi-submersible could still not be solved correctly. This resulted in a change of the plan of approach, the parameter study is conducted for a captive semi-submerisble and a quantitative assessment is made on the effects of the non-linear wave loads onto the total internal loads.

The first time that the higher harmonic response comes into play is at an operational draft, because the combination of the clearance between the pontoon top, the wave amplitude and wave length will influence the wave above the pontoon. When the Ursell number for the incoming waves above the pontoon top exceeds $U_r = \frac{H\lambda^2}{h^3} \leq \frac{32\pi^2}{3}$, the wave cannot be linear and energy is transferred to higher harmonic frequencies. An increase in wave amplitude will yield an increase in response contribution at a higher harmonic frequency; up to a maximum of 50% of the total response. A decrease in the water column above the pontoon and an increase in wavelength will also increase the higher harmonic response contribution. The higher harmonic response contribution is at its maximum when the free surface and draft fit in the range:$1 \leq \frac{\zeta_a}{T-H_{pontoon}} \leq 1.5$. A deeper draft or higher wave amplitude will cause the higher harmonic contribution to decrease. At a transit draft with $\frac{\zeta_a}{H_{pontoon}-T} \leq 1$ the response is again linear.

In order to obtain an insight into the higher harmonic response contribution due to the non-linear wave loads, a quantitative analysis is made. Using the wave loads obtained with the captive simulations in the CFD solver ComFLOW and the time domain simulator aNySim, the internal loads are calculated. It was found that the motions can be calculated in good agreement with model tests. The internal loads still present a challenge; for the 'linear' deep-draft model the provided calculation method shows higher harmonic response frequencies, whereas the expected solution should provide a solution with a linear relation to the incoming wave. In case of the inconvenient draft, the higher harmonic response contribution is larger than the applied contributions. In this case, the motions of the semi-submersible are linear; in other words, the total higher harmonic contribution cannot be larger in the internal loads compared to the applied wave loads. This might be caused by the way these models are set up with the spring damper measuring the internal loads. The stiffness of this joint has an influence on the higher harmonic contribution in the internal load response.

This mean the influence of the non-linear wave loads on the internal loads of a semi-submersible is unfortunately still not solved and the final goal of this research is not met.

7.2. Recommendations

To finalize this thesis recommendations are made to improve the current knowledge on the higher harmonic response contribution on the internal loads of a semi-submersible at an inconvenient draft.

- Model tests should be conducted to obtain the internal loads of a semi-submersible at an inconvenient draft. Model tests are not available at the time of this study and hence no direct validation is possible. During these model tests the internal loads should be measured on a semi-submersible at a deep draft and at the inconvenient draft. This would be of value for the validation of the CFD simulations and the quantitative analysis model.
- Conducting a parameter study for free-floating semi-submersibles. Currently the parameter study is conducted on captive tests as the motions of a free-floating semi-submersible could not be solved correctly. A free-floating parameter study would provide more insight into the combined problem of diffraction and radiation, as well as proving insight into the propagation of higher harmonic waves over the moving pontoon top. This might be done with a future version of ComFLOW in which the motions can be solved correctly or with a different CFD solver such as STAR-CCM+®.
- The effect of the interaction between the standing waves between the pontoons of the semi-submersible and the higher harmonic waves is as yet unknown, as are the effects on the higher harmonic response contribution. A more detailed research in these phenomena could decouple the effects from standing waves and higher harmonic waves resulting from the inconvenient draft.
- The effect of the non-linear hydrostatics. Due to the rapid change in water plane area the still water spring stiffness is non-linear. This can be implemented in the current model used in the quantitate analysis with a non-linear hydrostatic solver.

Bibliography

[1] American Bureau of Shipping. Rules for Building and Classing Mobile Offshore Drilling Units, 2015.

[2] J. A. Battjes and S. Beji. Spectral evolution In waves traveling over a shoal. In *Nonlinear Water Waves Workshop*, University of Bristol, 1991. URL `http://resolver.tudelft.nl/uuid:f837312b-1acc-4fa7-8f37-4b0ef821edde`.

[3] Simon Burmester, Sébastien Gueydon, Guilherme Vaz, and Bettar El Moctar. Surge decay simulations of a semi-submersible floating offshore wind turbine. 10 2017.

[4] Xing Chang, Ido Akkerman, Rene H M Huijsmans, and Arthur E P Veldman. Generating and Absorbing Boundary Conditions for Combined Wave-Current Simulations. In *12th International Conference on Hydrodynamics*, number September 2016, pages ID53 1–8, Delft, 2016.

[5] Rogier de Bruijn, Huijs Fons, Rene H.M. Huijsmans, Tim Bunnik, and Marc Gerretsma. Calculation of Wave Forces and Internal Loads on a Semi-Submersible at Shallow Draft using an IVOF Method. In *ASME 2011 30th International Conference on Ocean, Offshore and Arctic Engineering*, Rotterdam, 2011.

[6] J. de Weerd. Design of a Semi-Submersible Pladfrom for West-Africa (including modeltests). *Bsc Thesis*, 2004.

[7] S. E. Hirdaris, W. Bai, D. Dessi, A. Ergin, X. Gu, O. A. Hermundstad, R. Huijsmans, K. Iijima, U. D. Nielsen, J. Parunov, N. Fonseca, A. Papanikolaou, K. Argyriadis, and A. Incecik. Loads for use in the design of ships and offshore structures. *Ocean Engineering*, 78:131–174, 2014. ISSN 00298018. doi: 10.1016/j.oceaneng.2013.09.012.

[8] Leo H. Holthuijsen. *Waves in Oceanic and Coastal Waters*. Cambridge University Press, 2010. ISBN 9780123821003.

[9] Koichiro Iwata, Koji Kawasaki, and Do-sam Kim. Breaking Limit, Breaking and Post-Breaking Wave Deformation Due Bottom seated (Type I) Tautly-moored. In *25th International Conference on Coastal Engineering*, pages 2338–2351, Florida, 1996.

[10] Roel Luppes, Peter van der Plas, Bogdan Iwanowski, Tim Bunnik, Bulent Duz, Henri van der Heiden, Rik Wemmenhove, Peter Wellens, Arthur Veldman, Theresa, Helmholt-Kleefsman, Erwin Loots, and Joop Helder. Manual comflow version 3.9.x / 4.0, 2015.

[11] MARIN. aNySim. URL `https://www.marin.nl/publication/anysim-a-versatile-hydrodynamics-engineering-tool`.

[12] Michigan Institute of Technology. WAMIT - User Manual, 2019.

[13] Harald Ottens and Alessio Pistidda. Motion RAOS of a SSCV at Deep and Inconvenient Draft Using CFD. In *ASME 2015 34th International Conference on Ocean, Offshore and Arctic Engineering*, St. John's, 2015.

[14] Harald Ottens, Alessio Pistidda, and Radboud van Dijk. CFD Analysis of Waves Over a Submerged Cylinder in Close Proximity of the Free Surface. In *ASME 2014 33rd International Conference on Ocean, Offshore and Arctic Engineering*, volume 33, San Francisco, 2014.

[15] Zhiyong Pei, Shenyi Wu, Keqiang Chen, Xiaoming Hu, and Weiguo Wu. A Comparative Research on Computation Methods for Wave Loads of Semi-Submersible Platform. In *Proceedings of the ASME 2018 37th International Conference on Ocean, Offshore and Arctic Engineering*, Madrid, 2018.

[16] Ashkan Rafiee and Alireza Valizadeh. Non Linear Hydrodynamics of Bluff Bodies Oscillating Near Free Surface. In *Proceedings of the Twenty-eighth (2018) International Ocean and Polar Engineering Conference*, pages 307–315, Sapporo, 2018. ISBN 9781880653876.

[17] José Miguel Rodrigues and C Guedes Soares. Ship Vertical Loads From Using an Adaptive Mesh Pressure Integration Technique for Froude-Krylov Forces Calculation. In *ASME 2017 36th International Conference on Ocean, Offshore and Arctic Engineering*, volume 36, Trondheim, 2017.

[18] Peter van der Plas. *Local grid refinement for free-surface flow simulations*. PhD thesis, University of Groningen, 2017.

[19] J.J. van der Vegt. Slinger gedrag van Schepen. *KIVI-Lecture on seakeeping*, 1984.

[20] J.A. van Santen and G.J. Schepman. Structural Assessment of Floating Mobile Units - A Designers Point of View. In *8th International Conference on Offshore Mechanics and Arctic Engineering*, The Hague, 1989.

[21] Ivan van Winsen, Job S Bokhorst, and Rene H.M. Huijsmans. Calculation of Wave Height Dependent Force Rao ' S on Submerged Bodies in Close Proximity to the Free Surface. In *ASME 2013 32nd International Conference on Ocean, Offshore and Arctic Engineering*, Nantes, 2013.

[22] T.G. Vos, Rene H.M. Huijsmans, J. den Haan, Ivan van Winsen, and Radboud van Dijk. *Motion Analysis of a Semi-Submersible Crane Vessel at Inconvenient Draft - A Flooding Tank Approach*. PhD thesis, Delft University of Technology, 2015.

A

Literature study

In this part of the research thesis multiple papers with respect to this topic are discussed, the papers discussed in this part range from closely related topics to slightly broader applicable topic. Each of these papers has attributed in the scientific knowledge or theoretical background on which this thesis is build on. For all papers a small introduction is given and the main conclusions that can be used in the research are discussed. This section is split up into 4 different subjects, first of all multiple researches are discussed, in which CFD is used to compute the forces, motions or internal loads of floating object in close proximity to the free surface. Next two papers on improving linear potential theory to solve higher order responses are shown and discussed. The third part will elaborate the research conducted on the internal loads of a semi-submersible. To finalize this literature study, two papers on non-linear wave loads on submerged structures will be elaborated.

Computational Fluid Dynamics

In this part the most important paper is first described, as this is a direct predecessor of this research. Next three researches on solving motion and force RAOs on a cylinder and on a semi-submersible are shown. Finally, a paper on the hydrodynamic coefficients of a cylinder in close proximity to the free surface is described. In all of these papers, the results will be compared with the results for linear diffraction solvers.

Calculation of Wave Forces and Internal Loads on a Semi-Submersible at Shallow Draft using an IVOF Method by R. de Bruijn et al (2011).[5]

One of the most important papers from literature is written by Rogier de Bruijn in 2011 and is a direct predecessor of this research. The paper describes the non-linear effects that influence the internal loads of a semi-submersible at an inconvenient draft. An assessment is made on the feasibility of the linear diffraction and a CFD method, to determine the non-linear effects. The CFD solver that is used in this research is ComFLOW, the linear diffraction solver is WAMIT.

There are two main parts in this research, in the first part the wave loads of a fixed semi-submersible in regular waves are analysed, the results are compared to model test results. Secondly the internal loads are assessed of a free floating semi-submersible. The semi-submersible gets a prescribed motion which is obtained from a linear diffraction solver, as at that time ComFLOW was not able to solve for the motions of an object in waves. In both parts the semi-submersible is assessed for an operational and an inconvenient draft.

For the wave forces on a fixed semi-submersible a good comparison is shown, between the linear diffraction solver, ComFLOW and the model test when at a deep draft. Almost no non-linear wave effects are present at this draft. It is shown that for an inconvenient draft, the wave forces of the model test show a phase shift compared to a model test at a deep draft. The maximum force that is exerted is a few seconds later compared to the maximum wave elevation. This phase shift increases with an increasing wave height and can be related to the non-linear flow above the pontoon. As the diffraction solver does not solve the non-linear effects that cause this phase shift, the phase shift is not present in the wave force results. For strong non-linear situations the amplitude of the wave force are underestimated by the linear diffraction solver compared to the fixed model test. ComFLOW however

has a has a better approximation but is still off in some parts of the wave cycle, as can been seen in figure A.1. One final remark is made on this part, stating that only regular waves are assessed, no irregular waves. Further investigation into the irregular waves is needed.

In the second part where the semi-submersible is given a prescribed motion, the internal loads on the aft section are assessed. In this case F_x and M_y. As there are no model test which have measured the internal loads, only the internal forces obtained by linear diffraction and ComFLOW can be compared. For the simulations at the deep draft both F_x and M_y are in good agreement with each other, however for the inconvenient draft, the internal forces differ. The phases are in general correct but the ComFLOW calculations show for both the forces as the moment a lower amplitude. R. de Bruijn states that the semi-submersible is moving along with the waves, thereby the non-linear effects are reduced and are less present than the non-linear effects in case of the fixed semi-submersible. Two other remarks are made on this second part, firstly is the lack model test for the internal loads, so the findings for the semi-submersible with a prescribed motion can not be validated. Finally the prescribed motion itself, as ComFLOW at that time was not able to solve for the motions, the motions were prescribed, this causes an unrealistic flow around the pontoons and will influence the outcome of the simulations. As ComFLOW is now able to solve the motions of a floating object in waves this last problem can be solved.

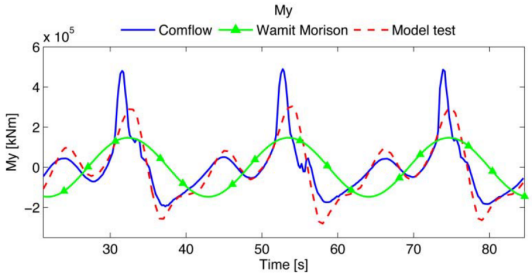

Figure A.1: Wave load M_y on a fixed semi-submersible (R. de Bruijn et al.(2011) [5])

Calculation of Wave Height Dependent Force RAO's on Submerged Bodies in Close Proximity to the Free-Surface by I. van Winsen, J.S. Bokhorst and R.H.M. Huijsmans. (2013) [21]

As a user of semi-submersible crane vessels (SSCV), Heerema Marine Contractors has conducted multiple researches with respect to the inconvenient draft. One of their papers is written by I. van Winsen and is a more fundamental paper on a cylinder in close proximity of the free-surface, without free-surface penetration. The paper starts with a mention of model tests for various wave spectra (on a submerged cylinder and a model SSCV), the outcome of these test were compared with the outcome of a linear diffraction solver and showed an over prediction of the motion RAOs for the linear diffraction solver. In this research a parameter study is conducted to get a better understanding why the linear diffraction solvers over predict the force and motion RAOs in heave direction. With this outcome a method is created to calculate the wave height dependent force and motion RAOs of a submerged body in close proximity of the free surface.

In the parameter study the diameter and the submergence is varied, next the forces on the top and bottom of the cylinder were decoupled to assess which plane has the most influence on the over prediction. This study showed that the over predictions of force RAOs were caused by a large water column above the cylinder which causes a high pressure on the top of the cylinder. This phenomena is caused by a pumping mode on top op the cylinder, that decreased in height and pressure if the cylinder submergence was increased.

To cope with this problem a dampening lid is introduced, which would decrease the severity of the pumping mode. With this dampening lid the peak period and amplitude of the RAOs decreased, but still not enough. So two two setups are suggested to predict the wave height dependable RAOs. For these setups it is stated that the assumption of a constant submergence height above the cylinder is not valid for regular wave heights, as is assumed in linear diffraction theory. The first setup is based on regular waves to calculate the time varying RAO signals over a wave cycle, this is integrated over time to obtain a time average force RAO for each frequency component. The second setup uses the wave spectrum with a set wave height and peak period to calculate the force signal.

To compare the methods, three wave spectra are used with a different significant wave height. At each spectra the peak period is kept the same whilst the significant wave height is varied for a value of Hs=1m, 2m and 4m. For a small wave height Hs=1, the dampening lid model and both of the setups are a better fit on the model test compared to the linear diffraction theory. For larger wave heights Hs=2m and 4m, the dampening lid calculation is starting to differ more and more, whilst the results

of the two setups presented are still close to the model test results. For a deeper submergence the setups presented are still in good arrangement with the model tests whilst the dampening lid gives a slight under prediction of the heave force. For even deeper submergence's, all models are in good agreement, as almost no non-linearity's are present in the movements. The linear diffraction solver is also able to solve the heave force RAO with a good arrangement to the model tests.

CFD Analysis of Waves Over a Submerged Cylinder in Close Proximity of the Free Surface by H. Ottens, A. Pistidda and R. van Dijk.(2014) [14]

As a follow-up on the study from I. van Winsen, H. Ottens also from Heerema Marine Contractors performed a study on a fixed cylinder in close proximity of the free surface in a CFD solver, also without free-surface piercing motions. In this study the wave effects on the cylinder for different wave heights, periods and different submerged drafts are assessed. The study is started with a assessment of the numerical setting on the wave propagation. Parameters like: turbulence, laminar and a inviscid flow are assessed and evaluated as these have a large influence on the computational time of the simulations. After simulations with model-scale turbulence, full-scale turbulence and an inviscid model it is shown that the results are almost identical. It is concluded that a inviscid flow is good enough to simulate the cylinder, this causes a reduction in computational time as the turbulent equations does not needs to be solved and no boundary layer mesh is needed.

With the CFD solver the process of one wave cycle is analysed. The heave force on the cylinder is at its maximum when there is a trough on the wave surface, as a small water column is present on top of the pontoon, resulting in a low pressure. As the water column start to increase the pressure beneath the cylinder increase. This force is at its maximum just before the wave brakes. The minimum heave force occurs if the wave crest is passing the cylinder. Another remark is pointed out, as the maximum heave force for both a 1m wave as a 4m wave are in absolute numbers almost the same and thus it is not linear dependable on the wave height. The minimum wave height shows more of a correlation between the force and the wave height, however not a factor of four as expected in linear theory.

If the model tests with the CFD calculations for regular waves are compared, multiple conclusions can be drawn. First for a wave height of 1 meter, the surge RAO almost shows a linear dependency, only a deviation occurs at the peak value. The heave RAO a has larger deviation and is non-linear with respect to the wave height. The CFD calculations show wave height dependable results, however the results are under predicted compared with the model tests heave force RAO. Different submergence depths are also compared, this showed a lower surge RAO for a deeper submergence. This also caused the peak period to shift to longer periods. The CFD program used is able to capture this behaviour. The heave RAO gave to low of a result for a submergence of 1m whist for the deeper submergence's this becomes a over prediction but stays within a 15% difference of the model-test results. The regular wave part is concluded by stating the CFD solver gives a good results and is able to predict the wave height dependable RAOs to an acceptable level.

The next step in the research is the response on a irregular wave. Three simulations are conducted with a Hs of 1m, 2m and 4m all with a duration of 20 minutes to obtain a good insight in the irregular wave response. The overall results of the CFD calculations shows a nice fit to the model test results. The heave force RAO are within 10% of the model tests, for the surge there is less of a fit as the ROA shows a peak which is not present in the model test result. This increases the difference to 20%. The rest of the RAO surge is within a 10% difference.

Motion RAOS of a SSCV at Deep and Inconvenient Draft Using CFD by H. Ottens and Alessio Pistidda.(2015) [13]

After his research on a cylinder H. Ottens extended the research to a SSCV's. Together with Alessio Pistida they tried to solve the motions with the CFD solver STAR-CCM+ and with an Euler Overlay Method. This method is used to force a certain wave on the outsides of the domain and to counter wave reflection. With a relative small simulation of 10 wave cycles and using Discrete Fourier Transformation (DTF) filtering, the time series from the CFD solutions could be used to create the motion RAOs.

With this method the motion response at a deep draft is calculated and analysed. The calculated heave RAO is in good agreement with the linear diffraction results. Same holds for the pitch RAO, however the roll RAO for a semi-submersible in deep water does not coincides with the results for linear diffraction theory. The roll motion is more damped in the CFD result compared with the diffraction theory. This part is concluded with thee remarks. First it is concluded that this CFD tool is suitable to

calculate the motion RAOs of an SSCV in regular waves. Secondly, the pitch and roll RAO are non-linear with respect to the wave heights. Thirdly, the difference between the linear diffraction solver and the model tests could be caused by non-linearity's.

In the second part the motion RAOs for a SSCV at the survival draft are solved. With 3 meters of water above the pontoons. The paper shows that the CFD calculations show similar trends as in the model tests for the pitch and the heave motion. In both the pitch and heave RAOs are the over prediction in the linear diffraction solver at the natural frequencies not visible in the results from the CFD solver. For the roll motion the trend is the same as in the model test, only the amplitude is still to high. It is shown that increasing the wave height results in non-linear RAOs(wave height dependable). Finally, it is stated that the difference between the linear diffraction solver and the model tests could come from the non-linear responses in high waves.

Non Linear Hydrodynamics of Bluff Bodies Oscillating Near Free Surface
by A. Rafiee and Alireza Valizadeh.(2018) [16]
A fundamental paper on the diffraction/radiation problem of objects near the free-surface is written by Ashkan Rafiee and Alireza Valizadeh. The difference in hydrodynamic radiation coefficients (added mass and added damping) are studied in both a linear diffraction solver as in a fully non-linear CFD solver. For the fully non-linear method it uses OpenFOAM, an open source CFD toolbox with a turbulence model.

In the study a cylinder with a prescribed motion in close proximity of the surface is used. For heave, surge and pitch the different hydrostatic components are analysed. For the heave motion both the trend for the added mass as the added damping are coinciding for the linear and non-linear result, but in both cases has the linear solver a higher peak value. If the heave force is plotted against the frequency of the oscillation, it can be seen that a second order harmonic force is present. This is caused by the formation of a jet when the cylinder is moved upwards. For the surge motion the linear and the non-linear solution are almost the same. In a surge oscillation the free-surface above the cylinder is less influenced compared to the heave oscillations and thus less non-linear effects are visibly. This can also been seen if the surge force is plotted with respect to the oscillation frequency, as only one distinctive peak is present in the spectrum. The least correlation between the linear and non-linear calculations is with the pitch motion. This motion has the most influence on the free-surface and in some cases even penetrates the free-surface. In case of the added mass is the distinctive peak around the natural period not visible in the non-linear calculations, whilst for the linear calculations it is clearly visibly. For the added damping the peak value is only half the peak value of the linear calculations. The existence of non-linear effects can be clearly seen in the frequency plots, as multiple peaks can be distinguished.

A final remark is made on the amplitude of these forced oscillations, if the amplitude for the heave and pitch motion increases the difference between the linear and non-linear results will increase. Whilst a increase in amplitude of the surge motion gives less deviation.

Linear Potential Solver

In this part two researches are described, in the first one a linear diffraction solver with a non-linear ad on is shown. It solves the wave induced forces on the wetted hull taking the instantaneous free surface in account. The second research is on a method to solve the motions of a semi-submersible at a shallow draft by modelling free flooding tanks on top of the pontoons.

Ship Vertical Loads From Using an Adaptive Mesh Pressure Integration Technique for Froude-Krylov Forces Calculation by J.M. Rodrigues and C.Guedes Soares.(2017) [17]
In the paper of J.M. Rodrigues and C. Guendes Soares a research is conducted on a linear radiation and linear diffraction pressures on a quad-tree driven adaptive mesh. With these pressures the Froude-Krylov forces and the vertical bending moment RAO are computed. In the introduction of the paper a reverence is made to another article in which the six levels from linear to complete non-linear are described. This is written in an article of S.E. Hirdaris (2014) [7]. The six levels are described as follows:

1. Linear
2. Froude-Krylov non-linear
3. Body non-linear
4. Body exact - Weak Scatterer

5. Fully non-linear - Smooth waves
6. Fully non-linear

The paper of J.M. Rodrigues is a method for to solve for the level 2 non-linear Froude-Krylov forces. Use is made of WAMIT, a linear diffraction solver. Instead of solving the oscillating pressure on the compete hull, it is solved for each panel. This is done by subtracting the incident wave potential from the diffraction potential to obtain the scattering pressure at each panel. This results in the hydrostatic and undisturbed wave forces each time step and on the adaptive mesh which takes care of the instantaneous wave height.

This method predicts a lower dynamic vertical bending moment RAO compared to linear diffraction theory, and compared to the model test in frequency domain a closer fit.

Motion Analysis of a Semi-Submersible Crane Vessel at Inconvenient Draft - A Flooding Tank Approach by T.G. Vos.(2015) [22]
In another research of Heerema a method is developed by T.G. Vos to capture the motion behaviour of a SSCV at the inconvenient draft. In this approach a free flooding tank on top of the pontoons is modelled. At each time step in the numerical calculation the amount of water in the free flooding tank is calculated, this causes a static force on top of the pontoons, that depends on the amount of water in the tank. To calculate the diffraction and radiation forces a linear diffraction solver is used.

In the first step a fixed cylinder in close proximity of the free-surface with a free-flooding tank on top is modelled. In these simulations is was found that the model is able to capture the force RAO for certain submergence's, however for submergence's where a pumping mode occurred on top of the cylinder the model overestimated the forces. The test on the cylinder is concluded by stating the model is not able to cope with the wave height dependability of the forces, as this influences the pumping mode on top of the cylinder. After the cylinder, the free-flooding tank model is tested on a SSCV, these test are concluded with stating that the model is not able to compute the non-linearity's that occur at the inconvenient draft. However the calculated force RAOs are closer to the model tests, compared with the standard linear diffraction solver WAMIT.

Internal Loads

In this part two researches are described, the first one gives a overview of the critical wave directions and wave lengths for a semi-submersible. The second paper describes a method which couples the linear diffraction results to a finite element method to solve the internal loads.

A Comparative Research on Computation Methods for Wave Loads of Semi-Submersible Platform by Zhiyong Pei et al.(2018) [15]
In general this paper compares three different methods to design for wave loads, this is not within the scope of this research. However, it gives a nice overview of the internal loads for a semi-submersible and which wave lengths/directions give the highest loads. All this is summed in table: A.1. This table is based on the ABS, Rules for Building and Classing Mobile Offshore Drilling Units. (2015) [1]

Structural Assessment of Floating Mobile Units - A Designer Point of View by J.A. van Santen and G.J. Schepman. (1989) [20]
In this research a structural analysis method is presented which combines the hydrodynamics, motions and structural response of a semi-submersible in waves. It uses a linear diffraction solver and the forces on the wetted-hull are determined. The structure is modelled by membranes that are able to distribute these forces throughout the structure. Eventually the target of this method is to determine the internal structural stress variation of floating structures caused by waves.

To calculate the dynamics forces acting on the semi-submersible, the wave induces motions of the vessel should be calculated first. The dynamic forces are split up into three parts. First the inertia forces, to calculate these inertia forces the semi-submersible is modelled as a large amount of masses. In this case the correct mass en moment of inertia can be obtained. In combination with the correct motions from the diffraction solver, the dynamic inertia forces can be obtained. The second dynamic forces are the gravitational forces, as the pitch and heel of the vessel influence the direction of this force, it is implemented in the same way as the inertia forces. Thirdly, the hydromechanic forces. These can also be split into three forces, hydrostatic, radiation and diffraction forces. These three hydromechanic

Characteristic Response	Main control members	Critical Waves
Split Force	Horizontal bracing bear the maximum axial force	A beam wave with a length of tow times the breadth
Twisting Pitch Moment	Diagonal bracing bear the maximum axial force	A diagonal wave with a length of about the diagonal distance
Longitudinal Shear Force	Horizontal bracing bear the maximum bending moment	A diagonal wave with a length of about one and half times the diagonal distance
Vertical Wave Bending Moment	Pontoon bear the maximum bending moment	A head wave with a length of about the pontoon length
Longitudinal Accelerations	Columns bear the maximum bending moment and shear force	The critical direction are Head sea's
Transverse Accelerations	Diagonal bracing bear the axial force, columns bear the maximum bending moment and shear force	The critical direction are Beam sea's

Table A.1: Table from Z. Pei et al.(2018) [15]

forces can be simply summed using the correct phase shift. These three dynamic forces are coupled with a Finite Element (FE) model to compute the stresses throughout the structure.

To verify the results the internal loads are compared with model tests, this shows a good agreement between the two. For the transverse forces, vertical forces and longitudinal moments the results are in good agreement. The research states that at survival draft a large wave height is the limiting factor (deckbox impact). Whilst for the transit draft its the shear forces in the deck to column connection.

Waves over submerged structures

Breaking Limi, breaking and Post-breaking wave deformation due to submerged structures by K. Iwata, K. Kawasaki and D. Kim [9]

A paper initially targeted for the field of civil engineering, but of great importance on the physical understanding on the fluid behaviour above the pontoons. The main target of the paper is a experimental en numerical investigation on the breaking limit, breaking and post-breaking wave deformation due to submerged structures. Three types of structures are analysed: bottom seated, fixed-non-bottom seated and tautly-moored, each of which is analysed on multiple variations of the dimensions. First the breaking limit, breaking type, breaking position and breaking zone length are discussed. After which the most important part for this research is stated, the generation of high harmonic wave components. It is stated that the fundamental harmonic wave component increases in front of the submerged structure and decreases on the aft side of the submerged structure. This is caused by the wave energy dissipation due to the breaking of waves. Much more important is the occurrence of higher harmonic wave components above the structure. Due to the wave energy transfer from the fundamental harmonic component to the higher harmonic wave components caused by the nonlinear interaction between the waves and the submerged structure. In this paper four different submerged structures are shown, each of these structures causes a different distribution of wave components. Wave components until the 5th harmonic wave frequency are measured in the experiments, the second and third harmonic components show a significant contribution. This gives the indication that the linear relation of the response is caused by a higher harmonic wave pattern above the pontoons, as this causes higher harmonic wave forces on the structure the linear relation with respect to the incoming wave is lost.

B

Model Test Setup

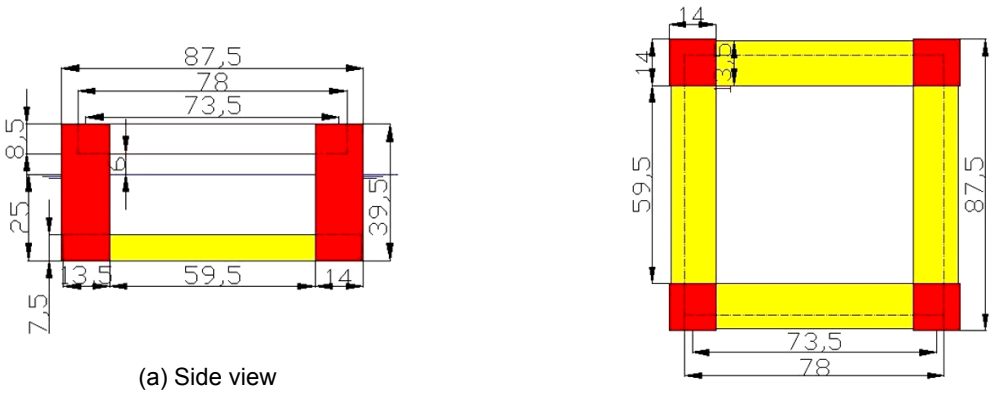

(a) Side view

(b) top-down view

Figure B.1: Dimensions of model tests (centimeters)

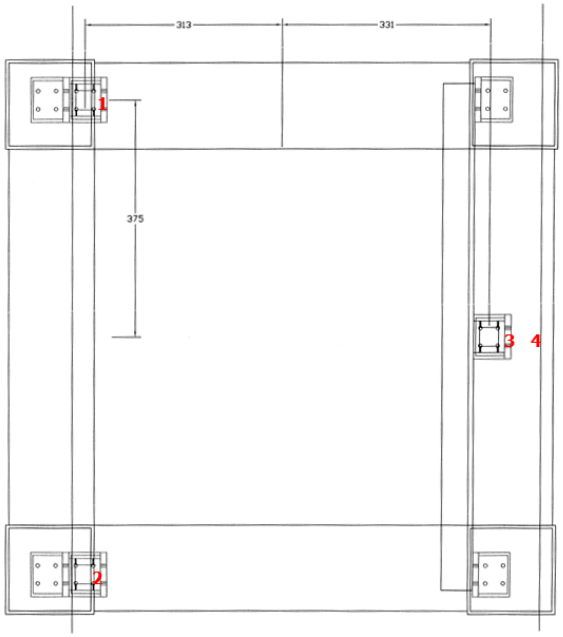

Figure B.2: Position of force sensors - vertical sensors 1,2,3 - horizontal sensor 4.

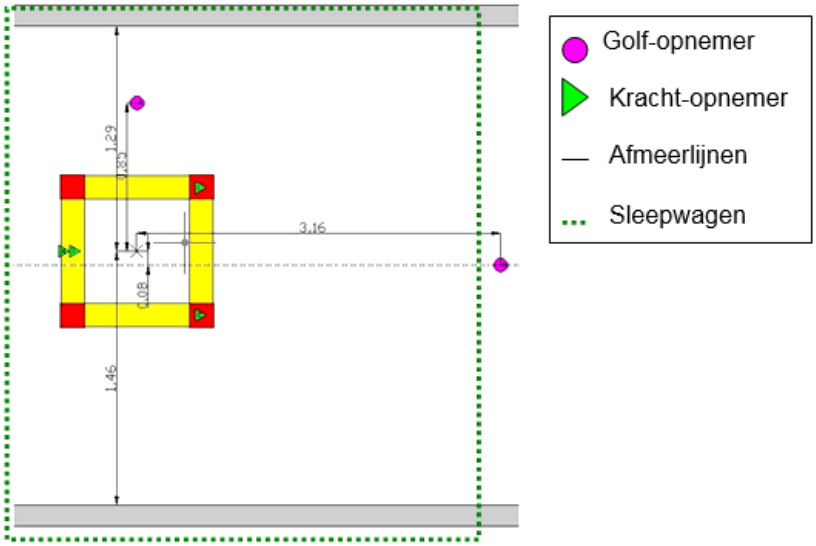

Figure B.3: Setup of Captive test (in meters)

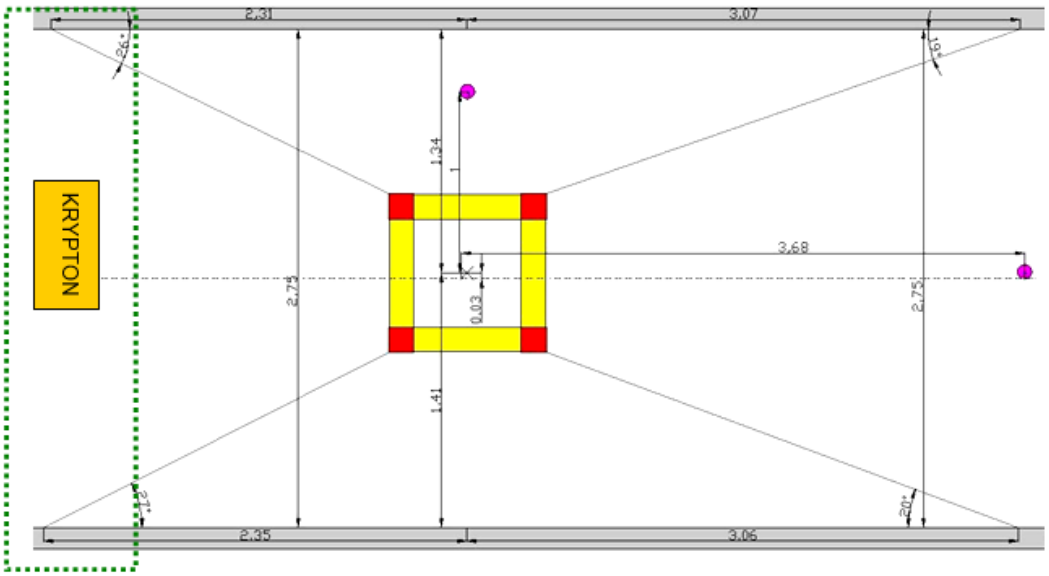

Figure B.4: Setup of Free Floating test (in meters)

C

Figures Comparison Modeltests, Linear Diffraction and Computational Fluid Dynamics

C.1. Model Test

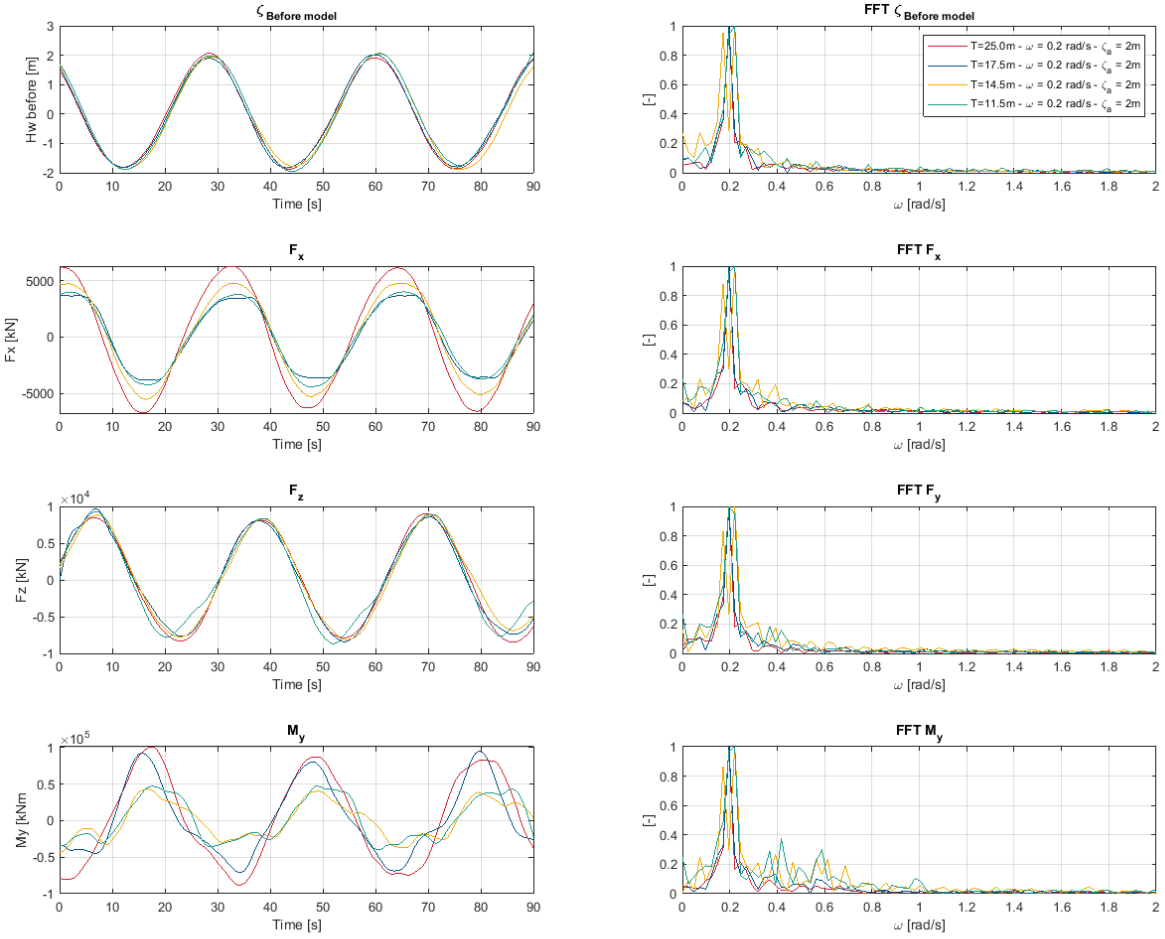

Figure C.1: Model test data at $T = 25,\ 17.5,\ 14.5,\ 11.5\ m$ with $\omega = 0.2\ rad/s$, $\zeta_a = 2\ m$

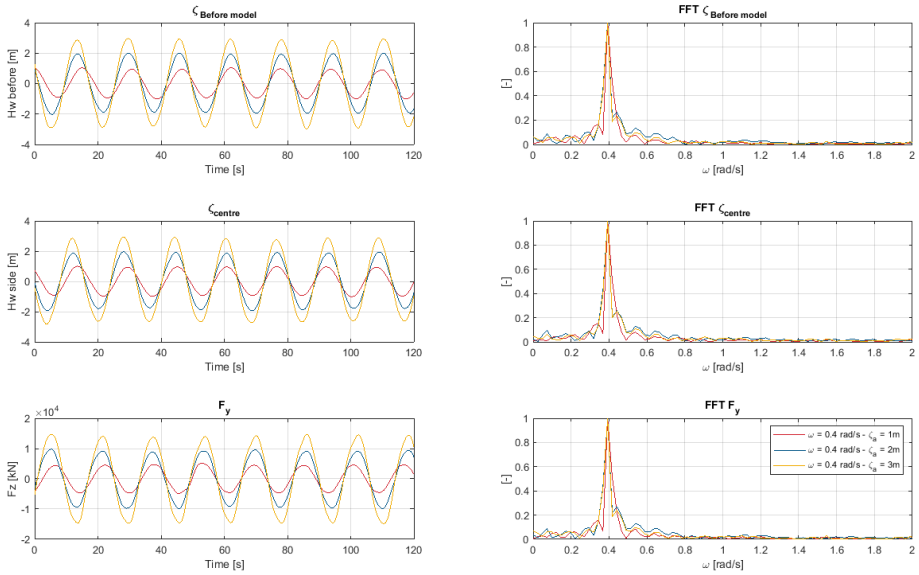

Figure C.2: Model test data at $T = 25\ m$ with $\omega = 0.4\ rad/s$, $\zeta_a = 1, 2, 3\ m$

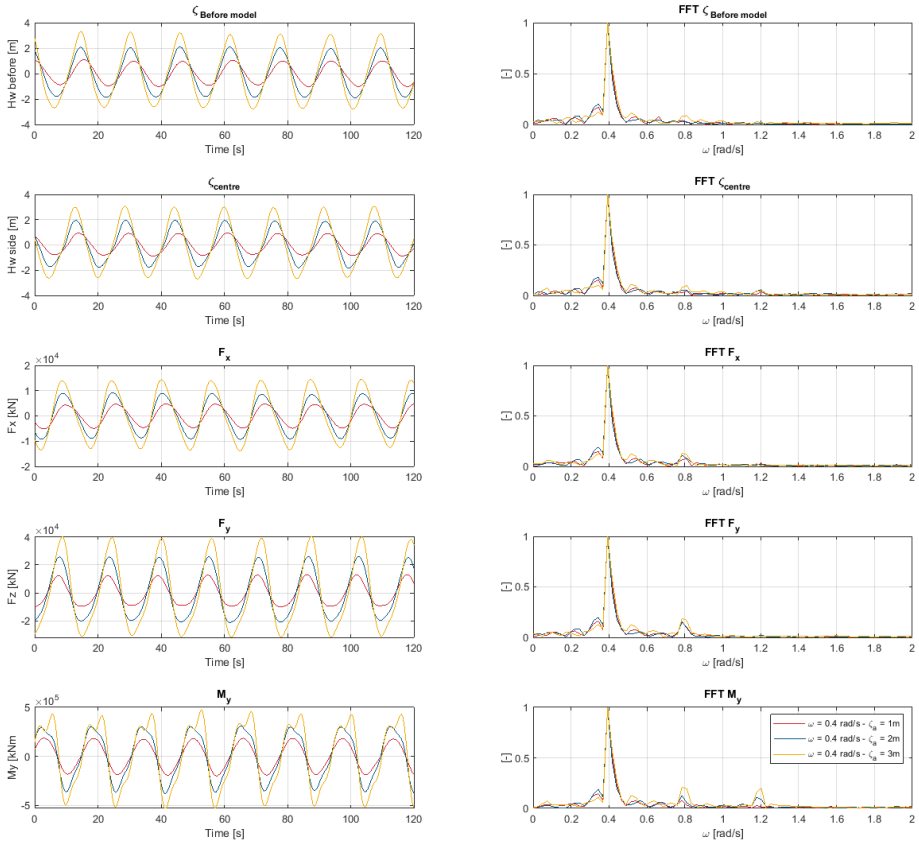

Figure C.3: Model test data at $T = 11.5\ m$ with $\omega = 0.4\ rad/s$, $\zeta_a = 1, 2, 3\ m$

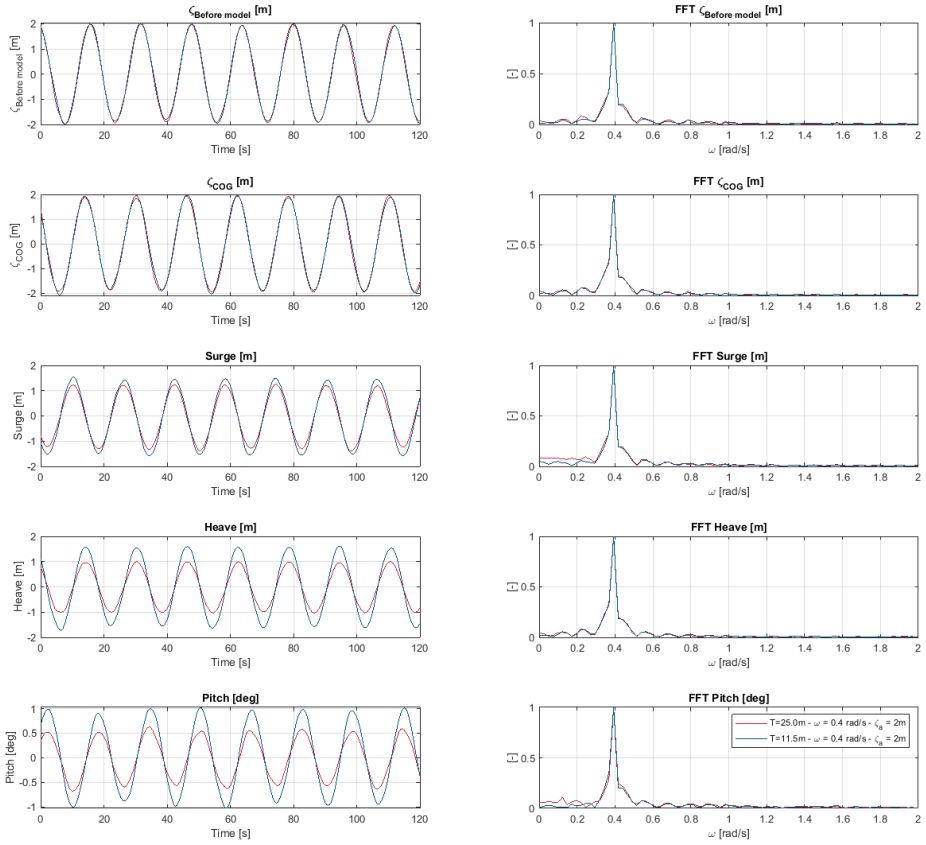

Figure C.4: Model test data at $T = 25,\ 11.5\ m$ with $\omega = 0.4\ rad/s$, $\zeta_a = 2\ m$

C.2. Numerical Solvers

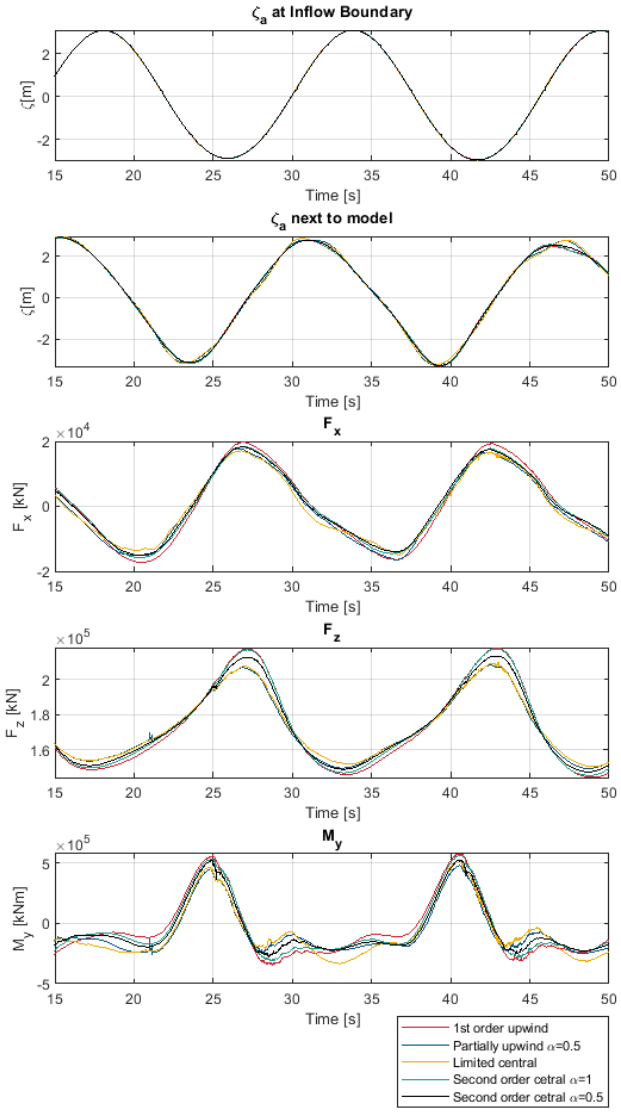

Figure C.5: Convection schemes

C.3. Wave simulations

Table C.1: Absolute values for different number of cells per wavelength

	Required Input		Inflow Boundary		Middle of domain	
	$Period[s]$	$\zeta_a[m]$	$Period[s]$	$\zeta_a[m]$	$Period[s]$	$\zeta_a[m]$
$\lambda/30\ h_w/10$	7.923	1.7127	7.922	1.7995	7.594	0.8819
$\lambda/60\ h_w/10$	7.923	1.7127	7.924	1.8193	7.905	1.7017
$\lambda/120\ h_w/10$	7.923	1.7127	7.924	1.8201	7.913	1.7376
$\lambda/240\ h_w/10$	7.923	1.7127	7.924	1.8190	7.914	1.7657

Table C.2: Absolute values for different number of cells per wave height

	Required Input		Inflow Boundary		Middle of domain	
	$Period[s]$	$\zeta_a[m]$	$Period[s]$	$\zeta_a[m]$	$Period[s]$	$\zeta_a[m]$
$\lambda/120\ h_w/4$	7.923	1.7127	7.924	1.8201	7.914	1.7316
$\lambda/120\ h_w/8$	7.923	1.7127	7.924	1.8200	7.913	1.7333
$\lambda/120\ h_w/12$	7.923	1.7127	7.924	1.8201	7.914	1.7418
$\lambda/120\ h_w/16$	7.923	1.7127	7.924	1.8203	7.914	1.7486

Table C.3: Absolute values for different number of cells with a fixed aspect ratio

	Required Input		Inflow Boundary		Middle of domain	
	$Period[s]$	$\zeta_a[m]$	$Period[s]$	$\zeta_a[m]$	$Period[s]$	$\zeta_a[m]$
$\lambda/60\ h_w/4$	7.923	1.7127	7.924	1.8190	7.909	1.6595
$\lambda/120\ h_w/8$	7.923	1.7127	7.924	1.8200	7.913	1.7333
$\lambda/240\ h_w/16$	7.923	1.7127	7.924	1.8194	7.917	1.7724

C.4. Comparing Captive Wave loads

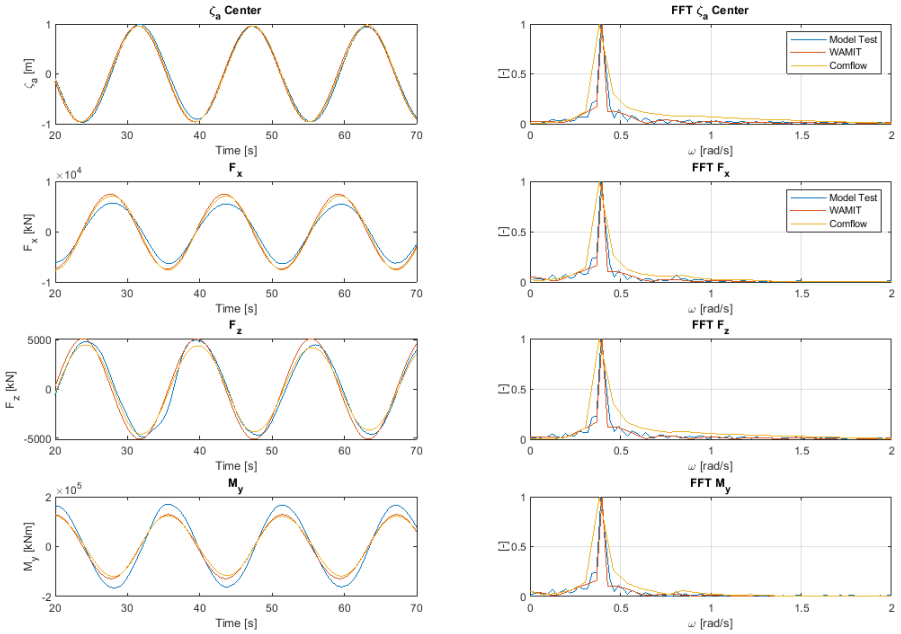

Figure C.6: Wave loads at $T = 25\ m$, $\omega = 0.4\ rad/s$ and $\zeta_a = 0.9\ m$

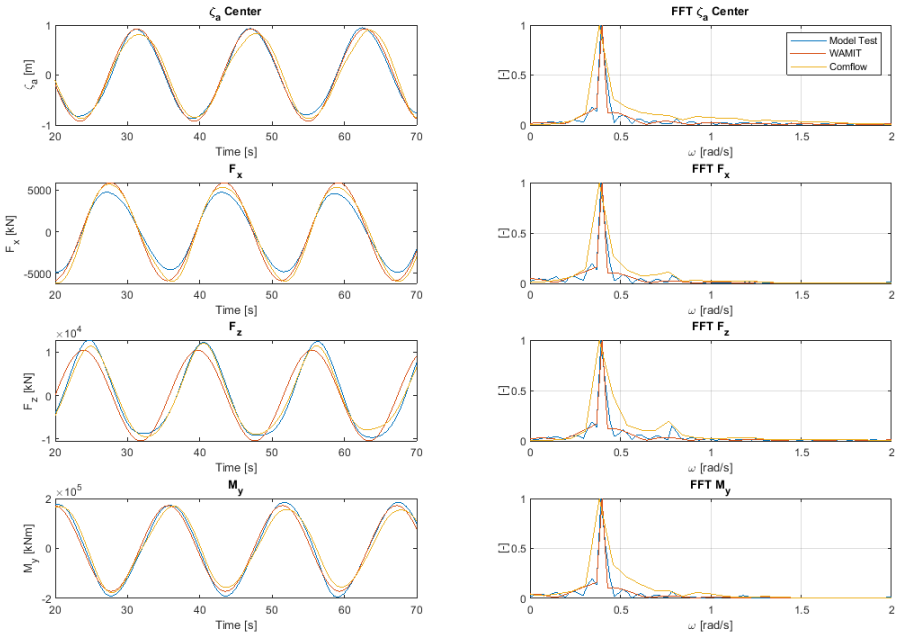

Figure C.7: Wave loads at $T = 11.5\ m$, $\omega = 0.4\ rad/s$ and $\zeta_a = 0.9\ m$

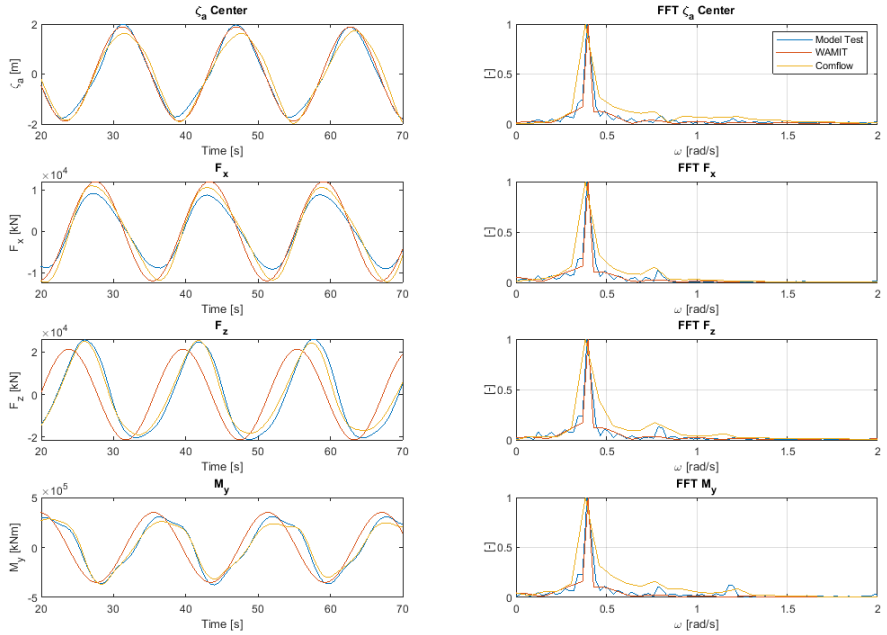

Figure C.8: Wave loads at $T = 11.5\ m$, $\omega = 0.4\ rad/s$ and $\zeta_a = 1.9\ m$

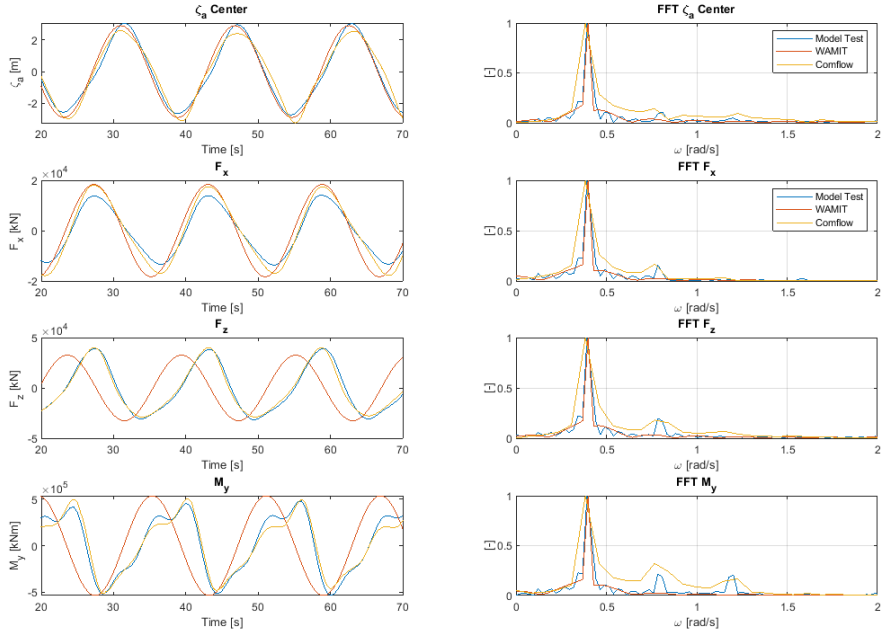

Figure C.9: Wave loads at $T = 11.5\ m$, $\omega = 0.4\ rad/s$ and $\zeta_a = 2.9\ m$

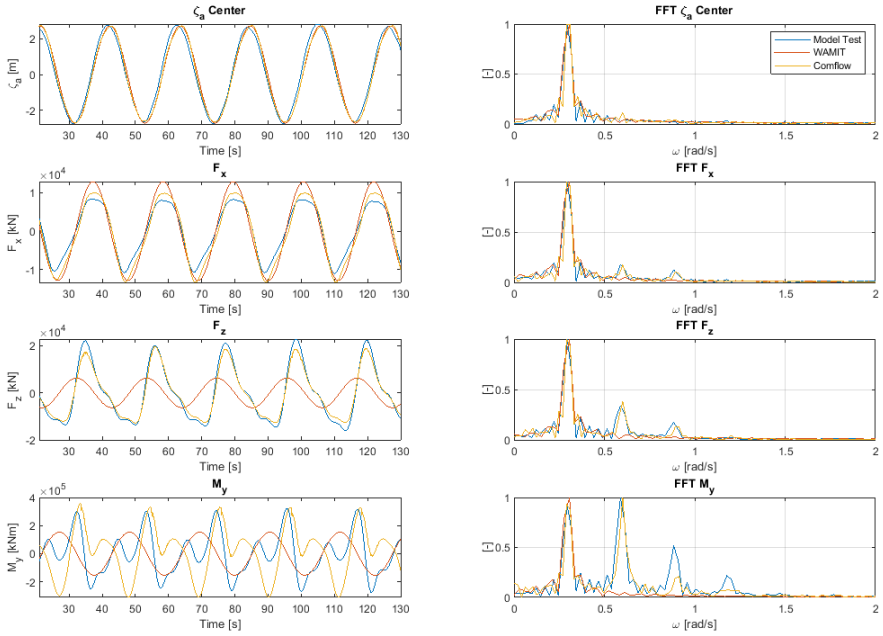

Figure C.10: Wave loads at $T = 11.5\ m$, $\omega = 0.3\ rad/s$ and $\zeta_a = 2.7\ m$

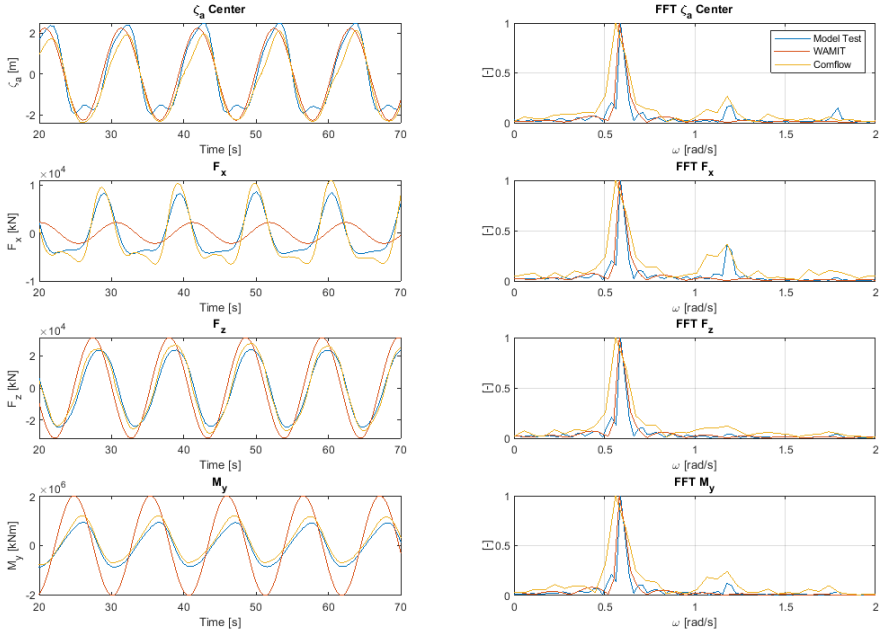

Figure C.11: Wave loads at $T = 11.5\ m$, $\omega = 0.6\ rad/s$ and $\zeta_a = 2.2\ m$

C.5. Comparing Motions

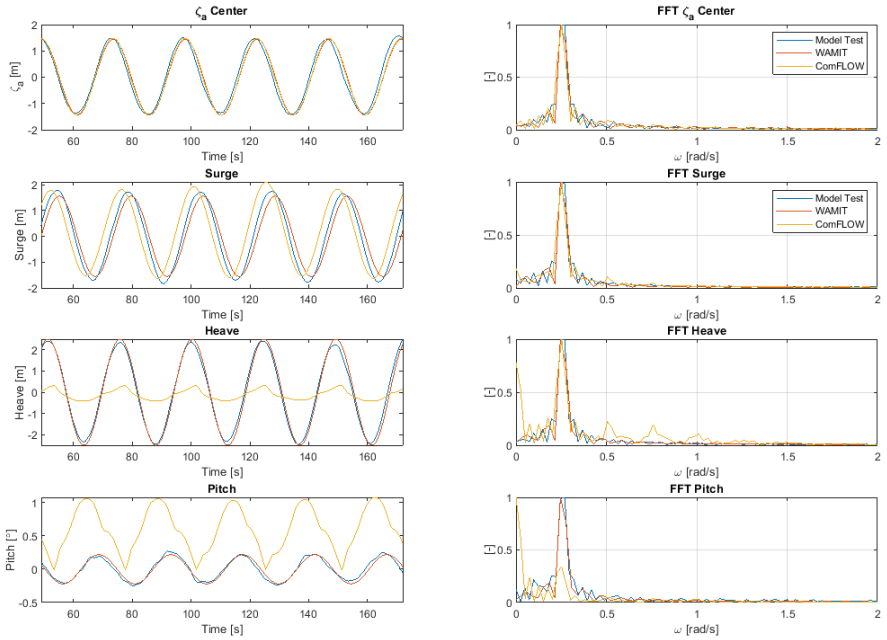

Figure C.12: Motions at $T = 25\ m$, $\omega = 0.26\ rad/s$ and $\zeta_a = 1.4\ m$

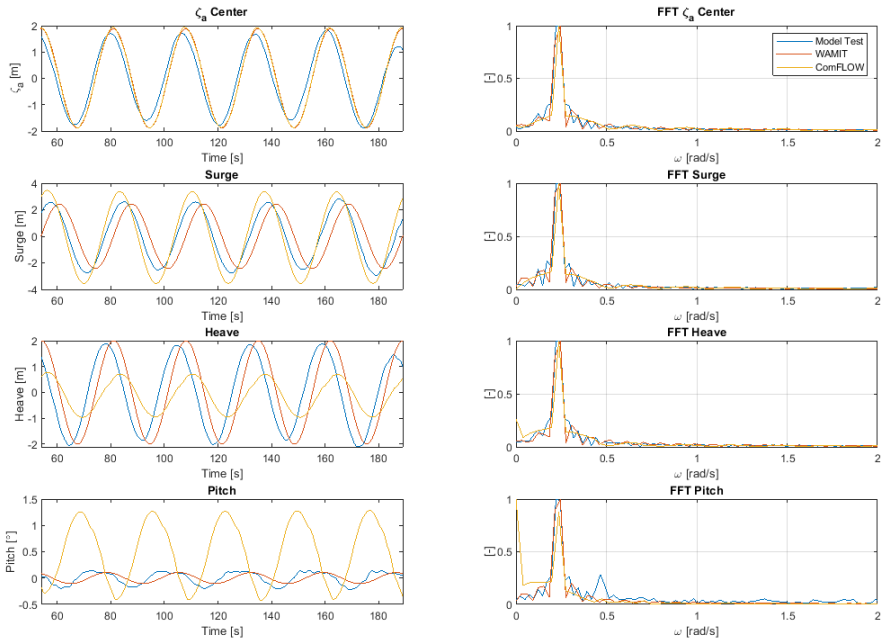

Figure C.13: Motions at $T = 11.5\ m$, $\omega = 0.23\ rad/s$ and $\zeta_a = 1.9\ m$

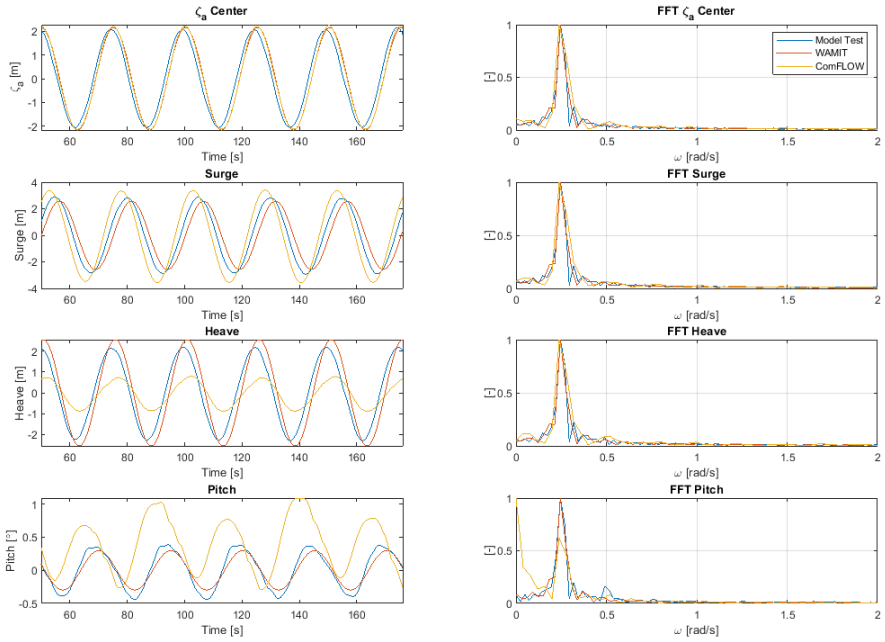

Figure C.14: Motions at $T = 11.5\ m$, $\omega = 0.25\ rad/s$ and $\zeta_a = 2.2\ m$

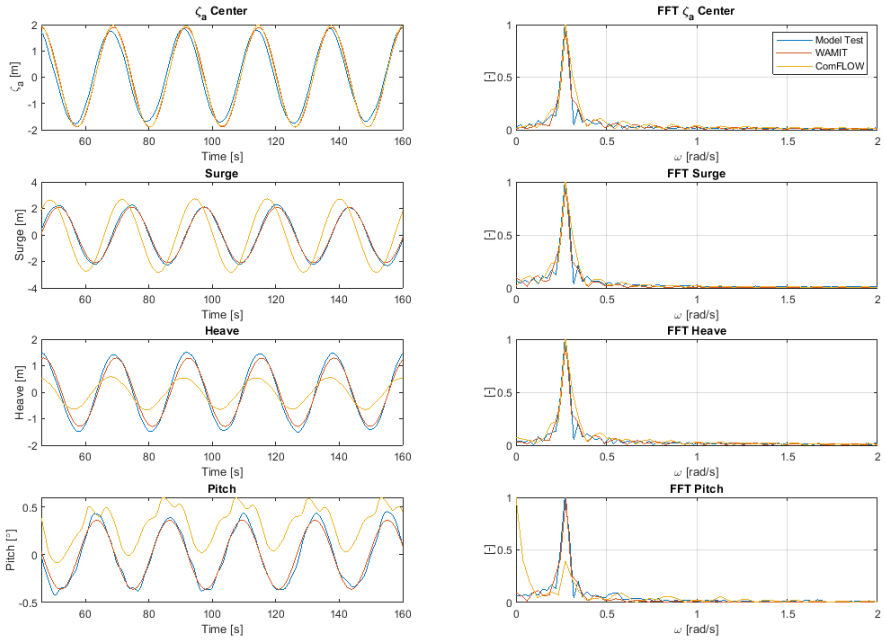

Figure C.15: Motions at $T = 11.5\ m$, $\omega = 0.27\ rad/s$ and $\zeta_a = 1.9\ m$

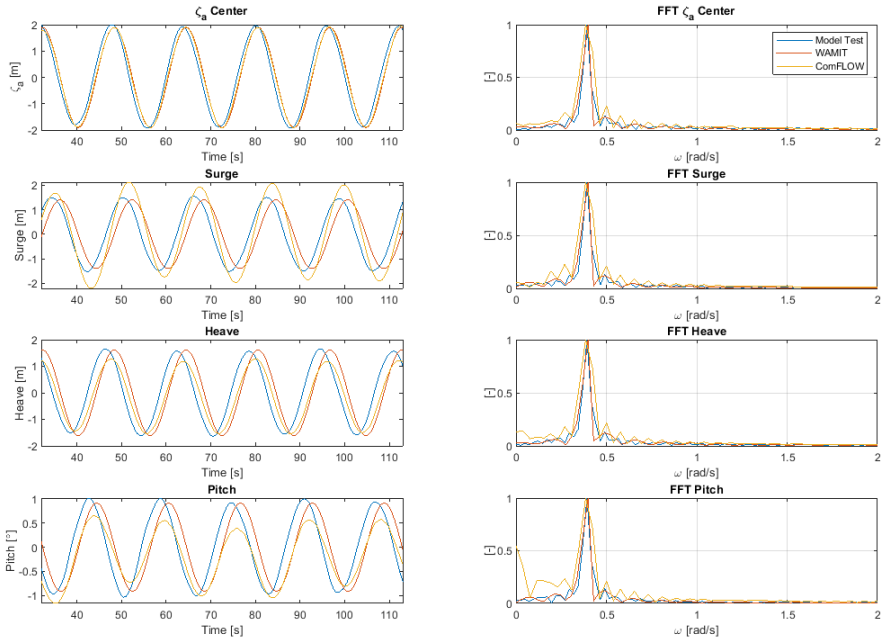

Figure C.16: Motions at $T = 11.5\ m$, $\omega = 0.39\ rad/s$ and $\zeta_a = 1.9\ m$

Table C.4: Modeltest and ComFLOW

ω	0.23	0.25	0.27	0.39
Surge difference [%]	33.69	24.27	31.65	46.05
Heave difference [%]	-54.94	-64.28	-61.39	-20.18
Pitch difference [%]	554.48	66.67	38.40	-42.35

Table C.5: Modeltest and WAMIT

ω	0.23	0.25	0.27	0.39
Surge difference [%]	-7.55	-9.59	-6.39	-6.34
Heave difference [%]	12.00	16.94	-13.27	-2.74
Pitch difference [%]	-22.56	-19.85	45.74	-9.49

C.6. Wave loads in free-floating cases

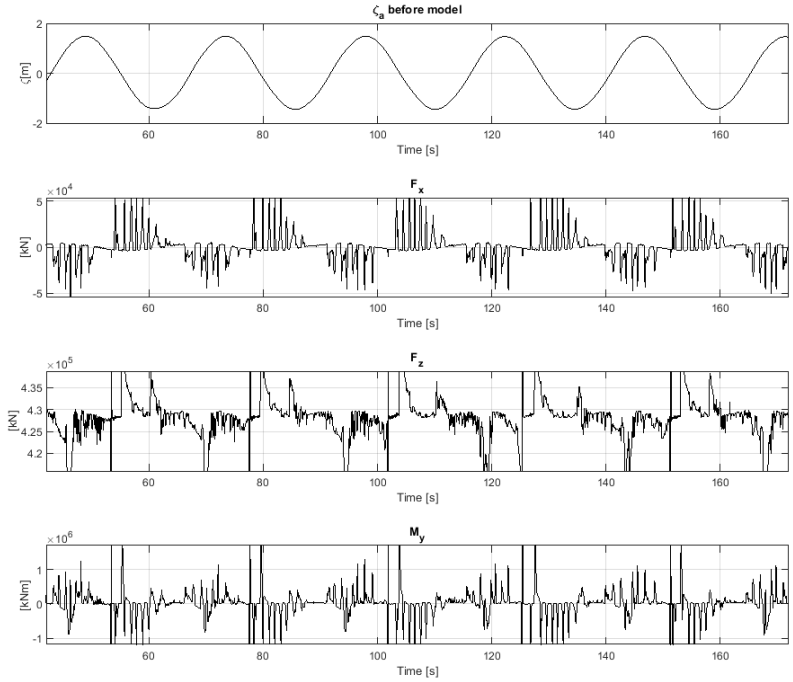

Figure C.17: Wave loads at $T = 25\ m$, $\omega = 0.26\ rad/s$ and $\zeta_a = 1.4\ m$

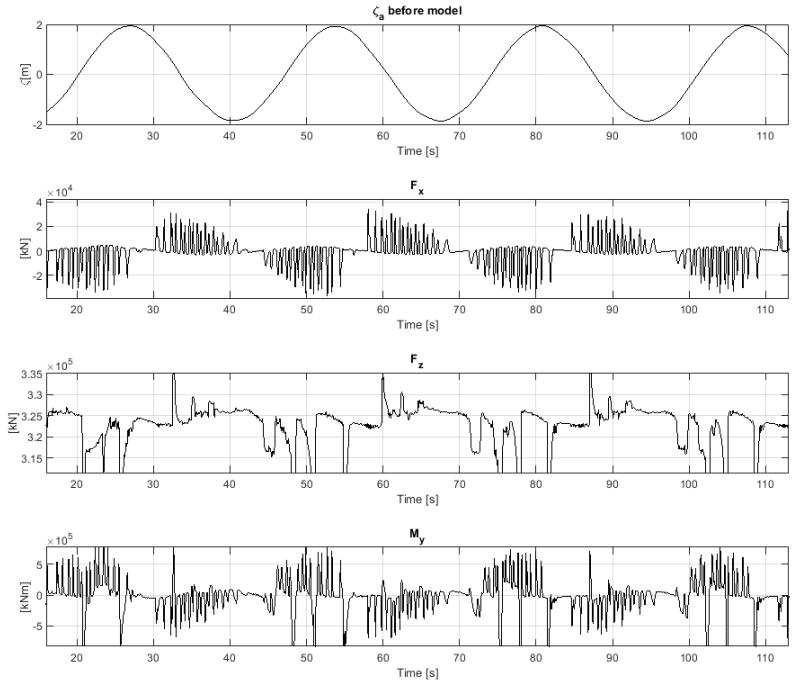

Figure C.18: Wave loads at $T = 11.5\ m$, $\omega = 0.23\ rad/s$ and $\zeta_a = 1.9\ m$

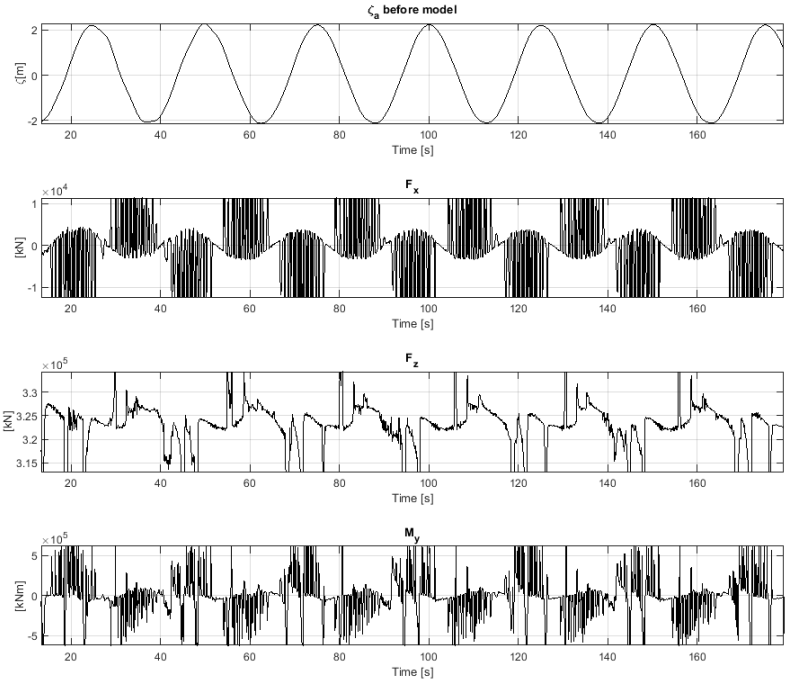

Figure C.19: Wave loads at $T = 11.5\ m$, $\omega = 0.25\ rad/s$ and $\zeta_a = 2.2\ m$

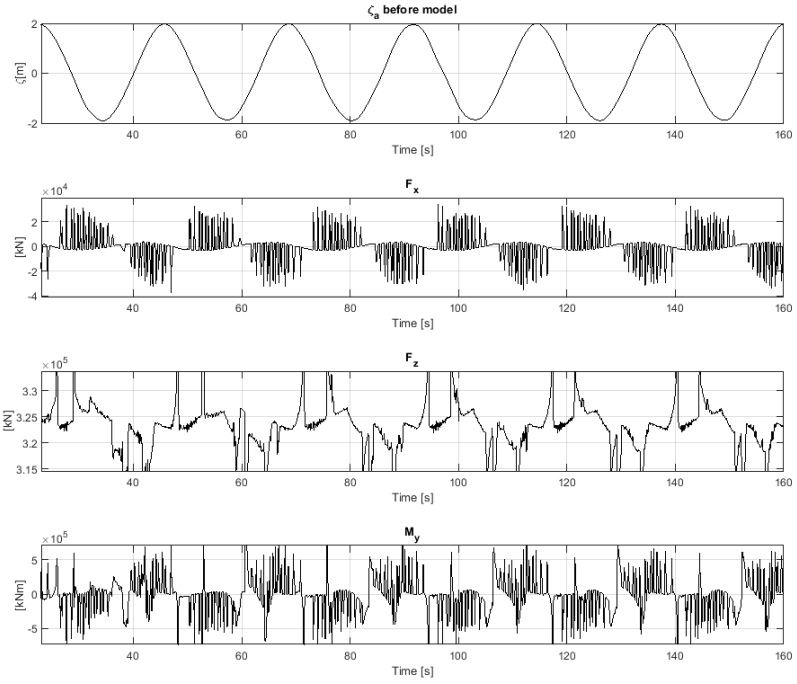

Figure C.20: Wave loads at $T = 11.5\ m$, $\omega = 0.27\ rad/s$ and $\zeta_a = 1.9\ m$

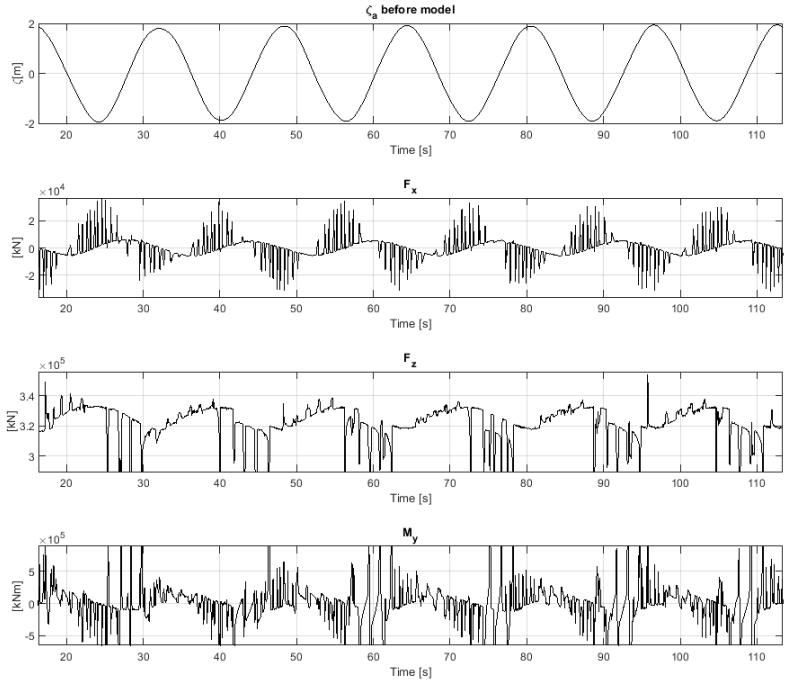

Figure C.21: Wave loads at $T = 11.5\ m$, $\omega = 0.39\ rad/s$ and $\zeta_a = 1.9\ m$

C.7. Comparing Internal Loads

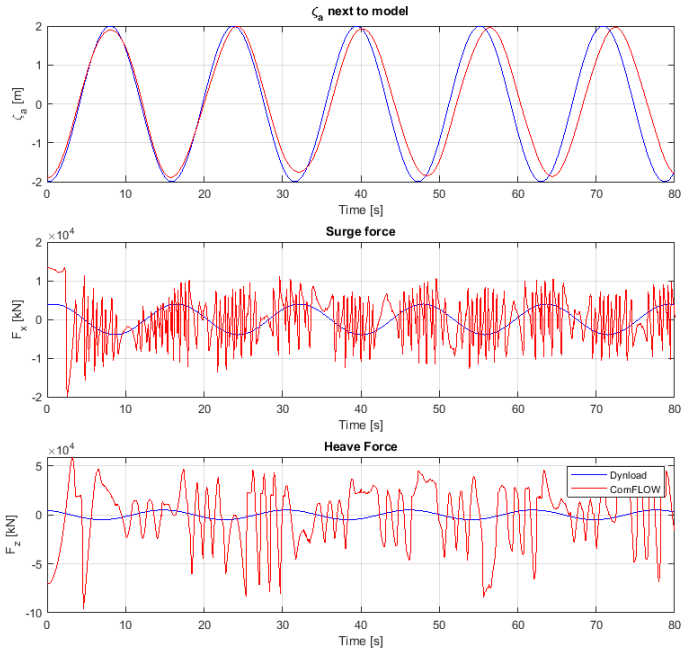

Figure C.22: Internal loads at $T = 11.5\ m$, $\omega = 0.39\ rad/s$ and $\zeta_a = 1.9\ m$

C.8. Physical cause

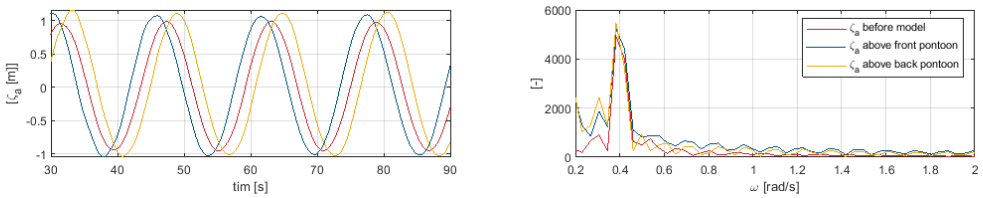

Figure C.23: Wave amplitude on three locations

D

Figures Parameter study

D.1. Fixed draft varying wave height

D.1.1. Total wave loads

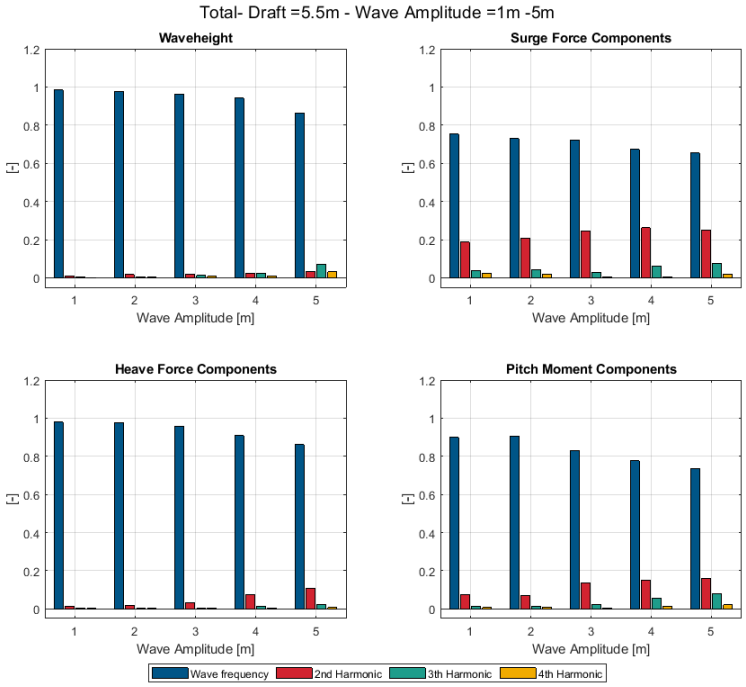

Figure D.1: Higher harmonic components of the total wave loads at $T = 5.5\ m$

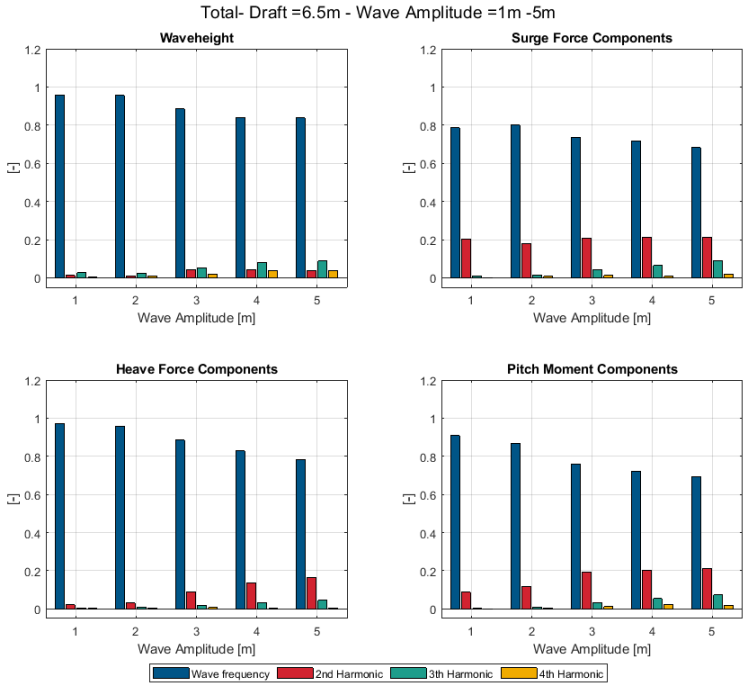

Figure D.2: Higher harmonic components of the total wave loads at $T = 6.5\ m$

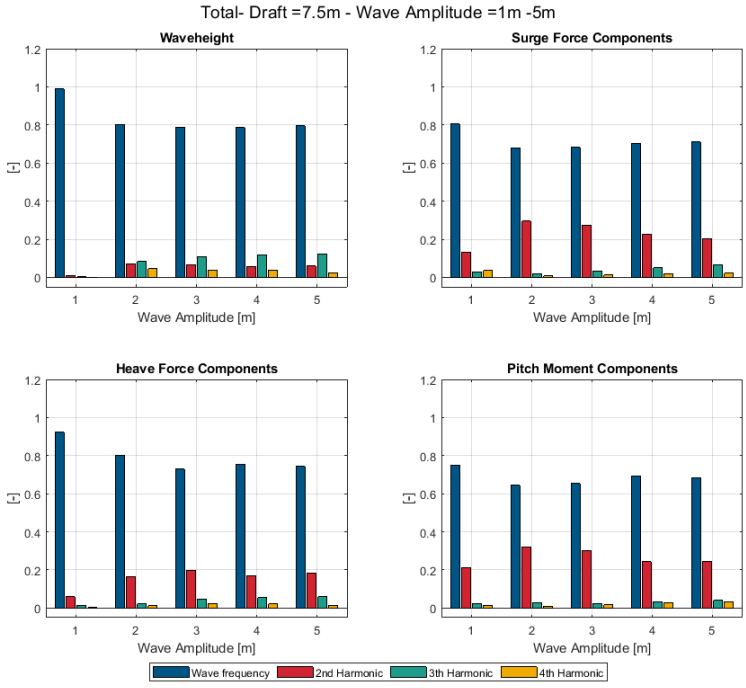

Figure D.3: Higher harmonic components of the total wave loads at $T = 7.5\ m$

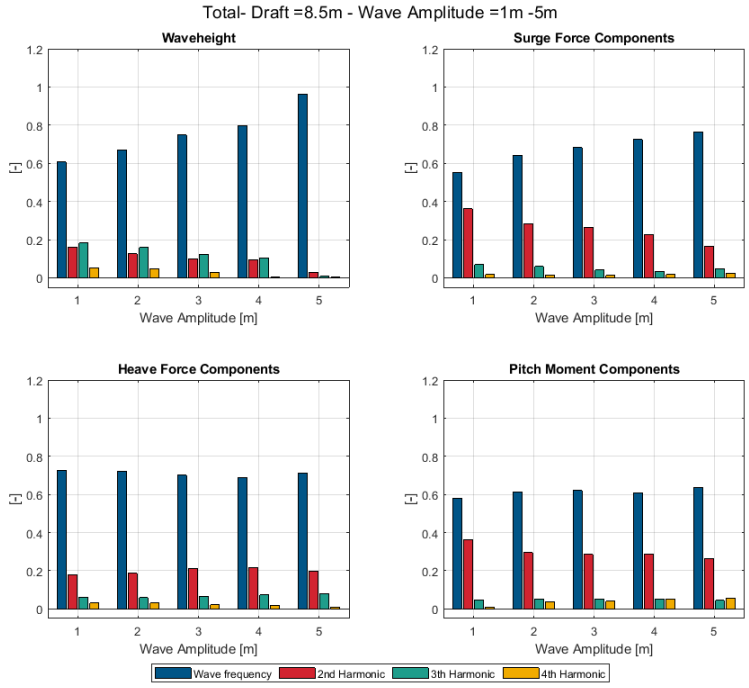

Figure D.4: Higher harmonic components of the total wave loads at $T = 8.5\ m$

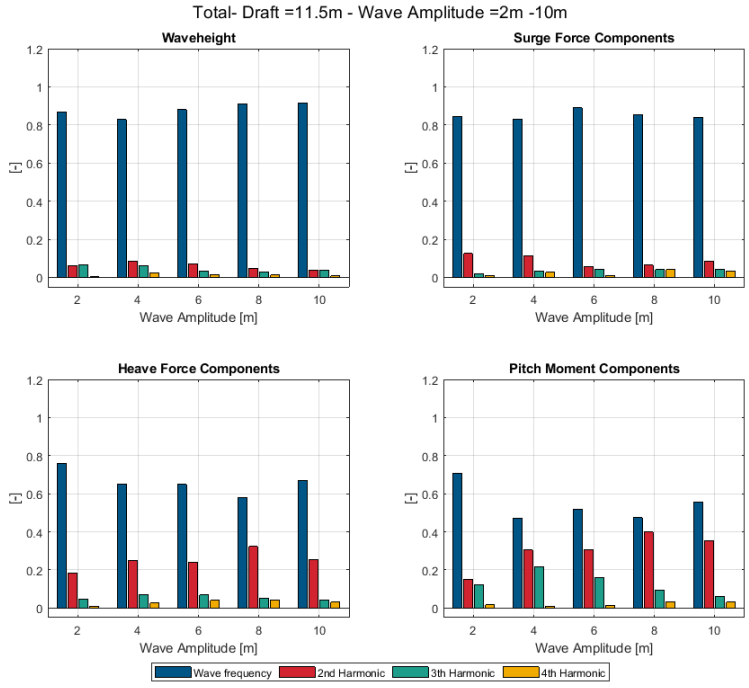

Figure D.5: Higher harmonic components of the total wave loads at $T = 9.5\ m$

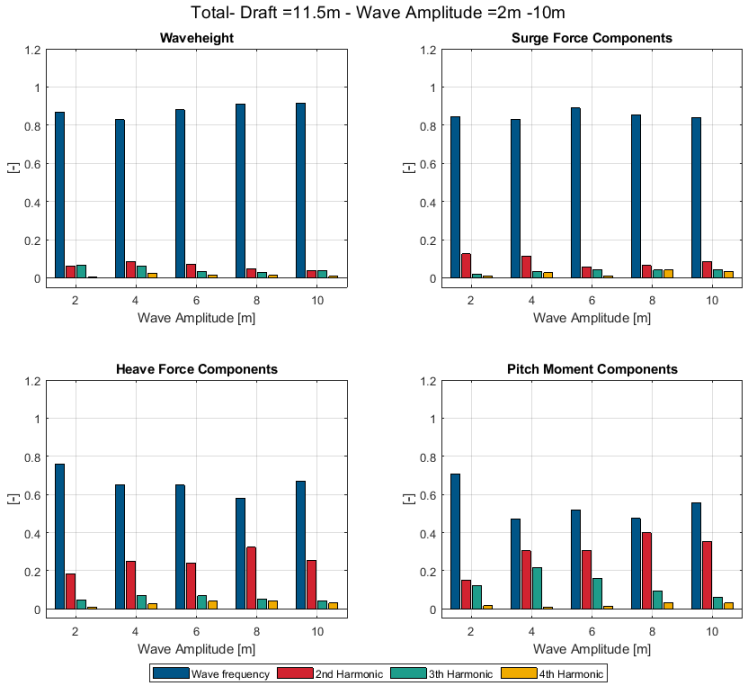

Figure D.6: Higher harmonic components of the total wave loads at $T = 11.5\ m$

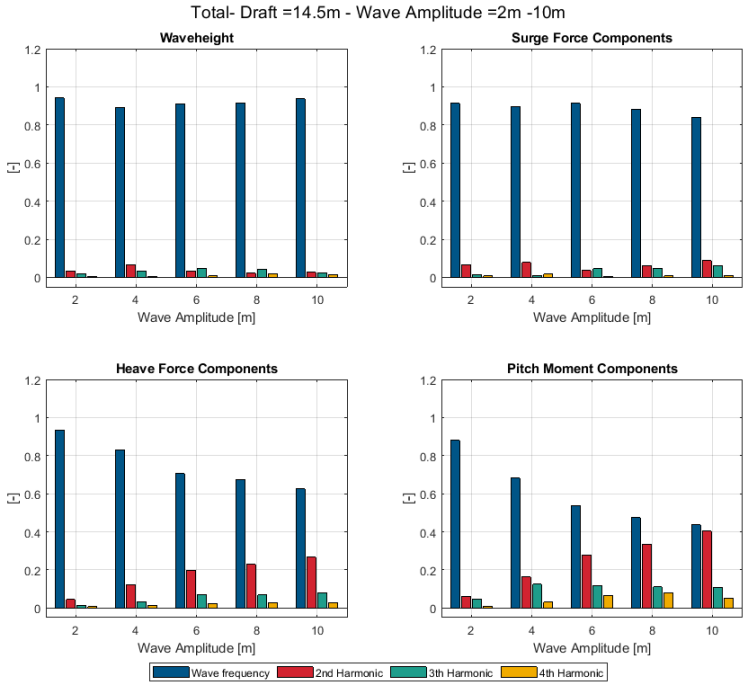

Figure D.7: Higher harmonic components of the total wave loads at $T = 14.5\ m$

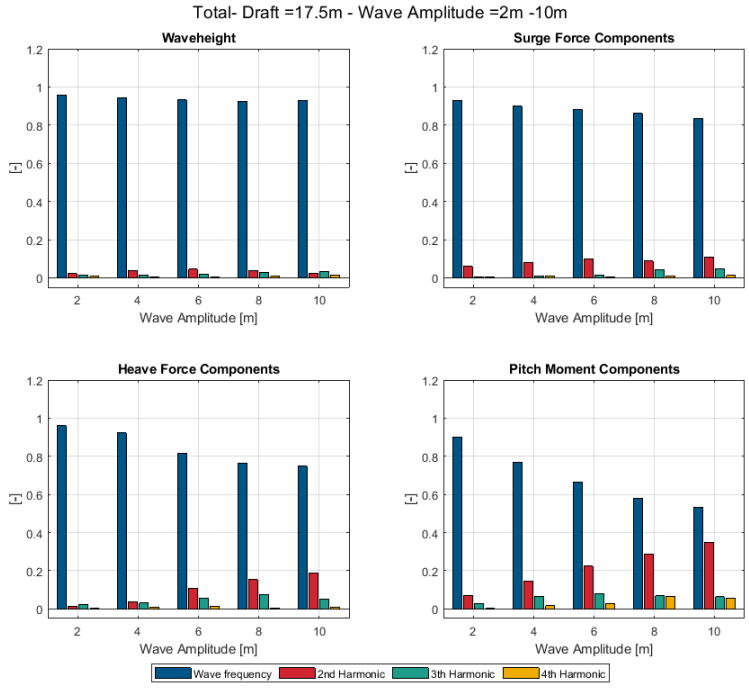

Figure D.8: Higher harmonic components of the total wave loads at $T = 17.5\ m$

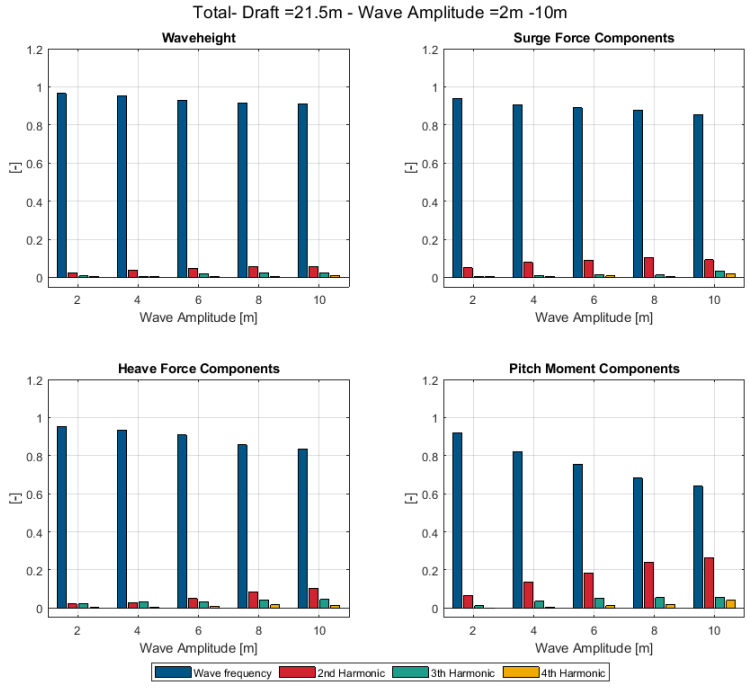

Figure D.9: Higher harmonic components of the total wave loads at $T = 21.5\ m$

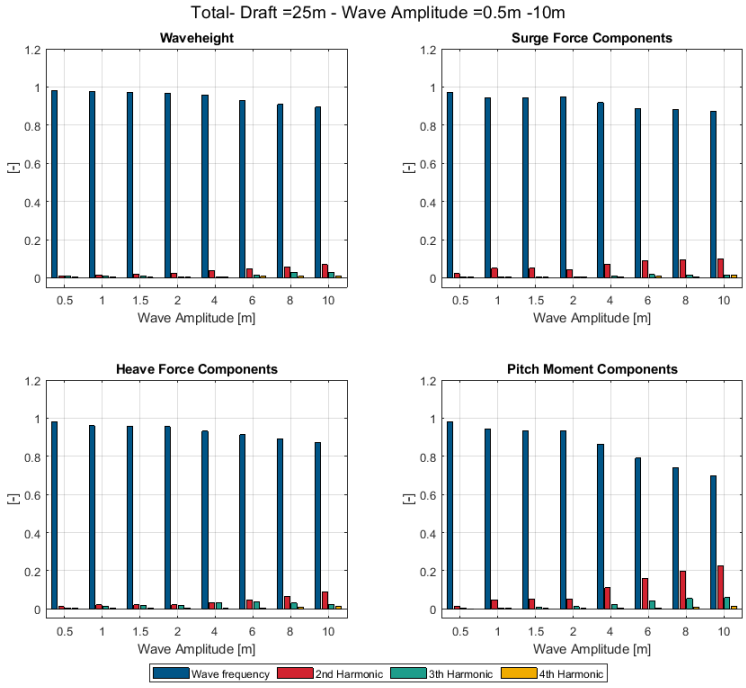

Figure D.10: Higher harmonic components of the total wave loads at $T = 25\ m$

D.1.2. Forward wave loads

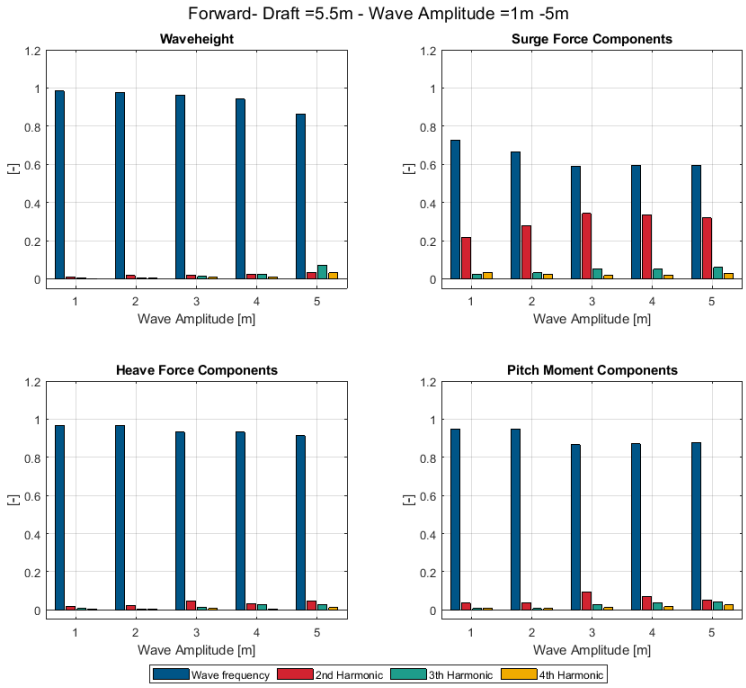

Figure D.11: Higher harmonic components of wave loads response of forward section at $T = 5.5\ m$

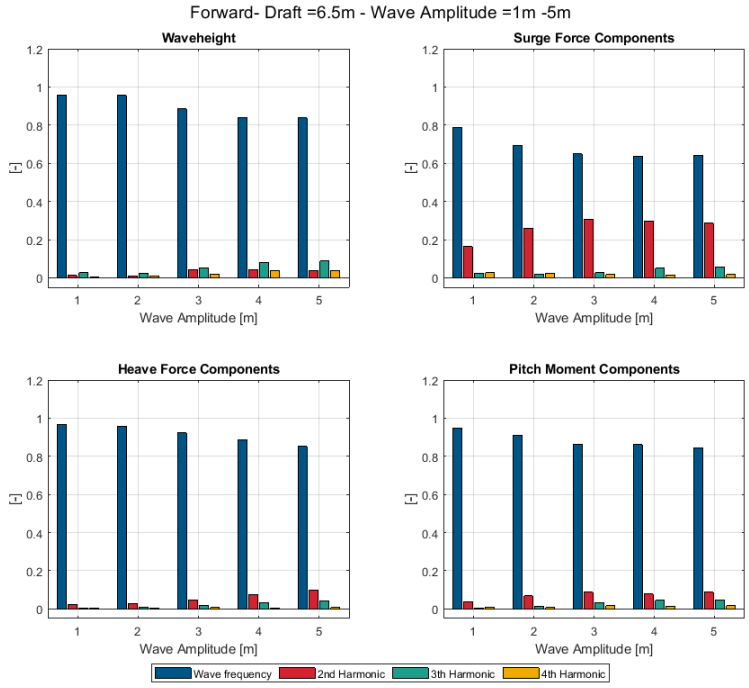

Figure D.12: Higher harmonic components of wave loads response of forward section at $T = 6.5\ m$

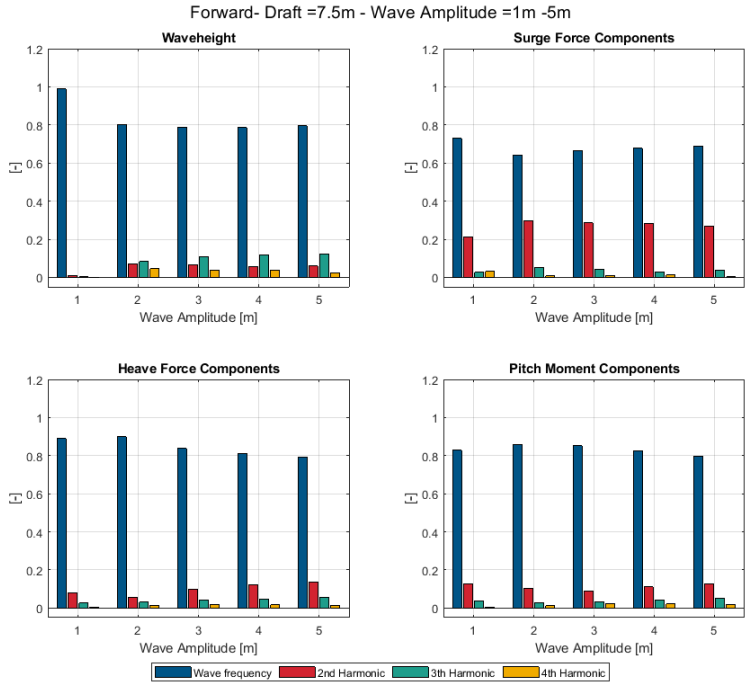

Figure D.13: Higher harmonic components of wave loads response of forward section at $T = 7.5\ m$

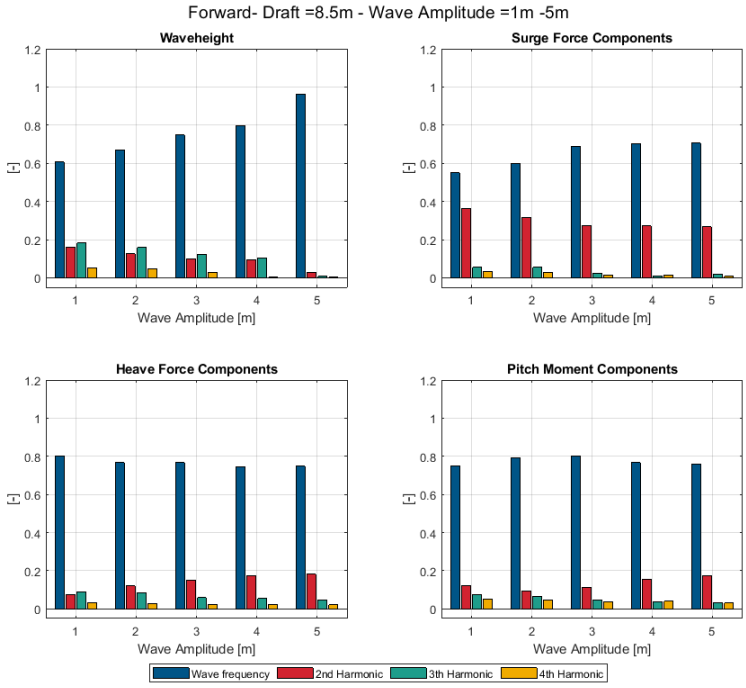

Figure D.14: Higher harmonic components of wave loads response of forward section at $T = 8.5\ m$

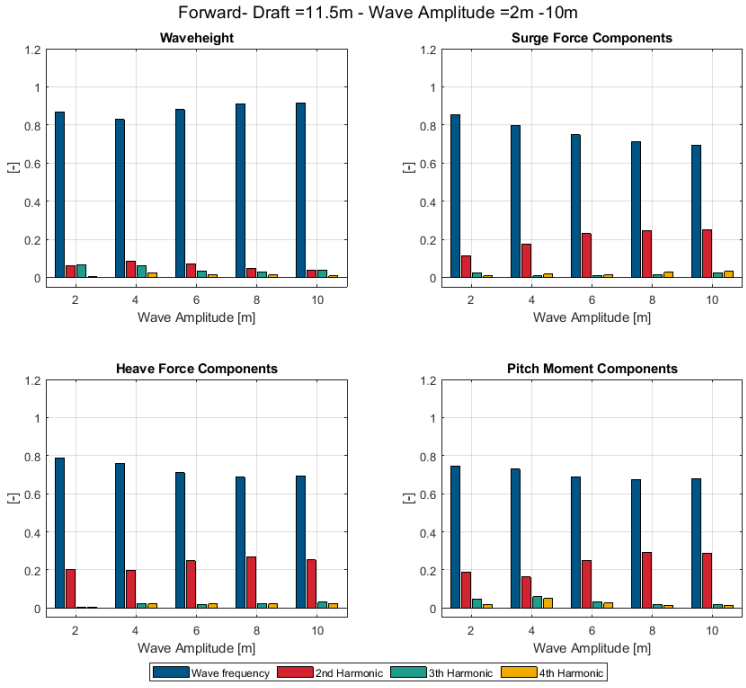

Figure D.15: Higher harmonic components of wave loads response of forward section at $T = 9.5\ m$

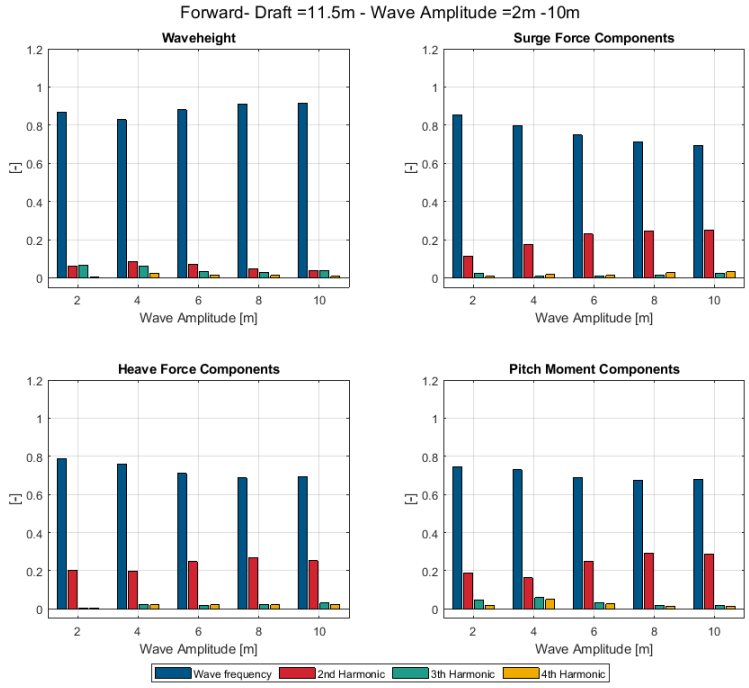

Figure D.16: Higher harmonic components of wave loads response of forward section at $T = 11.5\ m$

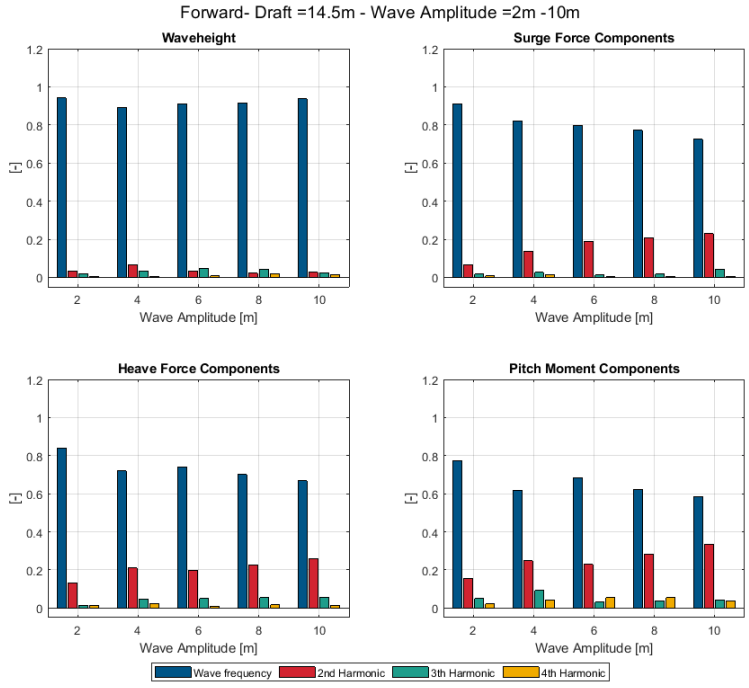

Figure D.17: Higher harmonic components of wave loads response of forward section at $T = 14.5\ m$

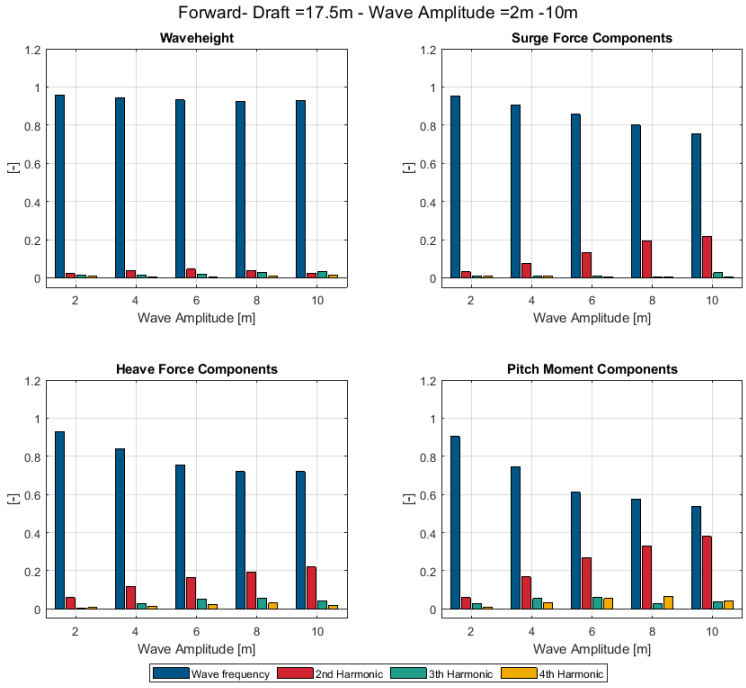

Figure D.18: Higher harmonic components of wave loads response of forward section at $T = 17.5\ m$

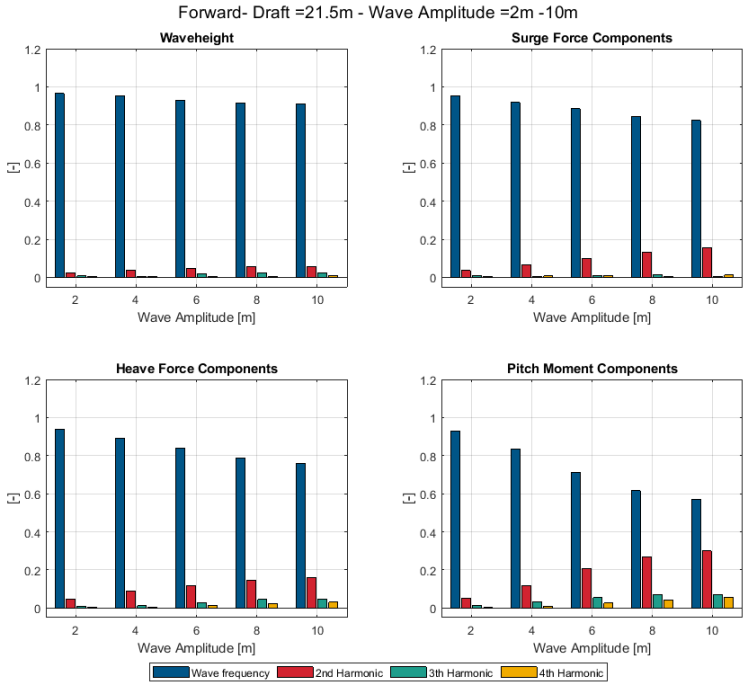

Figure D.19: Higher harmonic components of wave loads response of forward section at $T = 21.5\ m$

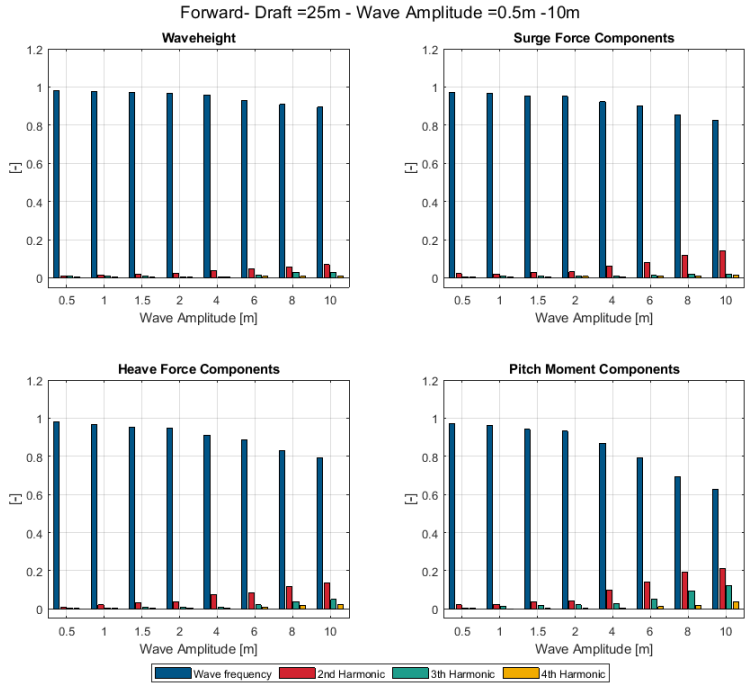

Figure D.20: Higher harmonic components of wave loads response of forward section at $T = 25\ m$

D.1.3. Aft wave loads

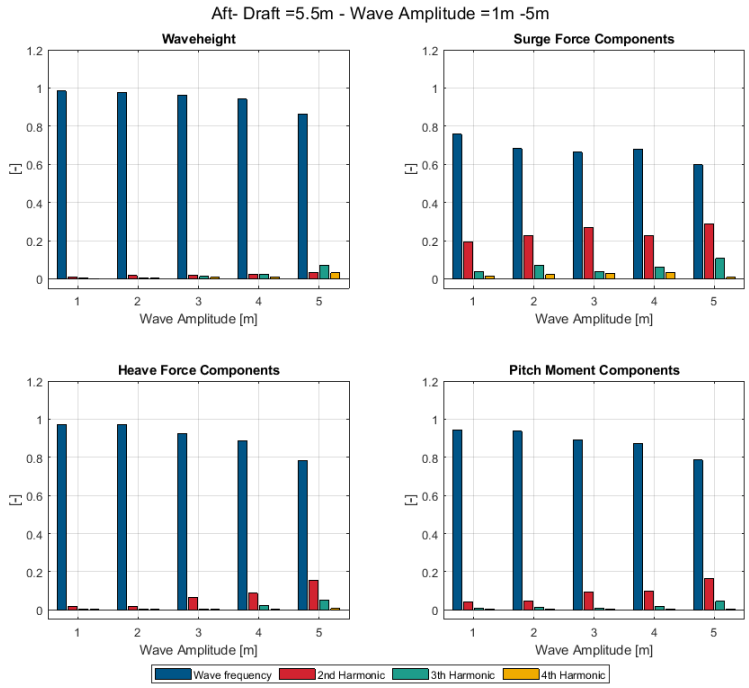

Figure D.21: Higher harmonic components of wave loads response of aft section at $T = 5.5\ m$

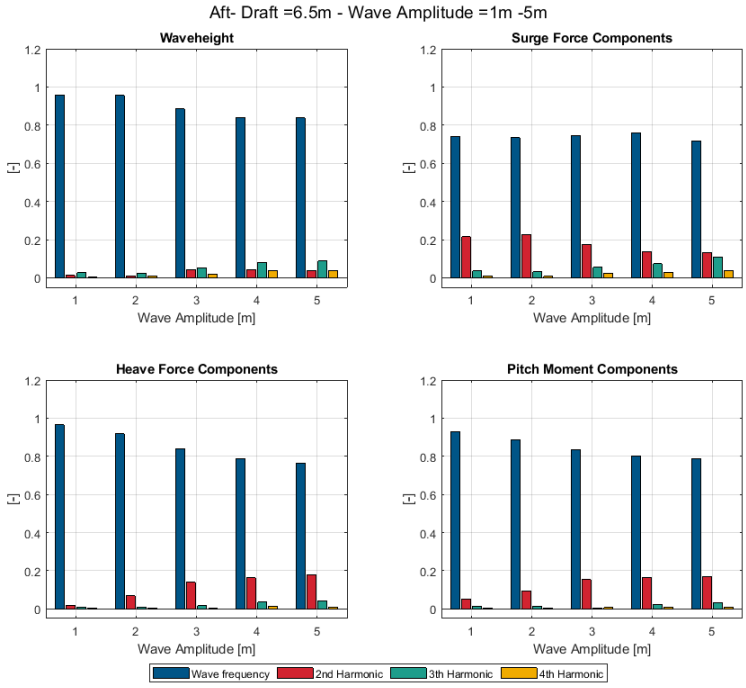

Figure D.22: Higher harmonic components of wave loads response of aft section at $T = 6.5\ m$

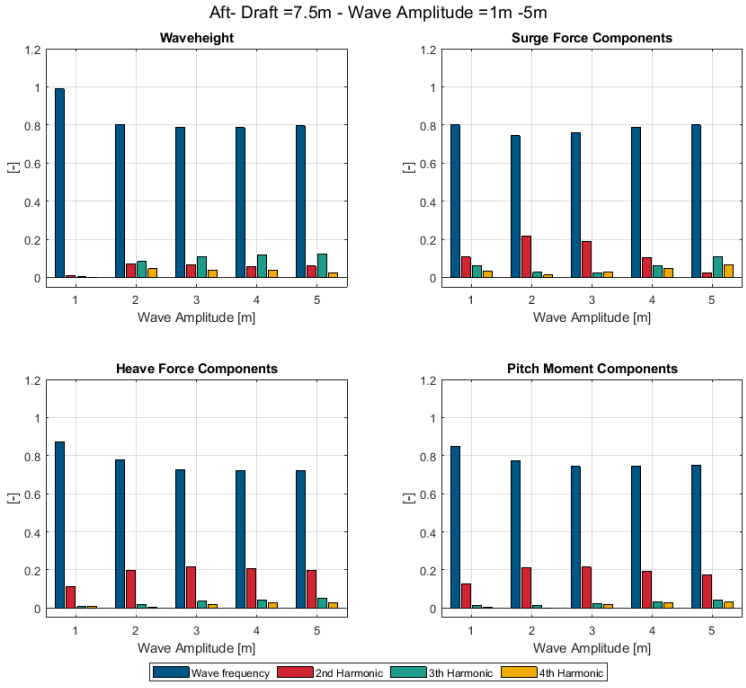

Figure D.23: Higher harmonic components of wave loads response of aft section at $T = 7.5\ m$

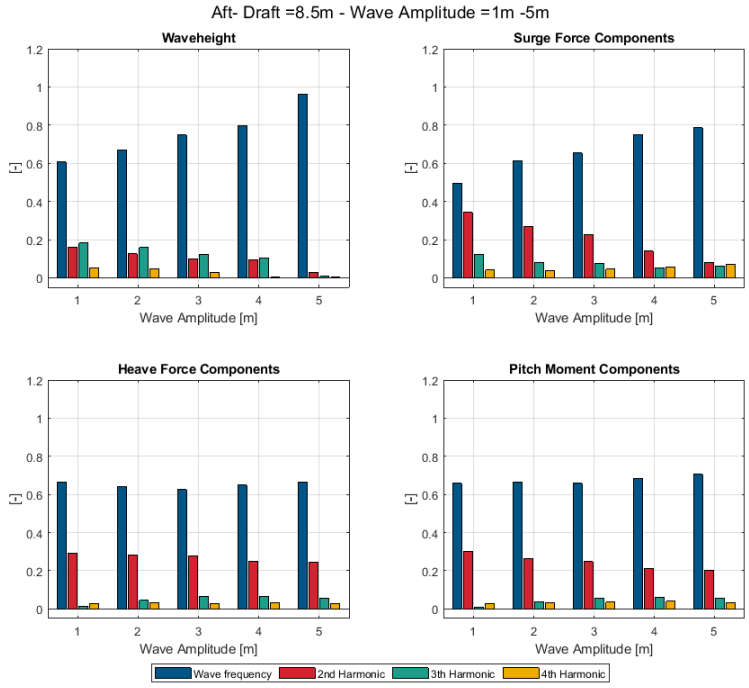

Figure D.24: Higher harmonic components of wave loads response of aft section at $T = 8.5\ m$

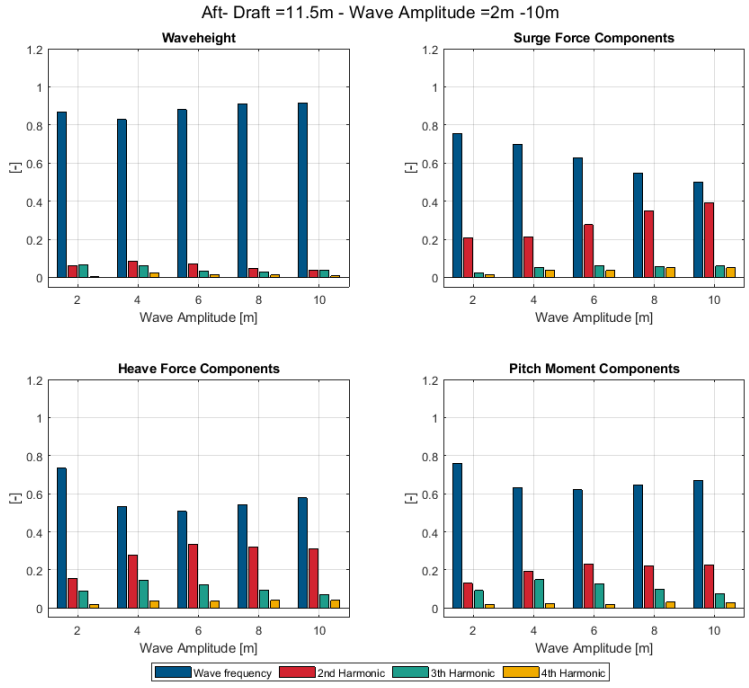

Figure D.25: Higher harmonic components of wave loads response of aft section at $T = 9.5\ m$

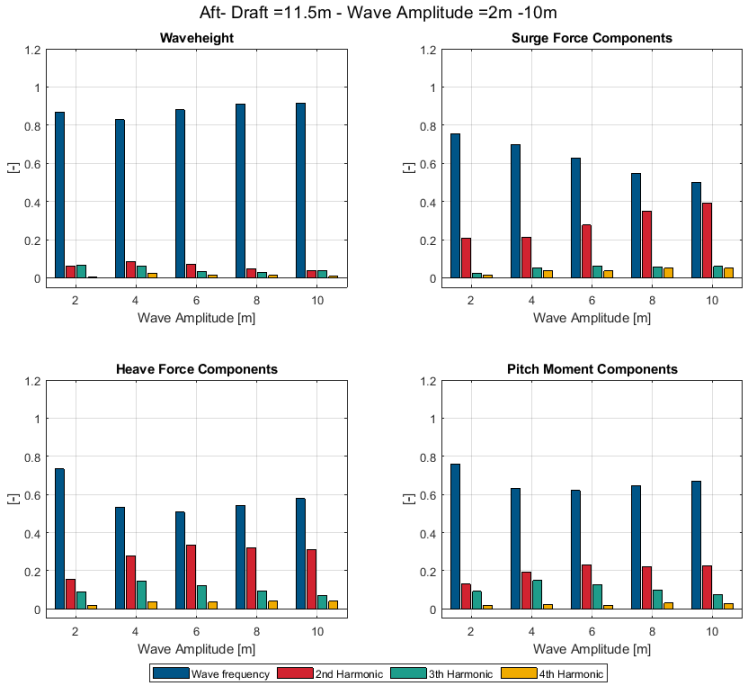

Figure D.26: Higher harmonic components of wave loads response of aft section at $T = 11.5\ m$

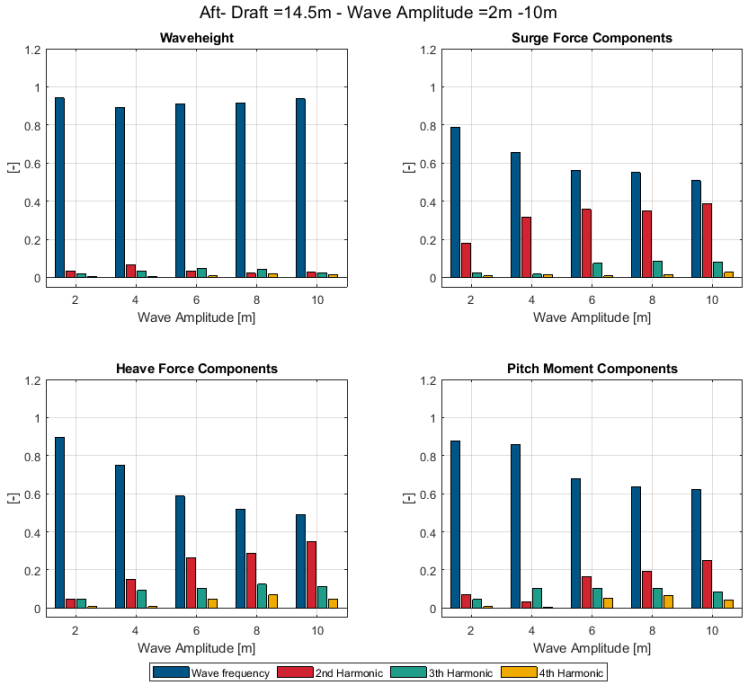

Figure D.27: Higher harmonic components of wave loads response of aft section at $T = 14.5\ m$

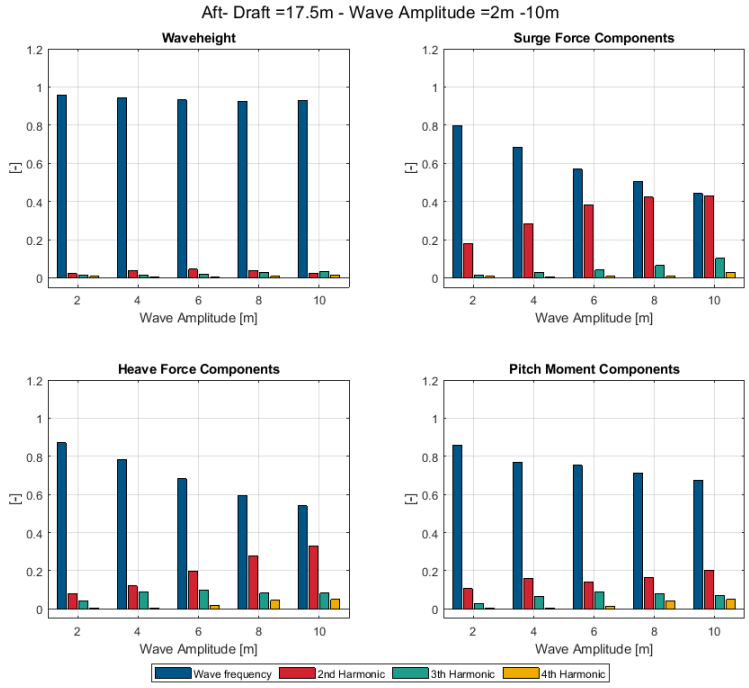

Figure D.28: Higher harmonic components of wave loads response of aft section at $T = 17.5\ m$

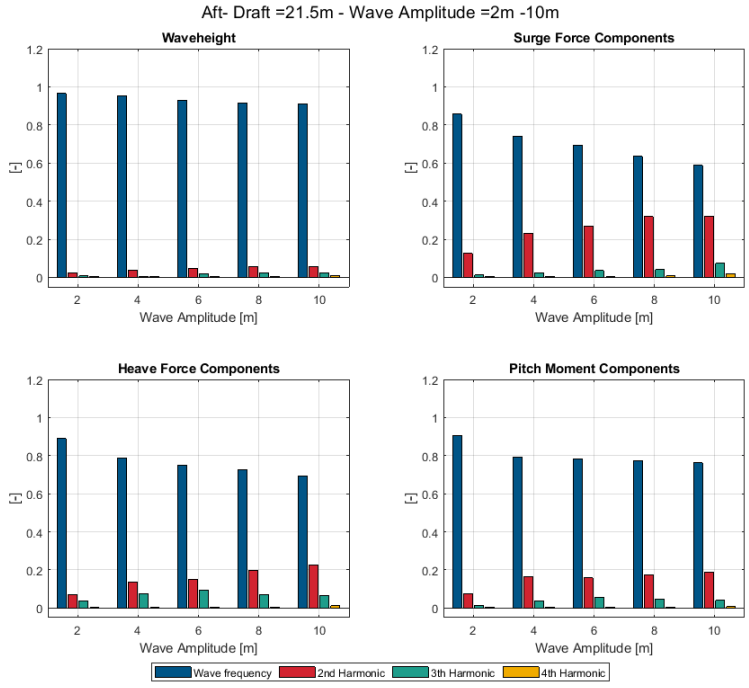

Figure D.29: Higher harmonic components of wave loads response of aft section at $T = 21.5\ m$

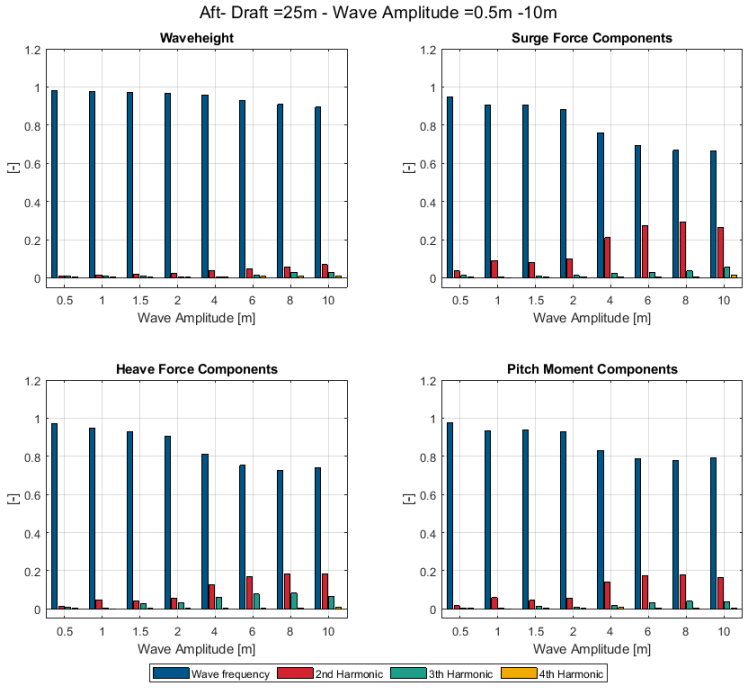

Figure D.30: Higher harmonic components of wave loads response of aft section at $T = 25\ m$

D.2. Fixed wave height varying draft

D.2.1. Total wave loads

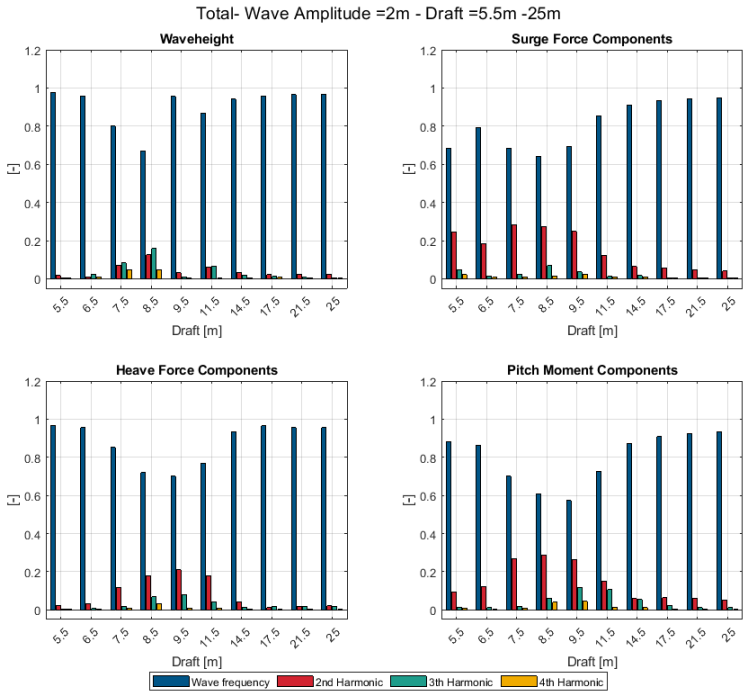

Figure D.31: Higher harmonic components of the total wave loads response at a wave amplitude of $\zeta_a = 2\ m$

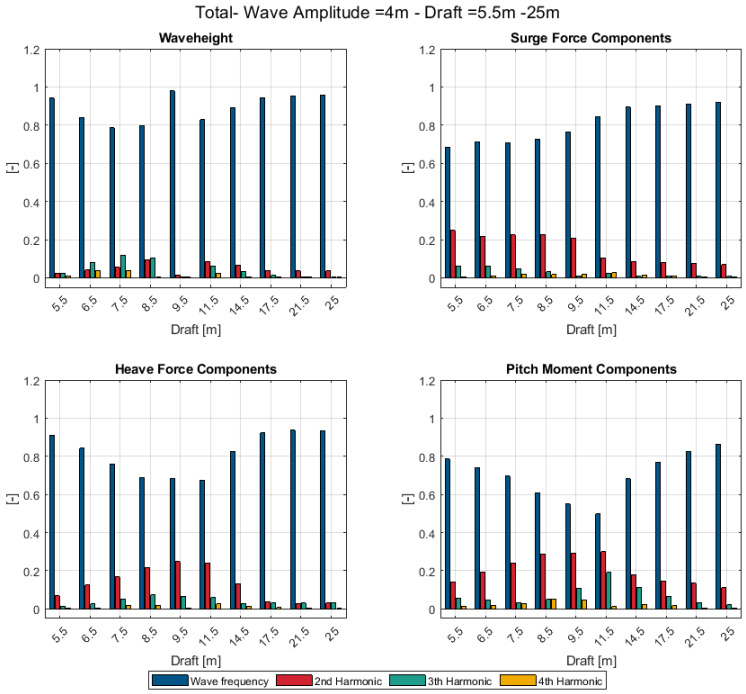

Figure D.32: Higher harmonic components of the total wave loads response at a wave amplitude of $\zeta_a = 4\ m$

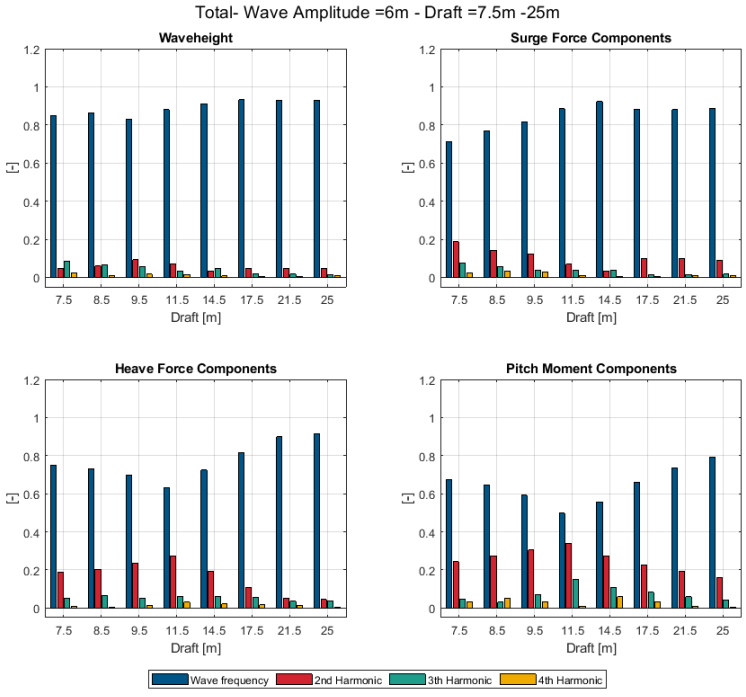

Figure D.33: Higher harmonic components of the total wave loads response at a wave amplitude of $\zeta_a = 6\ m$

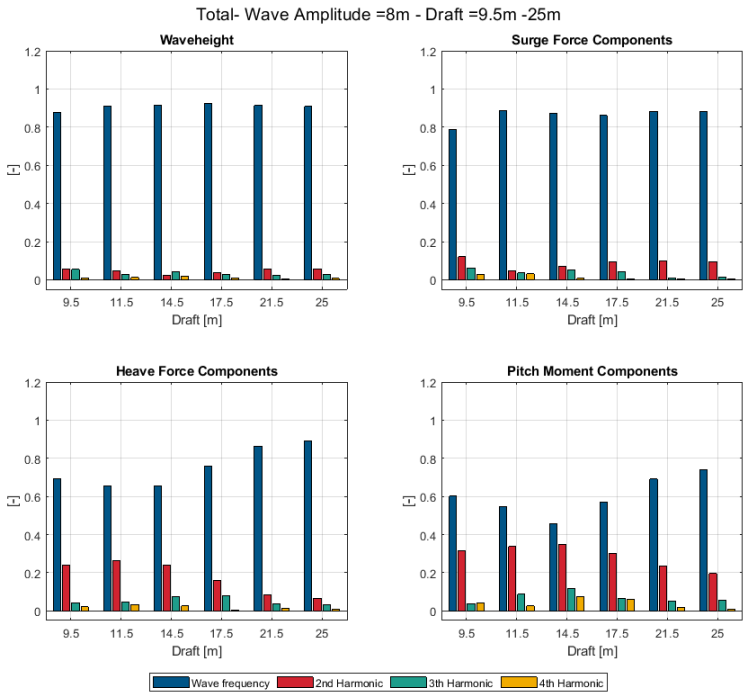

Figure D.34: Higher harmonic components of the total wave loads response at a wave amplitude of $\zeta_a = 8\ m$

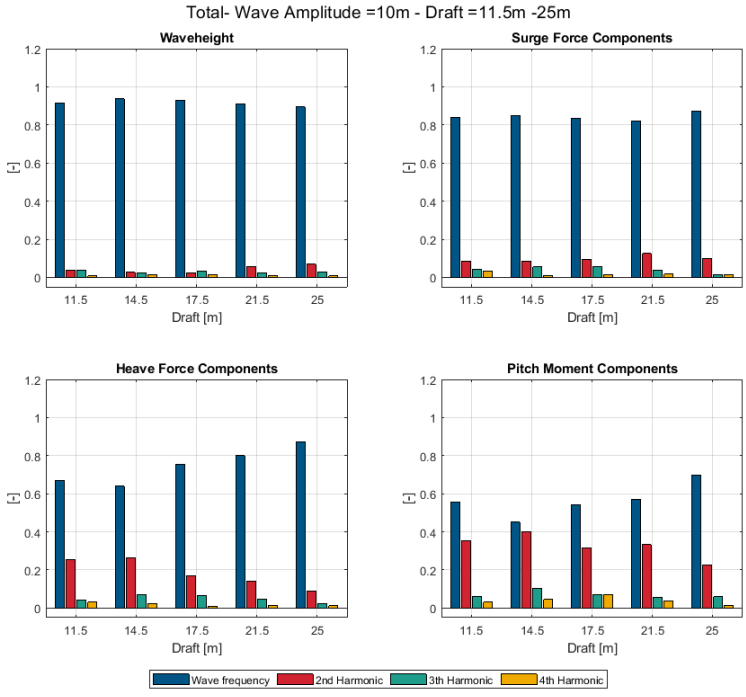

Figure D.35: Higher harmonic components of the total wave loads response at a wave amplitude of $\zeta_a = 10\ m$

D.2.2. Forward wave loads

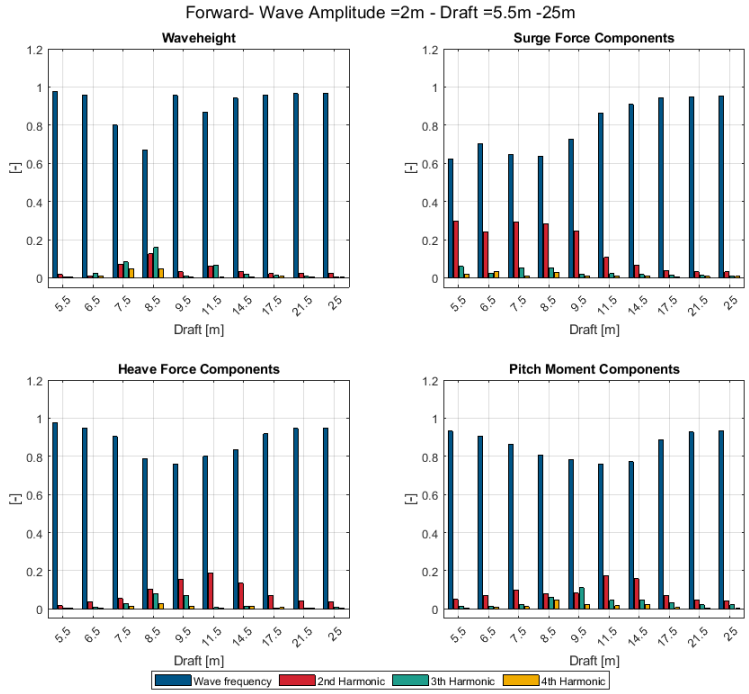

Figure D.36: Higher harmonic components of wave loads response of forward section at a wave amplitude of $\zeta_a = 2\ m$

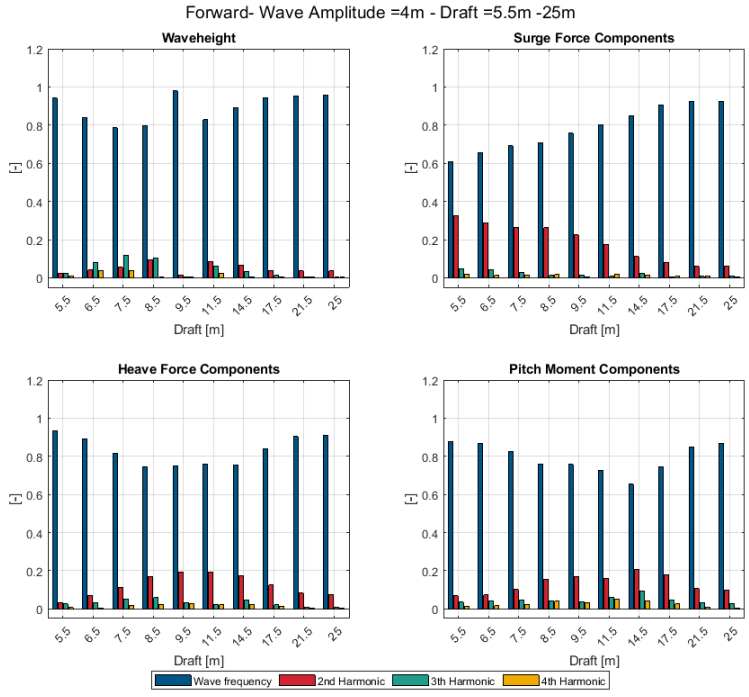

Figure D.37: Higher harmonic components of wave loads response of forward section at a wave amplitude of $\zeta_a = 4\ m$

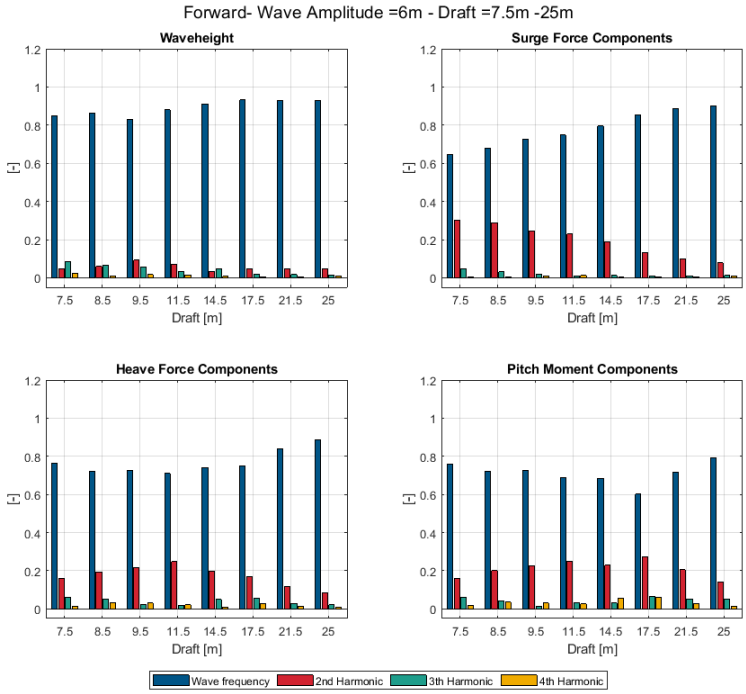

Figure D.38: Higher harmonic components of wave loads response of forward section at a wave amplitude of $\zeta_a = 6\ m$

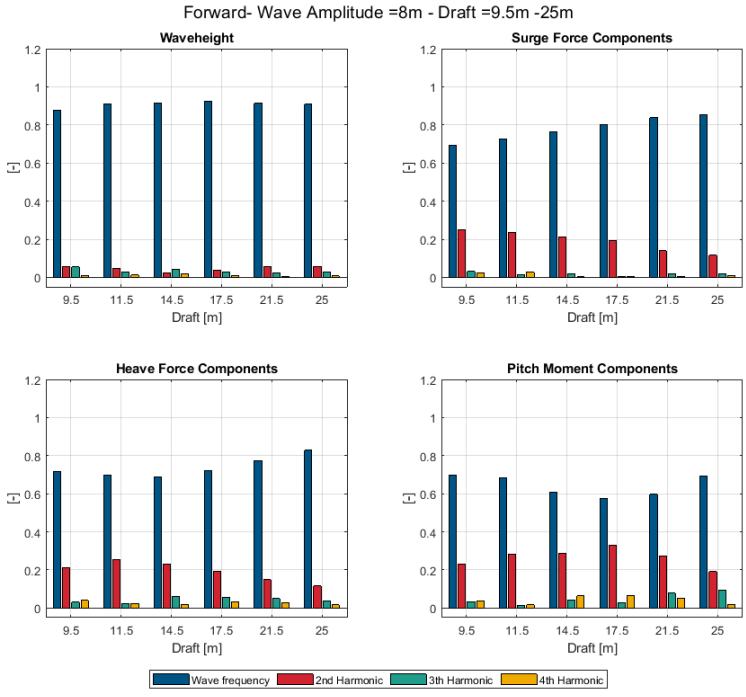

Figure D.39: Higher harmonic components of wave loads response of forward section at a wave amplitude of $\zeta_a = 8\ m$

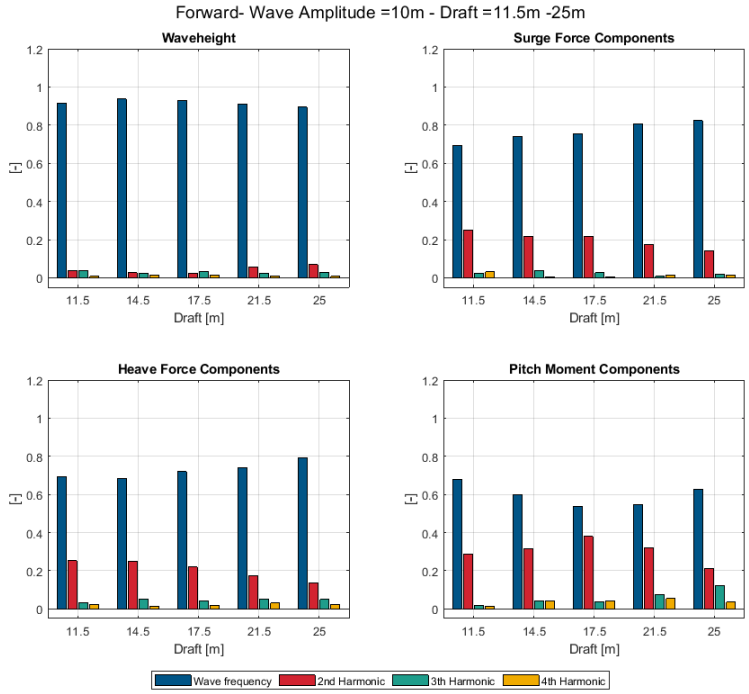

Figure D.40: Higher harmonic components of wave loads response of forward section at a wave amplitude of $\zeta_a = 10\ m$

D.2.3. Aft wave loads

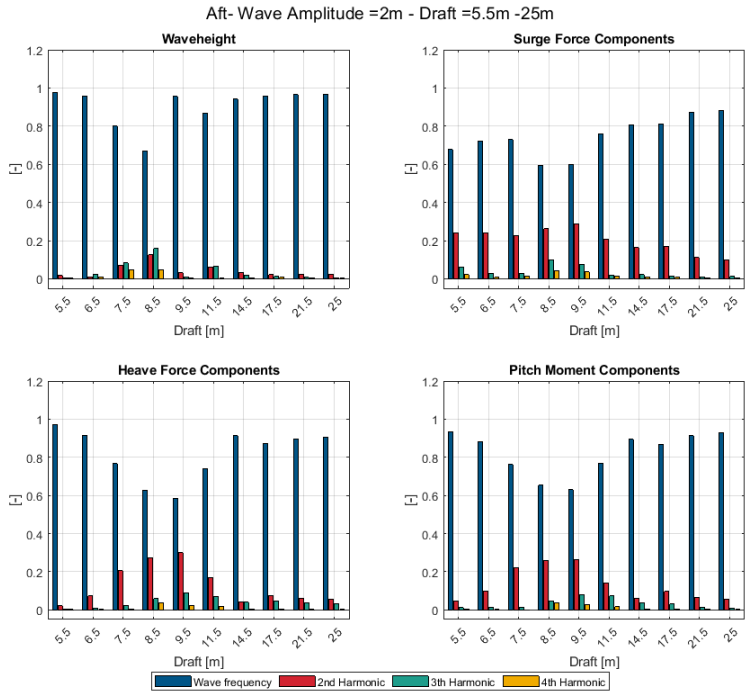

Figure D.41: Higher harmonic components of wave loads response of aft section at a wave amplitude of $\zeta_a = 2\ m$

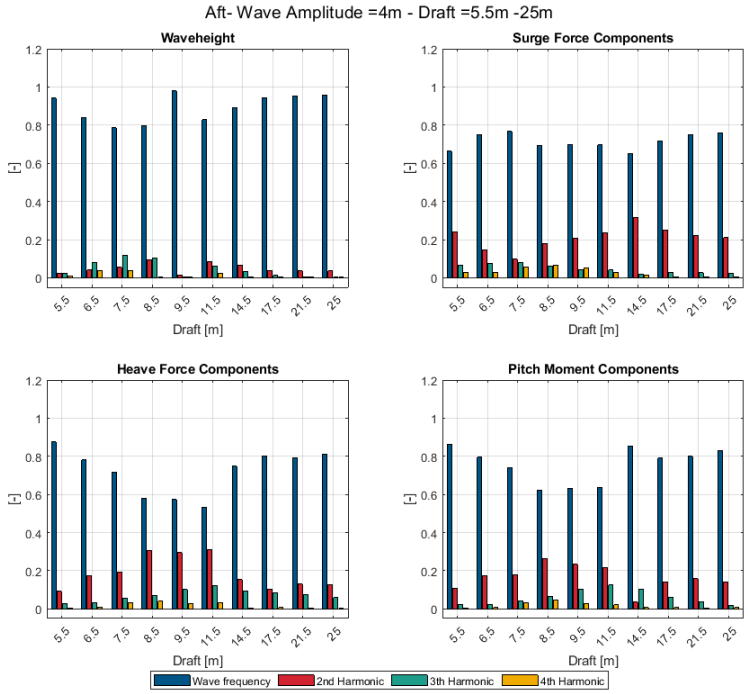

Figure D.42: Higher harmonic components of wave loads response of aft section at a wave amplitude of $\zeta_a = 4\ m$

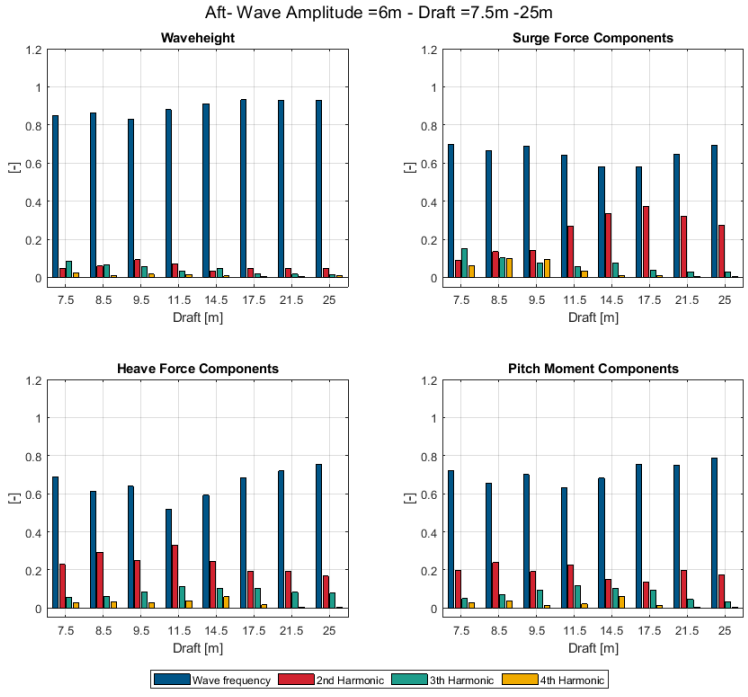

Figure D.43: Higher harmonic components of wave loads response of aft section at a wave amplitude of $\zeta_a = 6\ m$

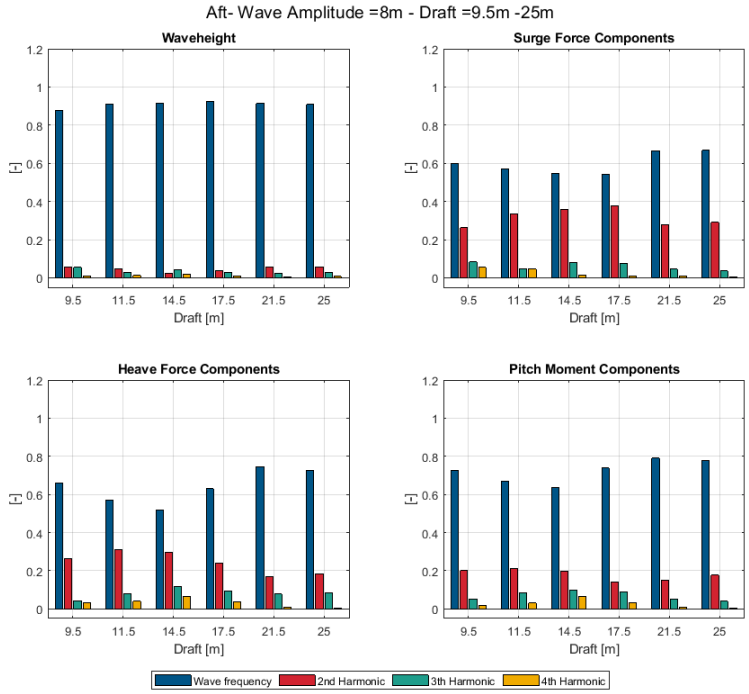

Figure D.44: Higher harmonic components of wave loads response of aft section at a wave amplitude of $\zeta_a = 8\ m$

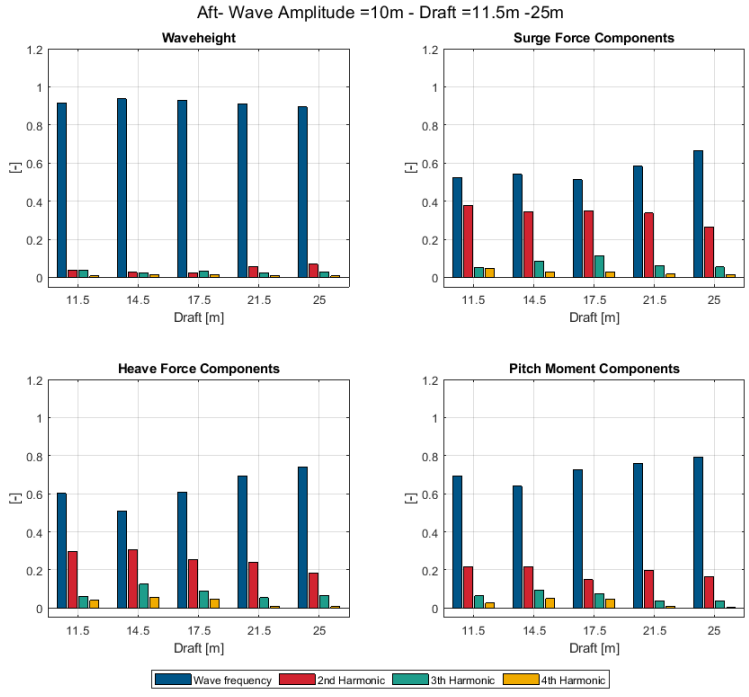

Figure D.45: Higher harmonic components of wave loads response of aft section at a wave amplitude of $\zeta_a = 10\ m$

E

ComFLOW versions

E.1. Version A

```
Welcome to ComFLOW4.1.1
 ---------------------------------------------------------------------------------------------------
 Version name    : ComFLOW release for the ComMotion JIP
 Release status  : Beta
 Platform        : Windows (x64)
 Version major   : 4
 Version minor   : 1
 Version patch   : 1
 Build date/time : 2018-02-05 17:47:24
 GIT branch name : mpi_amr
 GIT branch hash : 9161dd513756e764a1a364b0cca127098762092a
 GIT branch date : 2018-02-05 17:44:56 +0100
 Fortran compiler: Intel Fortran version 17.0.0
 OpenMP support  : Yes
 ===================================================================================================
 Rank: 1, World Size: 1, PID: 1372, Processor name: This executable does not support MPI
```

E.2. Version B

```
Welcome to ComFLOW4.1.1
---------------------------------------------------------------------------------------------------
Version name    : ComFLOW release for the ComMotion JIP
Release status  : Beta
Platform        : Windows (x64)
Version major   : 4
Version minor   : 1
Version patch   : 1
Build date/time : 2019-02-15 12:36:41
GIT branch name : 420_alpha_preparations
GIT branch hash : a99cbd66b90c09c6967ee77bc7c8167fbbb6c321
GIT branch date : 2019-02-12 10:03:23 +0100
Fortran compiler: Intel Fortran version 18.0.0
OpenMP support  : Yes
===================================================================================================
Rank: 1, World Size: 1, PID: 3592, Processor name: MPI_Get_processor_name_STUB, Simulation ID: 0
```

E.3. Version C

```
Welcome to ComFLOW4.1.1
-----------------------------------------------------------------------------------------------------
Version name    : ComFLOW release for the ComMotion JIP
Release status  : Beta
Platform        : Windows (x64)
Version major   : 4
Version minor   : 1
Version patch   : 1
Build date/time : 2019-04-11 11:40:25
GIT branch name : 420_alpha_preparations
GIT branch hash : 4103211bbb0a0582693a79625f9b38499382e817
GIT branch date : 2019-04-11 11:40:05 +0200
Fortran compiler: Intel Fortran version 18.0.0
OpenMP support  : Yes
=====================================================================================================
Rank: 1, World Size: 1, PID: 4192, Processor name: MPI_Get_processor_name_STUB, Simulation ID: 0
```

F

Figures Quantitative Analysis

F.1. joint stiffness

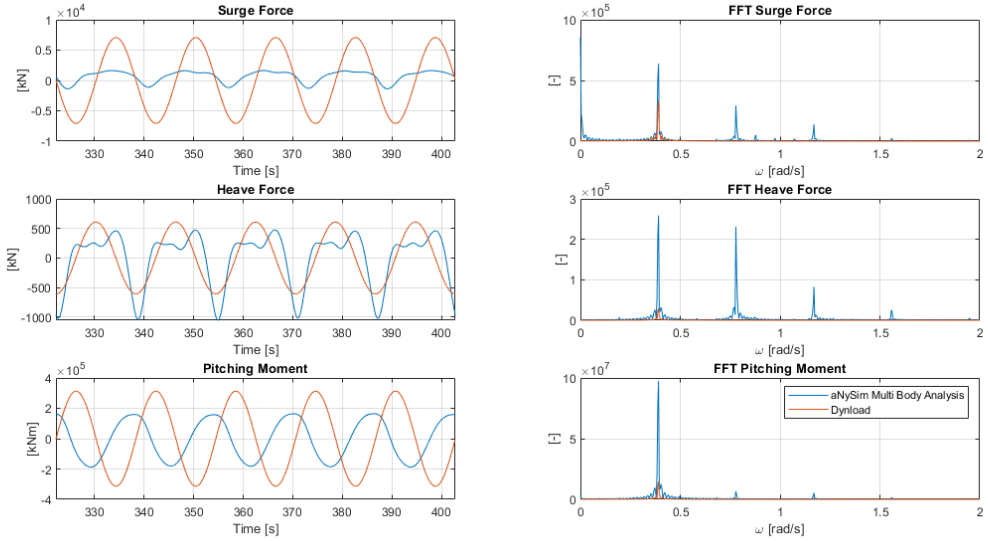

Figure F.1: Difference of internal load obtained with the weak joint at $T = 11.5\ m$

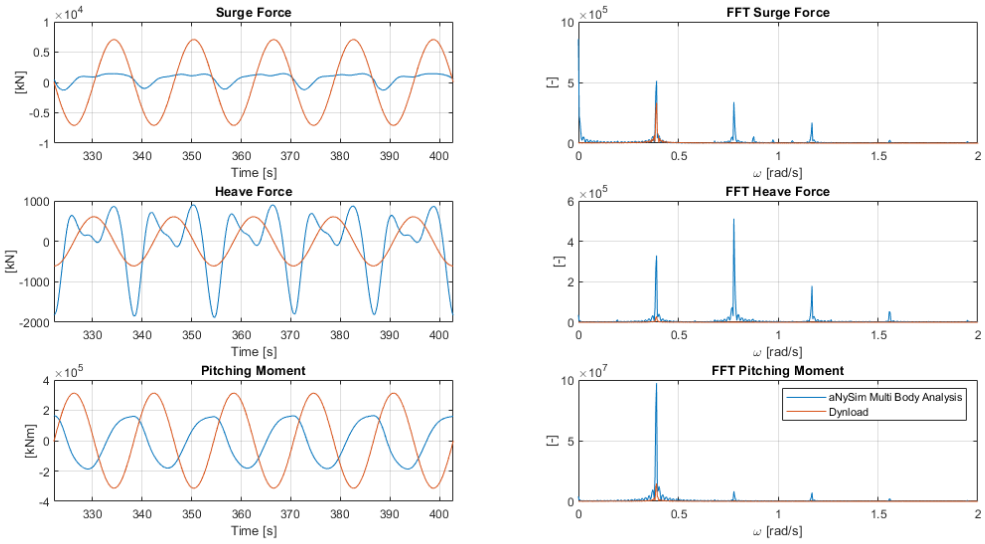

Figure F.2: Difference of internal load obtained with the medium joint at $T = 11.5\ m$

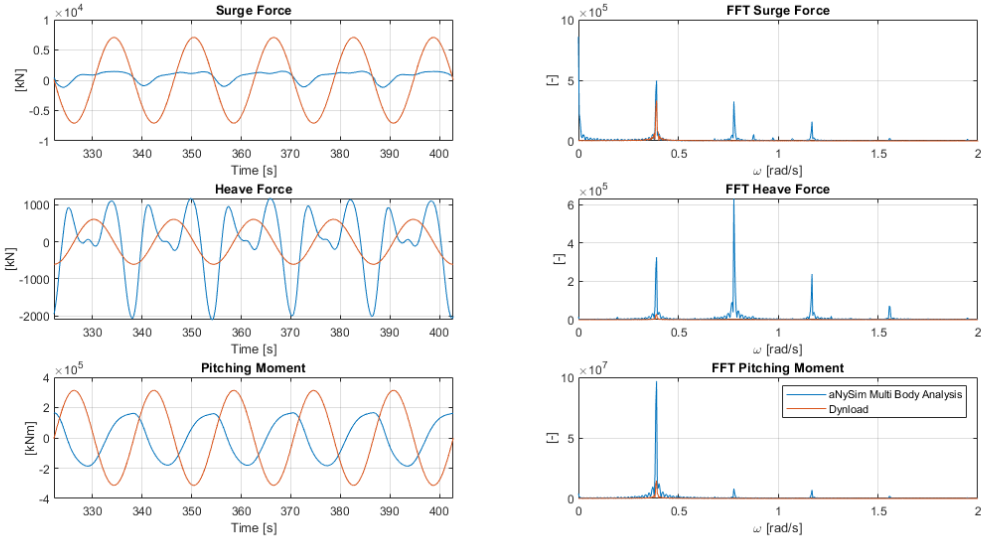

Figure F.3: Difference of internal load obtained with the stiff joint at $T = 11.5\ m$

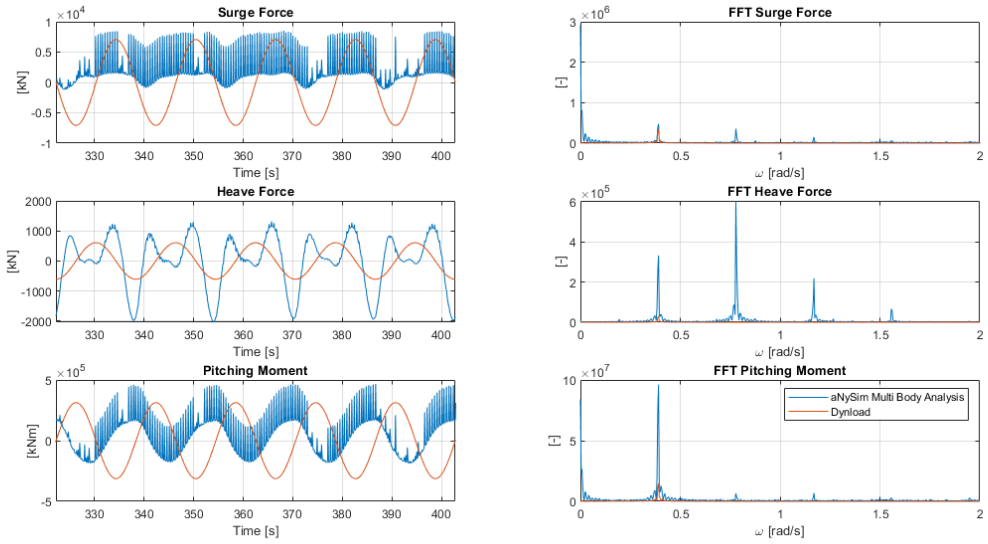

Figure F.4: Difference of internal load obtained with the Extra Stiff joint 2 at $T = 11.5\ m$

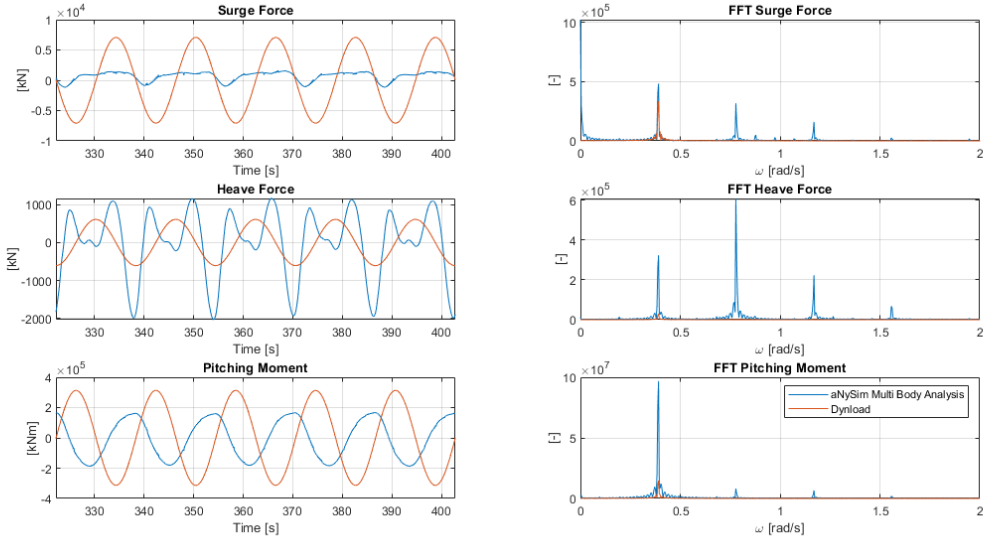

Figure F.5: Difference of internal load obtained with the extra stiff joint at $T = 11.5\ m$

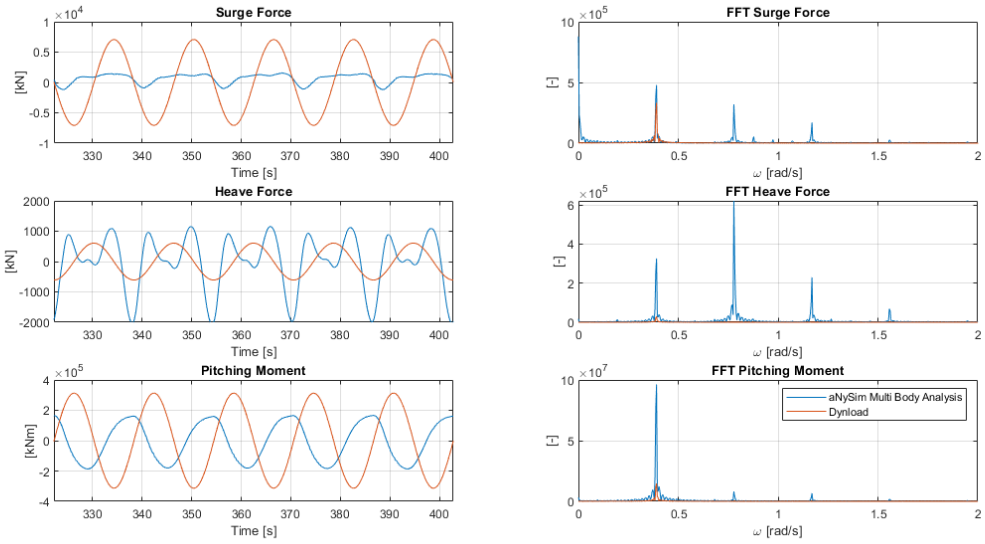

Figure F.6: Difference of internal load obtained with the stiff joint and a damping ratio of 1 at $T = 11.5\ m$

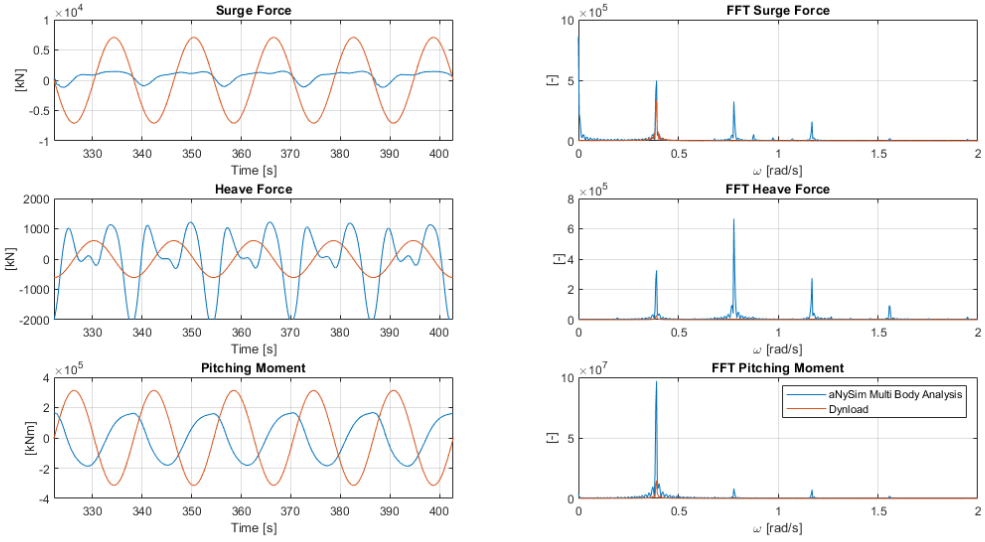

Figure F.7: Difference of internal load obtained with the stiff joint and a a damping ratio of 0.1 at $T = 11.5\ m$